UNIVERSITY OF CALIFORNIA,
IRVINE

Untangling the Complexities of Coronavirus Host Membrane Remodeling

DISSERTATION

Submitted in partial satisfaction of the requirements
for the degree of

DOCTOR OF PHILOSOPHY

in Biological Sciences

by

Megan Mary Angelini

Dissertation Committee:
Professor Michael J. Buchmeier, Chair
Professor Bert L. Semler
Professor Hung Y. Fan

2014

DEDICATION

For my friends and family,

both here and gone,

and all those who have helped along the way --

I could not have done this without you.

"To have one's hands among the unspeakable foundations, ribs, and very pelvis of the world; this is a fearful thing. What am I that I should essay to hook the nose of this leviathan!"

Herman Melville
Moby Dick

TABLE OF CONTENTS

LIST OF FIGURES

LIST OF TABLES

ACKNOWLEDGEMENTS

Thank you to my friends and family, especially my husband, Luke Avedon. Luke has been along for the ride during these five years of graduate school. His love, patience, kindness, support, and unwavering willingness to do dishes and laundry deserve the utmost praise. Thank you to my mother, Nancy Angelini, and my siblings, Brigid, Bill, and Frank, for their unending and unconditional support for all I've chosen to do. A special thank you to my father, Frank Angelini, who always fostered my interest in science and the arts. He's no longer here to read this, but his impact remains. A special thank you also goes to Allison Silverberg, my friend of 20 years, for love, support, and editing. I can't imagine what my graduate experience would have been like without my lab siblings: the other Buchmeier lab members. Specifically, Althea Capul, Cyrille Bonhomme, Lydia Bederka, and Kristeene Knopp. They taught me how to be an efficient, independent thinker and learner and guided me along the sometimes dimly lit path of molecular biology. They also formed a foundation of friendship, advice, and critique that I always knew I had supporting me. I'd like to thank my former undergraduate, Marzieh Akhlaghpour, who taught me what it means to be a mentor and who was always a joy to have around lab. Additionally, I'd like to thank JoEllen Brunner, administrator of the CVR, who was always kind and helpful with all my questions and PO forms and whose words of advice and encouragement I appreciate deeply. I'm extremely thankful to my undergraduate advisor, Ryan Z. Hinrichs, who exposed me to the world of scientific research and taught me how to design experiments and analyze data. Without him, I likely would not be where I am today.

Of course, this acknowledgement would not be complete without thanking the person who decided to take a chance on a liberal arts major five years ago, Michael J. Buchmeier. Mike has always challenged me to be the best scientist that I can be and has always supported my choices and career path, and for that I am eternally grateful.

I am grateful to my committee members, Dr. Bert Semler and Dr. Hung Fan, as well as my advancement committee members, Dr. Melissa Lodoen and Dr. Thomas Lane for their helpful feedback and support of my thesis project. I would also specifically like to thank Dr. Semler for the invaluable training I received during my first-year rotation in his lab and while on the CVR training grant.

I would like to express my gratitude to the University of California, San Diego Electron Microscopy Facility, specifically to Timo Meerloo and Ying Jones, without whom the EM studies presented here could not have been performed. I'd also like to thank Dr. Benjamin Neuman, who has been a collaborator, an advisor, and a mentor.

I would like to acknowledge the University of California, Irvine-Center for Virus Research for support and training via NIH Training Grant #5T32AI007319-23. I would also like to thank the California Center for Antiviral Drug Discovery MRPI (143226) for additional funding.

CURRICULUM VITAE

Megan Mary Angelini
University of California, Irvine - Department of Molecular Biology & Biochemistry
meg.angelini@gmail.com

EDUCATION

2009-2014 Doctor of Philosophy. University of California, Irvine.
Dept of Molecular Biology and Biochemistry
Thesis Advisor: Michael J. Buchmeier, Ph.D.

2003-2007 Bachelor of Arts. Sarah Lawrence College.
Concentration: Biology/Chemistry.
Mentor: Ryan Z. Hinrichs, Ph.D.

RESEARCH EXPERIENCE

2009-2014 University of California, Irvine. Irvine, CA
Graduate Student Researcher-Understanding coronavirus double membrane vesicle assembly

2005-2007 Sarah Lawrence College. Bronxville, NY
Undergraduate Researcher- The heterogeneous reactions of gaseous atmospheric pollutants on airborne mineral particles

HONORS AND AWARDS

2014 UCI School of Biological Sciences Edward Wagner Award in Virology
2010-2013 NIH-Training Grant #5T32AI007319-23
2011, 2012 American Society for Virology Student Travel Award
2011 International Nidovirus Symposium Student Travel Award
2011 NSF-GRFP Honorable Mention
2006 NY State Society for Applied Spectroscopy Undergraduate Award

PUBLICATIONS

2014 **Angelini MM**, Neuman, BW, Buchmeier MJ. "Untangling Membrane Rearrangement in the Nidovirales" *DNA Cell Biol.* 33(3): 122-7

2013 **Angelini MM,** Akhlaghpour M, Neuman BW, Buchmeier MJ. "Severe acute respiratory syndrome coronavirus nonstructural proteins 3, 4, and 6 induce double-membrane vesicles." *mBio*. 4(4):e00524-13

2013 Bonhomme CJ, Knopp KA, Bederka LH, **Angelini MM,** Buchmeier MJ. "LCMV glycosylation modulates viral fitness and cell tropism." *PLoS One.* 8(1):e53273

2007 **Angelini, MM**, Garrard, RJ, Rosen, SJ, Hinrichs, RZ. "Heterogeneous reactions of gaseous nitric acid and nitrogen dioxide on the clay minerals kaolinite and pyrophyllite." *J Phys Chem A*. 111(17), 3326-35.

ORAL PRESENTATIONS

2012 "Understanding the role of transmembrane nonstructural proteins in coronavirus double-membrane vesicle assembly" American Society for Virology (ASV) Annual Meeting, Madison, WI.

2012 "The Uninvited Guest: How Viruses Work and Why Understanding Them is Crucial" Sarah Lawrence College (invited speaker) Bronxville, NY.

2011-2013 "Understanding the role of coronavirus nonstructural proteins in double membrane vesicle assembly" Annual UCI CVR NIH Training Grant Symposium

POSTER PRESENTATIONS

2014 "FASN is important for coronavirus replication" UCI MB&B Departmental Retreat. Lake Arrowhead, CA.

2013 "SARS-Coronavirus non-structural proteins 3, 4, and 6 induce double membrane vesicles" Gordon Research Conference: Viruses and Cells. Lucca (Barga), Italy.

2011 "Understanding the role of nsp3, nsp4, and nsp6 in SARS-coronavirus double membrane vesicle formation" American Society for Virology 30th Annual Meeting, Twin Cities, MN.

2011 "Elucidating the importance of SARS-coronavirus nonstructural proteins 3, 4, and 6 in double membrane vesicle formation" Twelfth International Nidovirus Symposium, Acme, MI.

2006 "Spectroscopic Studies on the Heterogeneous Reactions of HNO3 and NO2 on Kaolinite and Pyrophyllite." American Geophysical Union Conference, San Francisco, CA.

TEACHING EXPERIENCE

2014 Teaching Assistant, *Viral Pathogenesis & Immunology*, UC Irvine
2012/13 Teaching Assistant, *Exp Microbiology Lab,* UC Irvine
2011/12/13 Teaching Assistant, *Virology*, UC Irvine
2011 Teaching Assistant, *Molecular Biology Lab*, UC Irvine
2007 School Group Workshop Educator, Hudson River Museum, Yonkers, NY

RELATED PROFESSIONAL EXPERIENCE

2007-2008 Manuscript Coordinator, Rockefeller University Press: Journal of Experimental Medicine, New York, NY

MEMBERSHIPS IN PROFESSIONAL ORGANIZATIONS

American Association for the Advancement of Science – AAAS, American Society for Microbiology – ASM, American Society for Virology – ASV

ABSTRACT OF THE DISSERTATION

Untangling the Complexities of Coronavirus Host Membrane Remodeling

By

Megan Mary Angelini

Doctor of Philosophy in Biological Sciences

University of California, Irvine, 2014

Professor Michael J. Buchmeier, Chair

Coronaviruses, like nearly all studied positive sense single-stranded RNA viruses, rely on host cell internal membranes to produce structures that support viral replication. These structures form in the cytoplasm and are called double membrane vesicles (DMVs) and convoluted membranes (CMs). DMVs are ~100-300 nm in diameter and are usually found in clustered groups. They are interconnected with regions of CM that can vary in size and extent. These membranous structures are the localized sites of viral genome replication and transcription within the infected cell. DMVs and CMs are distinct from structures that form later in the infection life cycle for purposes of virion assembly and budding. Ultrastructural studies have confirmed that the walls of DMVs and CMs are composed of two lipid bilayers in close proximity to each other and that the membranes are at least somewhat continuous with the membrane of the endoplasmic reticulum (ER). However, they do not stain for canonical ER markers. Despite the work that has been performed to discern the intricacies of DMV and CM assembly in coronavirus infected cells, the specific mechanisms and pathways involved have remained unclear. We present here the results of work done to elucidate both the viral proteins responsible for

DMV and CM formation as well as work to decipher which host cellular proteins and pathways might be important. We used plasmid constructs expressing nonstructural proteins (nsps) from the severe acute respiratory syndrome (SARS) coronavirus to determine that the combination of nsp3, nsp4, and nsp6 is sufficient for producing structures similar to DMVs and CMs induced during SARS-coronavirus infection. We also characterized structures induced by each of the three nsps individually and in paired combinations to theorize a general putative mechanism by which DMV and CM structures form. Additionally, we used inhibitors and siRNA technology to determine that host cellular fatty acid synthase (FASN) is an important protein for murine hepatitis virus replication and that, in the absence of FASN activity, DMVs and CMs are not observed. This work adds to the body of evidence characterizing membrane rearrangement by coronaviruses and will aid ultimately in a full description of the process.

CHAPTER 1

Introduction: Host cell membrane rearrangement in coronaviruses

Overview

Coronaviruses, members of the order *Nidovirales*, must induce internal membrane rearrangements in host cells in order to replicate and produce progeny virus. This chapter will examine membrane rearrangement as a general strategy utilized by nearly all positive sense single-stranded RNA viruses. Then, the basics of the *Nidoviruses* will be covered, segueing into the coronavirus family and the specifics of membrane rearrangement pertaining to them. This chapter will conclude with an examination of some possible host cellular proteins and pathways involved in membrane rearrangement.

Introduction to membrane rearrangement

Procreate or perish: it's the rule under which all biological entities persist. The reason for this is obvious enough—one must pass on genes to the progeny generation to maintain a population. This is especially pertinent with regards to viruses, biological entities that rely on their host in order to create progeny. Positive sense single-stranded RNA viruses (+RNA viruses) make up a diverse group of viruses. All +RNA viruses follow a similar basic schema of infection (Nagy and Pogany, 2012). The virus first enters the host cell and the virus' +RNA genome is released and translated to produce the viral proteins needed for replication. The proteins interact with the viral genome for replication on or within the replication complexes that have formed. Negative sense RNA is produced from the positive RNA template and is used for the production of more

positive sense molecules. This cycle continues until sufficient translation and genome replication have occurred for the viral particles to form and exit the initially infected cell. Host cell membrane remodeling is a tactic used by many viruses as a means of reaching their end game of using the host cell for viral production. The replication complexes of nearly all +RNA viruses are based on and around membranous structures composed of virally rearranged host cell membranes. (Ahlquist, 2006; Denison, 2008; Miller and Krijnse-Locker, 2008; Netherton and Wileman, 2011; Suhy et al., 2000)

Table 1.1 summarizes the virally-induced membranous replication structures for all currently studied +RNA viruses. A brief sampling includes flaviviruses, which induce an organized network of interconnected double-walled endoplasmic reticulum (ER)-derived membranes termed ‘‘vesicle packets’’ and ‘‘spherules” (Gillespie et al., 2010; Miorin et al., 2013; Welsch et al., 2009). Picornaviruses have been shown to reorganize ER, Golgi, and lysosomes into both single and double membrane vesicles (DMVs), the latter of which are similar to autophagosomes (Belov et al., 2012; Limpens et al., 2011; Suhy et al., 2000). Alphaviruses, members of the Togaviridae family, induce ~50nm in diameter single membrane vesicles termed ‘‘spherules,’’ seen to be derived from invaginated ER, plasma membrane, and endosomes/lysosomes depending on the virus (Froshauer et al., 1988; Kopek et al., 2007; Schwartz et al., 2002; Spuul et al., 2010). Nodaviruses reorganize the mitochondrial membrane into small ~50 nm vesicles. The walls of these vesicles are composed of a single membrane and are positioned between the inner and outer mitochondrial membrane (Kopek et al., 2010; Miller et al., 2001).

Table 1.1. Positive sense single-stranded RNA viruses, their proposed progenitor membranes, and viral proteins involved.
ER = endoplasmic reticulum, CH = chloroplast, M = mitochondria, L = lysosome, P = peroxisome, DMV = double membrane vesicle, SMV = single membrane vesicle, V = uncharacterized vesicle, VP = viroplasm (VP), CM = convoluted membrane, PM = paired membrane, T = tubule, X = data unknown. Gray shaded region = members of the *Nidovirales*.

Table 1.1. Membrane rearrangements in +RNA virus families

Family	Proposed Progenitor Membrane	Vesicle Designation	Viral Proteins Implicated	References
Arteriviridae	ER	DMV, PM	nsp2, 3	(Posthuma et al., 2008; Snijder et al., 2001; Wood et al., 1970)
Coronaviridae	ER	DMV, CM, S, PM	nsp3, 4, 6	(Angelini et al., 2013; Knoops et al., 2008; Maier et al., 2013)
Mesoniviridae	ER	PM, T	X	(Zirkel et al., 2011)
Roniviridae	X	V	X	(Spann et al., 1995)
Dicistroviridae	X	X	X	
Iflaviridae	X	Vesicle	X	(Gauthier et al., 2011)
Marnaviridae	X	V	X	(Takao et al., 2005)
Picornaviridae	ER	DMV	2BC, 3A	(Hsu et al., 2010; Richards et al., 2014; Suhy et al., 2000; Teterina et al., 1997)
Secoviridae	ER	V, CM	X	(Roberts and Harrison, 1970)
Alphaflexiviridae	ER	VP	TGB1	(Linnik et al., 2013; Tilsner et al., 2012)
Betaflexiviridae	ER	VP, DMV	X	(Edwardson and Christie, 1978; Rudzinska-Langwald, 1990)
Gammaflexiviridae	X	VP	X	(Boine et al., 2012)
Tymoviridae	C, M	DMV	X	(Lesemann, 1977)
Alphatetraviridae	X	VP	Rep	(Short and Dorrington, 2012)
Alvernaviridae	X	VP	X	(Tomaru et al., 2004)
Astroviridae	ER	DMV	nsP1a	(Guix et al., 2004; Méndez et al., 2007)
Barnaviridae	X	X	X	

Bromoviridae	ER	S	Protein 1a	(Moreira et al., 2010; Schwartz et al., 2002)
Caliciviridae	ER	V	P30	(Bailey et al., 2010)
Carmotetraviridae	X	VP	X	(Pringle et al., 2003)
Closteroviridae	X	VP, DMV	X	(Medina et al., 1998)
Flaviviridae	ER	Spherule	NS4A, 4B	(Gillespie et al., 2010; Gosert et al., 2002; Miller et al., 2007; Romero-Brey et al., 2012; Roosendaal et al., 2006; Welsch et al., 2009)

Hepeviridae	ER	Vesicle, PM	X	(Rehman et al., 2008)
Leviviridae	None evidenced			(Nishihara, 2003)
Luteoviridae	X	SMV, T	X	{Gill, 1979 #541}
Narnaviridae	X	X	X	
Nodaviridae	M	S	Protein A, viral RNA	(Kopek et al., 2007; Kopek et al., 2010)
Permutotetraviridae	X	X	X	
Potyviridae	ER	Vesicle	6K, 6K2	(Grangeon et al., 2012; Schaad et al., 1997; Wei and Wang, 2008)
Togaviridae	L, ER	S	P123	(Fontana et al., 2010; Magliano et al., 1998; Salonen et al., 2003)
Tombusviridae	P	S	X	(Barajas et al., 2009; Sharma et al., 2011)
Virgaviridae	ER	S	X	(Kawakami et al., 2004;
Virgaviridae	ER	S	X	(Kawakami et al., 2004; Reichel et al., 1999)

The reasons for +RNA viruses creating these membranous structures include the need to concentrate, localize, and anchor the host and viral proteins and precursors required for transcription. It is also thought that these structures aid in shielding double-stranded RNA replication intermediates from activating an innate immune response via toll-like receptor recognition and RIG-I pathway activation (Alexopoulou et al., 2001; Gantier, 2014; Perales-Linares and Navas-Martin, 2013).

Membrane rearrangements involved in viral genome replication and transcription for some members of the +RNA viruses have been well characterized and have a wide range of complexity of membrane involvement, numbers, and types of proteins responsible for the remodeling (den Boon et al., 2010; Kirkegaard and Jackson, 2005; Mackenzie, 2005; Novoa et al., 2005; Salonen et al., 2005). The "Type" column in Table 1.1 emphasizes that, although the overarching theme of membranous structures for viral replication is wide reaching in the +RNA viruses, the actual membrane morphologies can vary, even within the same family or order. Overall, the formation of these complexes across the families that have been studied appears to be well regulated. Observed regulatory mechanisms include RNA-RNA interactions as well as viral protein-protein and viral-host protein interactions. Regulation for some viruses appears very precise. One such example is hepatits C virus, for which the viral replication complexes have been shown to demonstrate specific balances in the numbers of negative strands, positive strands, and viral proteins present (Quinkert et al., 2005).

Although many studies on various aspects of membrane rearrangement have been performed, some very basic questions including which viral proteins are responsible for

membrane rearrangement remain largely unanswered for many of the families included in Table 1.1. Members of the *Nidovirales*, the order of focus for this thesis, have been shown to form double membrane vesicles (DMVs), convoluted membranes (CMs), paired membranes (PMs), spherules, tubules, and single membrane vesicles. The ultrastructural determinations of such structures are typically designated by mapping the intracellular localization of the double-stranded RNA (dsRNA) replicative intermediates, nascent RNA, and replicase proteins using immunogold labeling in electron microscopy. Once the membranous replicase structures have been identified, further characterization and description of the host and viral components involved can occur. Techniques used may include reverse genetics, immunofluorescence-based localization studies, genomic screening assays and proteomics approaches, *in vitro* replication modeling, and the more recently applied technique of three-dimensional electron tomography (Kopek et al., 2007; Subramaniam, 2005; Subramaniam et al., 2007).

Introduction to the Nidoviruses

The order *Nidovirales* contains families of positive sense nonsegmented single-stranded RNA viruses featuring an envelope and, notably, a mechanism of discontinuous transcription to produce the nested subgenomic mRNAs for which the order is named (the Latin *nidus* means nest) (González et al., 2003; Gorbalenya et al., 2006; Pasternak et al., 2006; Stern and Kennedy, 1980). This order contains families capable of infecting both vertebrates (*Coronaviridae*, *Arteriviridae*, and *Roniviridae*) and invertebrates (*Mesoniviridae*) (Cowley et al., 2000; Lauber et al., 2013). All nidoviruses share a genome with a similar genetic organization with the first two overlapping open reading frames (ORF1a and 1b) producing two large polyproteins (pp1a and pp1ab) that are co- and post-translationally cleaved into the nonstructural proteins (nsps) (Brian and Baric, 2005; Britton and Cavanagh, 2008). Processing of these polyproteins is directed by viral-encoded proteinases, which vary between families and species of these viruses (Snijder et al., 2013; Ziebuhr, 2006). For coronaviruses, the viral family that is the focus of this thesis, nonstructural protein 3 contains one or two papain-like protease (PLpro) subunits responsible for cleaving free nsp1, nsp2, nsp3, and the N-terminus of nsp4. Nonstructural protein 5 contains the main 3C-like protease (3CLpro or Mpro) responsible for cleaving free the C-terminus of nsp4 through nsp16. Figure 1.1 (A) illustrates the general Nidovirus genome organization and nonstructural protein production using severe acute respiratory syndrome coronavirus (SARS-CoV) as the example. Figure 1.4 shows an overview of the coronavirus life cycle. The nsps are part of the viral replicase machinery necessary for viral genome replication and transcription, in association with cellular membranes (Hagemeijer et al., 2010; van Hemert et al., 2008). For SARS-CoV, these

Figure 1.1. *SARS-coronavirus genome organization and protein production.* (A) The first two-thirds of the 29.7kb SARS-CoV genome is immediately translated into polyprotein 1a and, via a frameshift event, polyprotein 1b which are cleaved into 16 nonstructural proteins. (B) The last third of the genome encodes the structural and accessory proteins that are synthesized via discontinuous transcription of a nested set of subgenomic (sg) mRNAs. ORF=open reading frame, S=Spike, E=envelope, M=membrane, N=nucleoprotein

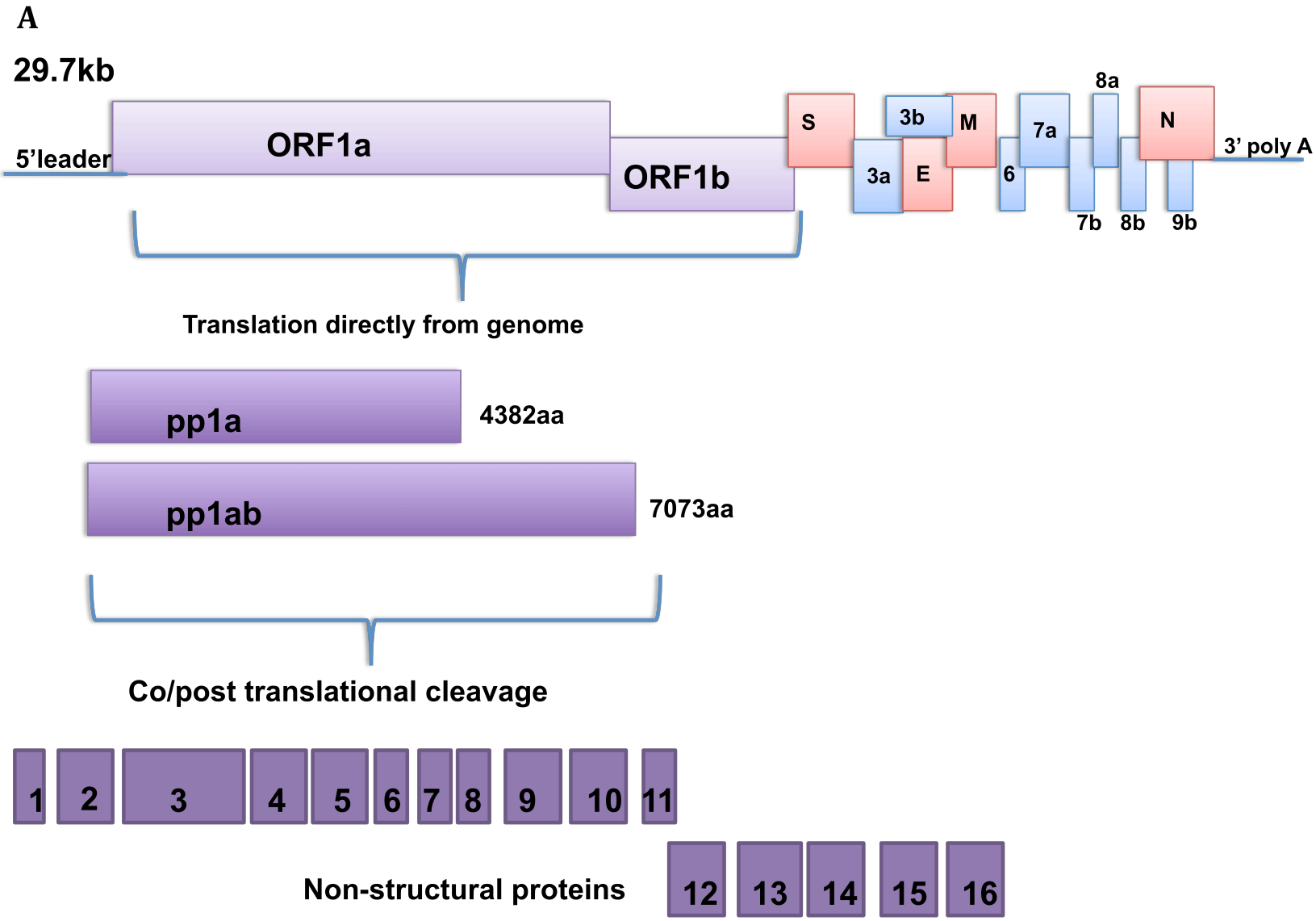
A
29.7kb
5'leader
ORF1a
ORF1b
S
3a
3b
E
M
6
7a
7b
8a
8b
N
9b
3' poly A
Translation directly from genome
pp1a
4382aa
pp1ab
7073aa
Co/post translational cleavage
1
2
3
4
5
6
7
8
9
10
11
Non-structural proteins
12
13
14
15
16

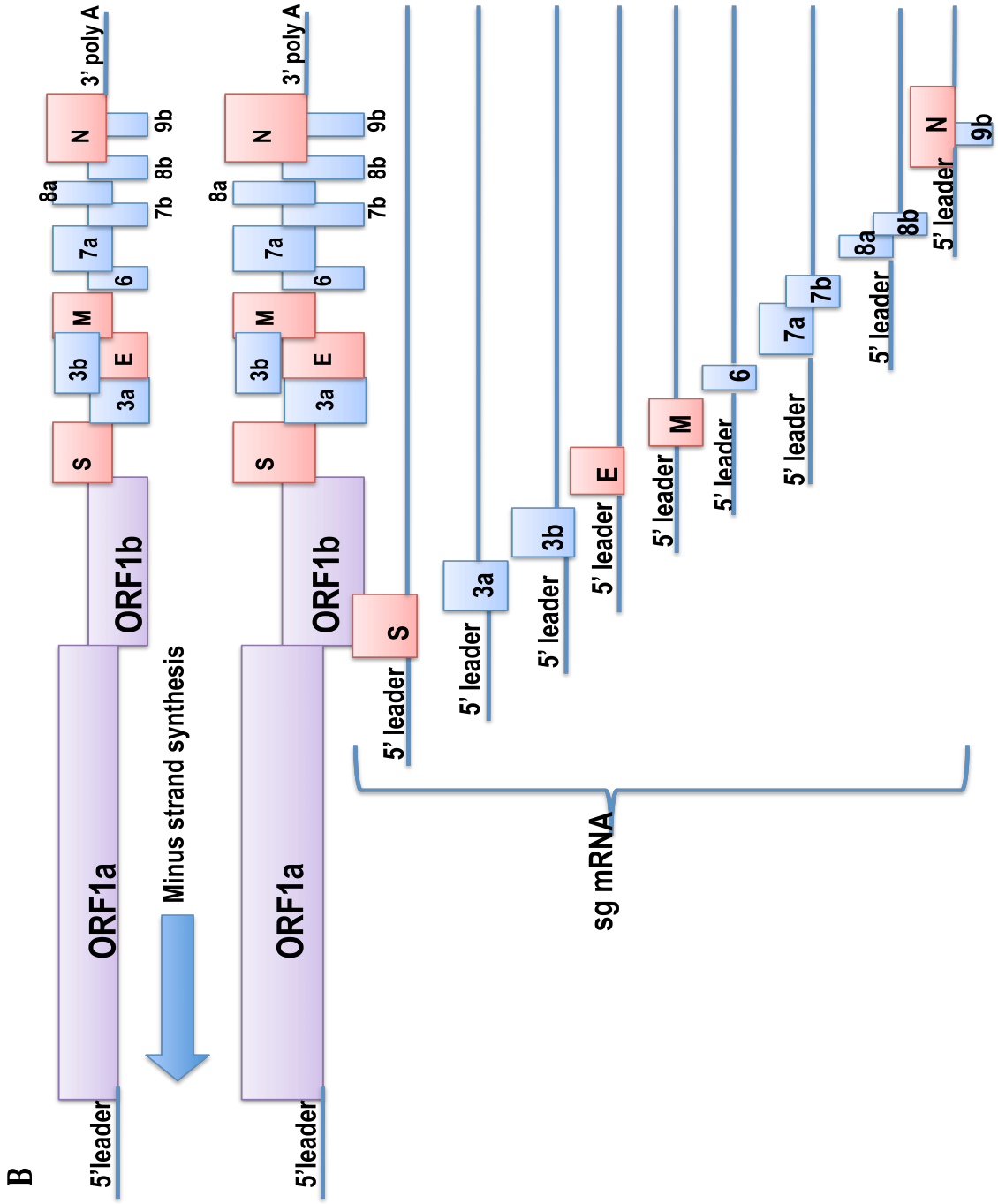
B
5'leader
ORF1a
ORF1b
S
3a
E
3b
M
6
7a
7b
8a
8b
9b
N
3' poly A
Minus strand synthesis
5' leader
sg mRNA

include an RNA-dependent RNA polymerase (nsp12), an RNA helicase (nsp13), an endoribonuclease (nsp15), an N7 methyltransferase (nsp14) a 2'-O methyltransferase (nsp16), a protein for shutting down host-cell mRNA synthesis (nsp1), the aforementioned proteases (nsp3 and nsp5), and a putative primase and/or RNA-dependent RNA polymerase (nsp7+nsp8) (Prentice et al., 2004b; Sawicki et al., 2005; Ulferts et al., 2010). ORFs downstream from ORF1a and 1b encode varying structural and accessory proteins (Figure 1.1 B). These structural and accessory proteins are produced from nested 3′ co-terminal subgenomic mRNAs via a discontinuous transcription process (Faaberg, 2008; Hogue and Machamer, 2008). The sub-genomic mRNAs have identical 3' and 5' ends. The 5' ends match the 5' leader sequence of the viral genomic RNA. The structural proteins are the spike (S) glycoprotein, the membrane (M) protein, the envelope (E) protein, and the nucleocapsid (N) protein. (Figure1.3C-right panel) Additionally, although the SARS-coronavirus does not, some coronaviruses also encode a haemagglutinin-esterase (HE) protein in this portion of the genome. In addition to these structural proteins, coronaviruses also encode from one to eight genes for accessory proteins in the 3'-third of the genome (Sawicki et al., 2007; Ziebuhr, 2004). While Nidovirus genomes range significantly in sequence and size, from 12.7kb for the smaller arteriviruses to 31.7kb for the large coronaviruses, they share some commonalities (Gorbalenya et al., 2006). Figure 1.2 highlights the conservation across the *Nidovirales* in the pp1a-based nsps thought to be involved in membrane rearrangement. Coronaviruses and arteriviruses remain the best-studied and characterized nidoviruses.

Figure 1.2. *Conservation of DMV producing proteins in the Nidovirales.* Domain annotations were based on conserved amino acid sequences (solid colors) or secondary structure patterns (diagonal stripes). Positions of transmembrane and hydrophobic nontransmembrane regions were predicted by TMHMM 2.0 and amended to reflect known topologies wherever possible. Virus names are abbreviated as follows: Human coronavirus 229E (HCoV-229E), severe acute respiratory syndrome coronavirus (SARS-CoV), infectious bronchitis virus (IBV), munia coronavirus HKU13 (MuCoV), equine torovirus (EToV), white bream virus (WBV), fathead minnow virus (FHMV), equine arteritis virus (EAV), lactate dehydrogenase elevating virus (LDV), porcine reproductive and respiratory syndrome virus (PRRSV), simian hemorrhagic fever virus (SHFV), Cavally virus (CAVV), and gill-associated virus (GAV). The amino-terminal region of the polyprotein is shown for CAVV and GAV because no obvious homolog of nsp3 was detected. A jagged line denotes the uncertain position of the amino termini of EToV, WBV, FHMV, and GAV.

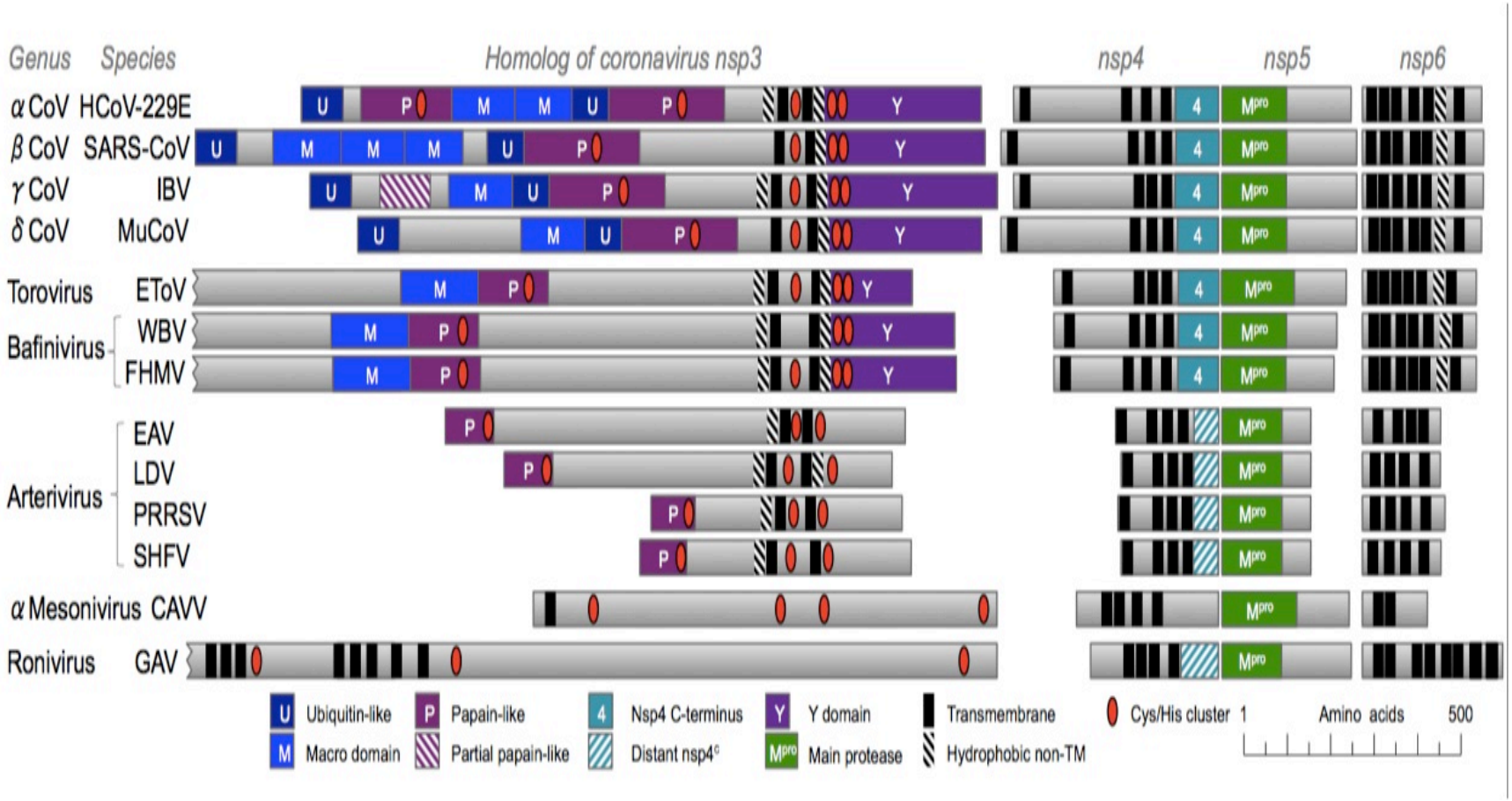
Genus
Species
Homolog of coronavirus nsp3
nsp4
nsp5
nsp6
α CoV HCoV-229E
β CoV SARS-CoV
γ CoV IBV
δ CoV MuCoV
Torovirus EToV
Bafinivirus WBV
FHMV
Arterivirus EAV
LDV
PRRSV
SHFV
α Mesonivirus CAVV
Ronivirus GAV
U Ubiquitin-like
M Macro domain
P Papain-like
Partial papain-like
4 Nsp4 C-terminus
Distant nsp4c
Y Y domain
Mpro Main protease
Transmembrane
Hydrophobic non-TM
Cys/His cluster
1
Amino acids
500

Coronaviruses

Coronaviruses are named for the "crowned" appearance of the virion due to the protruding spike protein (Figure 1.3C). Although estimated to cause up to 15% of common colds in humans as well as disease ranging from moderate to severe in many domesticated animals, coronaviruses were not known to result in life-threatening illnesses in humans, except in rare cases in infants, immunocompromised patients, and geriatric patients (Kupfer et al., 2007; Pyrc et al., 2007; Reed, 1984; Simon et al., 2007). The well-studied prototypic murine hepatitis virus (MHV) coronavirus can even be thought of as an asset to human health, in that it can cause a demyelinating disease in mice that is used as a model system for studying multiple sclerosis (Knobler et al., 1983; Tirotta et al., 2010). Severe acute respiratory syndrome, or SARS, first emerged as a life-threatening disease of unknown origin in late 2002 in the Guangdong Province of Southern China. The disease presented as an atypical penumonia with symptoms including fever, dry cough, shortness of breath, headache, and hypoxemia (low blood oxygen content). The disease subsequently spread via international travel of infected individuals and appeared to be caused by a unique and unidentified pathogen. The World Health Organization reports that the disease ultimately reached at least 30 countries, with approximately 8000 confirmed cases resulting in 774 deaths ((CDC), 2003; Braden et al., 2013). Interestingly, the disease had an age related coincidence of morbidity and mortality, with an increasing incidence of death with increased age (Fowler et al., 2003; Lau et al., 2010; Leong et al., 2006; Leung et al., 2004). By the spring of 2003, multiple laboratory groups had identified the causative agent as a novel coronavirus: the SARS-

coronavirus (Drosten et al., 2003; Ksiazek et al., 2003; Pfefferle et al., 2011; Poutanen et al., 2003).

The possibility of re-emergence or of the emergence of another similarly pathogenic coronavirus remains, despite the relative brevity of the SARS pandemic. This fear was realized in late 2012 when the Middle Eastern Respiratory Syndrome (MERS)-coronavirus appeared with estimates of an approximate 25% to 40% mortality rate, highlighting the importance of studying coronaviruses for public health reasons (Cotten et al., 2014; de Groot et al., 2013; de Wilde et al., 2013; Graham et al., 2013). Insight into and an understanding of the molecular biology of coronaviruses will prove beneficial for the development of potential treatments and therapeutics.

Figure 1.3. *Coronavirus microscopy and virion schematic.* (A) MHV induced double membrane vesicles and convoluted membranes as imaged by electron microscopy (B) SARS-CoV induced double membrane vesicles and convoluted membranes as imaged by electron microscopy. Red asterisks indicated DMVs, blue arrowheads indicate CMs. (C) MHV virion as imaged by atomic force microscopy (left) and cartoon representation of SARS-CoV virion (right). Red=spike (S) protein, yellow=envelope (E) protein, Purple=membrane (M) protein, Green=nucleocapsid (N) protein. Atomic force microscopy image credited to Yurii Kuznetzov, McPherson Lab, UCI. Cartoon schematic credited to former Buchmeier Lab member Cromwell T. Cornillez-Ty.

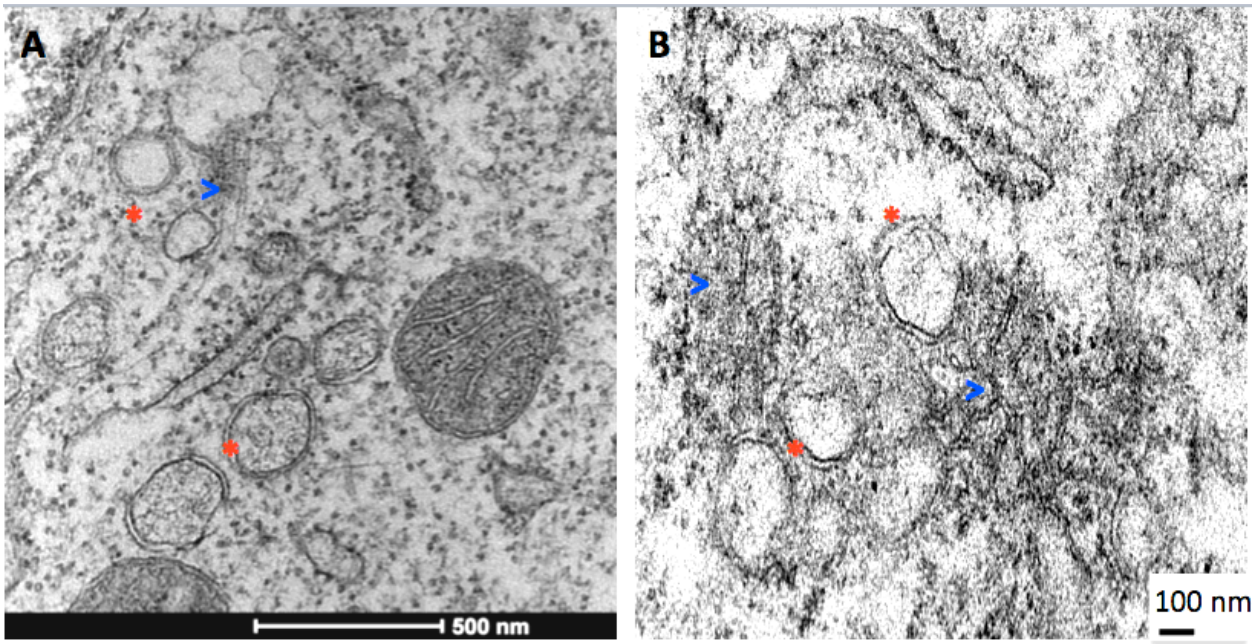
A
500 nm
B
100 nm

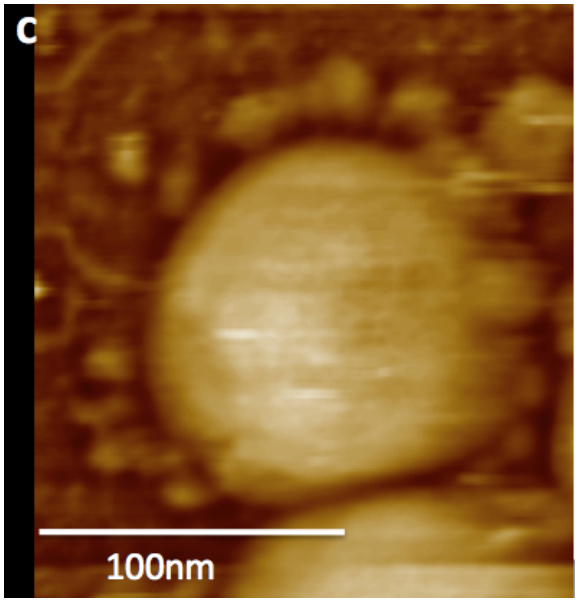
C
100nm

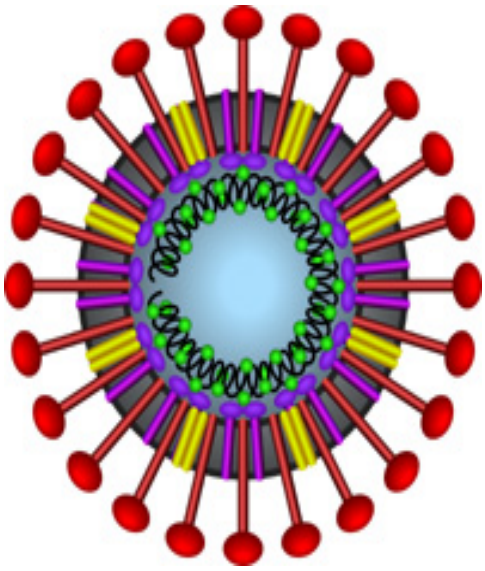

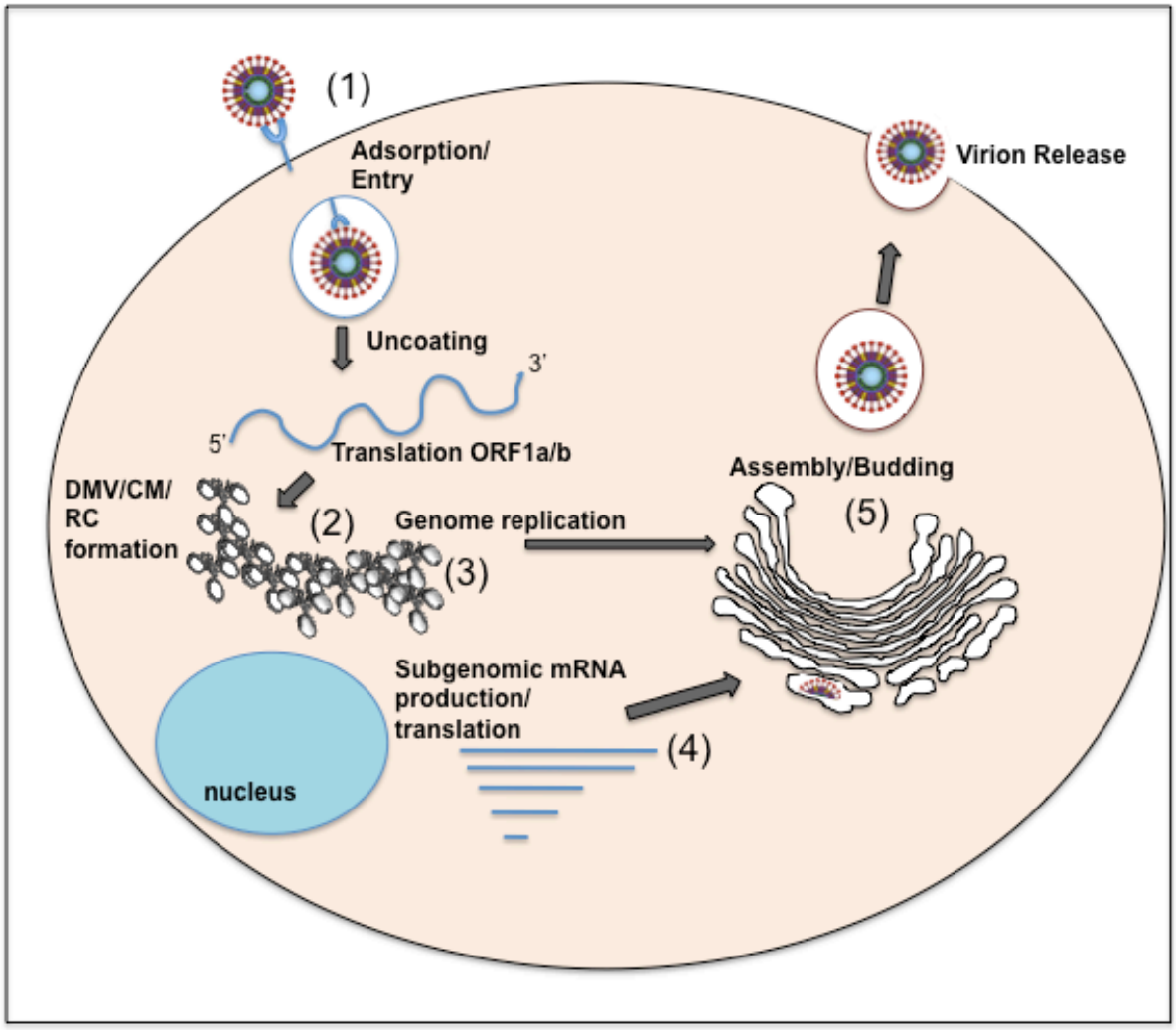

Figure 1.4 *Schematic of coronavirus replication cycle*. (1) Adsorption/entry into host cell. (2) First two-thirds of positive sense ssRNA genome translated and replication complex formation begins (3) Subgenomic (sg)RNA transcription and genome replication follow at replication complex (4) Structural and accessory proteins translated from sgRNAs (5) Virion assembly, budding, and release

The coronavirus life cycle (Figure 1.4) begins upon binding of the viral S glycoprotein to the host cell receptor. Host cell receptors have only been defined for a few coronaviruses. The receptor for the SARS-coronavirus is angiotensin converting enzyme 2 (ACE2) (Li et al., 2003). The receptor for MHV is carcinoembryonic antigen adhesion molecule 1 (CEACAM1) (Dveksler et al., 1991; Tan et al., 2002). Other identified coronavirus receptors include aminopeptidase N (APN) and 9-O-acetylated sialic acid (Perlman and Netland, 2009).

Following entry and uncoating, the 5'-capped, positive sense single-stranded RNA genome is released to the cytoplasm and translation begins of ORF1a and ORF1a/b. The latter ORF1ab is translated via a programmed -1 frameshifting event (Plant and Dinman, 2008). During and following the production of the polyproteins, pp1a and pp1ab, proteolytic cleavages of the pp1a- and pp1ab-encoded nonstructural proteins are completed (Weiss et al., 1994). The virally encoded proteases responsible for these cleavages are encoded within coronavirus nsp3 and nsp5 and, respectively, are papain-like proteases and chymotrypsin-like proteases (Hagemeijer et al., 2012). The number of papain-like protease domains varies between viruses, as shown in Figure 1.2. Once translation of ORF1a and 1ab begins, the host cell internal membrane environment begins rearranging and the formation of double membrane vesicles and regions of convoluted membranes commences, the viral determinants of which will be discussed in **Chapter 2.**

After translation of sufficient amounts of the nsps, the viral replicase proteins, negative strand synthesis from the positive sense RNA precursor starts. A subset of these negative sense RNAs will be used for producing more positive sense template, while others will be used to produce the coronavirus subgenomic mRNAs encoding the viral

accessory and structural proteins. The accessory proteins vary depending on the virus and their roles remain largely undefined (McBride and Fielding, 2012). The nascent full length positive-sense single-stranded RNAs are transported in a manner still not understood to the ER-Golgi intermediate compartment (ERGIC) between the ER and the Golgi apparatus, where they meet with the translated structural proteins assembling there. The virus assembles and buds intracellularly at the ERGIC. The nucleoprotein-encapsidated genome incorporates into the virion, comprised of the E integral membrane protein which alters the membrane's permeability, the M transmembrane glycoprotein, the S spike glycoprotein, and depending on the virus the HE haemagglutinin-esterase protein (Satija and Lal, 2007; Weiss and Leibowitz, 2011). The Golgi cisternae increase in size and become fragmented as more and more virus is produced and the virions travel through the Golgi and are released by the cell (Cong and Ren, 2014; Ruch and Machamer, 2012).

The hallmark membrane rearrangements formed upon coronavirus infection of a host cell are double membrane vesicles (DMVs), named for their distinct double membrane bilayer walls as seen in electron microscopy, and characteristic convoluted membranes (CMs) (Figure 1.3A & B) (Figure 1.4 Step 2) (Gosert et al., 2002). These DMVs are generally around 200 nm in diameter and, as expected, co-localize with both viral RNA and the nonstructural proteins. Multiple groups have reported double-stranded RNA (dsRNA) within the coronavirus-induced DMVs, marking the intermediate stage of viral RNA synthesis. Despite many ultrastructural electron microscopy studies examining coronavirus-induced DMVs, their precise membrane of origin has remained elusive. Electron microscopy (EM), immuno-electron microscopy (iEM), and 3-

dimensional electron tomography (ET) have been used to examine coronavirus rearranged membranes (Ulasli et al., 2010). These techniques have pointed to the endoplasmic reticulum (ER) as the most likely progenitor membrane, due to its proximity to the rearranged membranes as well as its sometimes-observed continuity with it. Despite this, the DMVs have failed to consistently stain for canonical ER membrane markers, including calnexin, calreticulin, and PDI (Table 1.2) (Knoops et al., 2010; Prentice et al., 2004a; Snijder et al., 2006; van den Worm et al., 2011). Transfection of two nonstructural proteins of the arteriviruses was sufficient to induce double membrane vesicles (Posthuma et al., 2008; Snijder et al., 2001). The two arterivirus nsps responsible for this, nsp2 and nsp3, are related to the SARS-Cov nsps 3 and 4. Figure 1.2 aligns the regions of similarity in arterivirus nsp2 and coronavirus nsp3 as well as arterivirus nsp3 and coronavirus nsp4. Both of these nsps, as might be expected for a protein capable of rearranging membranes, contain transmembrane domains. In addition, coronaviruses have a third nsp that contains transmembrane domains—nsp6. These three coronavirus nonstructural proteins will be the focus of this thesis.

The largest non-structural protein is nsp3, at 1922 amino acids and approximately 213kD. SARS-CoV nsp3 is a glycosylated, membrane-spanning, multi-domain protein. Several domains of nsp3 are conserved among all coronaviruses (Figure 1.2). Identified domains conserved in nearly all coronavirus nsp3s include one or two papain-like protease domains (PLpro) that are partially responsible for polyprotein cleavage. These domains also include an N-terminal acidic domain which may bind RNA; an "X" or "ADRP" domain which has been shown to have ADP-ribose 1-phosphatase function and poly-ADP ribose binding function; carboxy-terminal Y domains of unknown function;

ubiquitin-like domains; and a nucleic acid binding (NAB) region (Barretto et al., 2005; Egloff et al., 2006; Imbert et al., 2008; Johnson et al., 2010; Neuman et al., 2008; Saikatendu et al., 2005; Serrano et al., 2009). Additionally, nsp3 of SARS-CoV features the SARS unique domain, or SUD, which has not been found in any other coronaviruses (Neuman et al., 2008). All coronaviruses have three predicted transmembrane domains within nsp3. However, it has been shown that only two of these predicted domains are actually membrane spanning, leaving nsp3 with both its amino and carboxy termini exposed on the cytoplasmic side of the replication complex membranes (Kanjanahaluethai et al., 2007).

Nonstructural protein 4 (nsp4) is the second of the non-structural proteins featuring transmembrane domains. Nsp4 has four transmembrane domains, all of which are membrane spanning--yielding the same amino and carboxy cytoplasm-exposed termini conformation as nsp3 (Oostra et al., 2007). Compared to nsp3, nsp4 is a smaller protein, having predicted molecular mass of around 55kDa, with two glycosylation sites. In addition it lacks multiple domains and has not been implicated in any non-DMV related viral processes. Nsp4 of MHV has been shown to be required for viral replication. Mutation of an asparagine residue located near the second transmembrane domain (N258T) results in a temperature-sensitive mutant that causes nsp4 to be relocalized to the mitochondria and leads to reduced DMV formation. Cells infected with mutants featuring a loss of glycosylation of MHV nsp4 showed irregular DMV formation (Clementz et al., 2008; Gadlage et al., 2010; Hagemeijer et al., 2011; Sparks et al., 2007).

Nonstructural protein 6, at approximately 23-25kDa, is the smallest of the three transmembrane domain-containing nonstructural proteins and features six membrane spanning domains, yielding a conformation in which both the amino and carboxy termini are on the cytoplasmic-facing side of the membrane (Baliji et al., 2009; Oostra et al., 2008). Unlike nsp3 and nsp4, a homologue of nsp6 has not been shown to be involved in inducing the DMV formation for arteriviruses. However, for MHV, SARS-CoV, and infectious bronchitis virus (IBV), one group has implemented a screen using individual nonstructural proteins to demonstrate that nsp6 from each of these viruses, as well as homologues from arteriviruses, activated autophagy via induction of omegosome (autophagosome precursors) intermediates which then matured into autophagosomes (Cottam et al., 2011; Maier et al., 2013). Also, treatment of human coronavirus 229E (HCoV-229E) infected cells with the antiviral compound K22 resulted in loss of DMV formation and creation of a resistant virus with mutations mapping within nsp6 (Lundin et al., 2014).

We hypothesized that SARS-coronavirus nsp3, nsp4, and nsp6, either alone or in combination, are responsible for DMV induction in host cells, the results of which are discussed in **Chapter 2.**

Host cell protein involvement and fatty acid synthase

In addition to identifying which viral proteins are important for coronavirus-induced membrane rearrangement, we sought to determine which host cell proteins might also be important for this process**.** Although research into coronavirus double membrane vesicles and convoluted membranes has been moving at a rapid pace recently, few

conclusions have developed regarding which membranes comprise the precursor membranes hijacked to form DMVs and CMs and which host cell pathways and proteins are necessary. Table 1.2 provides examples of the inconclusive nature of these results. In these studies we have not observed colocalization of transfected nsp3 with the ER markers calnexin and calregulin, as shown in **Chapter 2.** Despite ultrastructural studies showing apparent continuity with the ER membranes and the observation that nsp3 and nsp4 are glycosylated, the lack of canonical markers suggests that the formation of these vesicles does not occur via a conventional cellular secretory pathway.

For both the coronaviruses and arteriviruses, components of the cellular autophagy machinery have been implicated in DMV formation (Maier and Britton, 2012). The autophagosomes themselves are double membrane vesicles, which initially suggested the possibility of this pathway's involvement. Multiple studies have shown activation of autophagy machinery upon coronavirus infection or in the presence of coronavirus proteins (Cottam et al., 2011; de Haan and Reggiori, 2008; Prentice et al., 2004a). Additionally, microtubule-associated protein light chain 3 (LC3) has been shown to associate with the DMVs of both arteriviruses and coronaviruses, and loss of LC3 had an overall negative effect on DMV formation (Monastyrska et al., 2012; Reggiori et al., 2010b). During autophagy, cytoplasmic LC3-I becomes lipidated and studs the autophagosome, serving as a marker for these vesicles. This is in contrast to the LC3 that has been shown to decorate the DMVs, which is the nonlipidated LC3-I form. This nonlipidated form has also been implicated in the ER-associated degradation (ERAD) pathway. Additionally, chaperone members of the ERAD machinery were shown to be present in the DMVs, suggesting a role for ERAD in DMV formation (Calì et al., 2008;

Reggiori et al., 2010b). The ERAD pathway is responsible for removing unfolded/misfolded glycopolypeptides from the ER for degradation (Bernasconi and Molinari, 2011). Two major players in this pathway are EDEM1 and OS-9. Both of these proteins are maintained at low levels with rapid turnover via LC3-I coated vesicles, termed EDEMosomes, under normal conditions (Bernasconi et al., 2008; Calì et al., 2008). This clearance of these ERAD chaperones is important to maintain balance and to prevent the degradation of newly produced polypeptides.

Table 1.2. *DMV/CM membrane/pathway markers*. Inconclusive results from studies attempting to pinpoint progenitor membranes of double membrane vesicles and convoluted membranes

Membrane (Marker)	Present at DMV/CM?	Ref
Endoplasmic Reticulum (PDI)	Negative	(Ulasli et al., 2010)
ERGIC (ERGIC53)	Negative	(Snijder et al., 2006; Ulasli et al., 2010)
Golgi (GM130, TGN46)	Negative	(Ulasli et al., 2010)
Endosome/Lysosome (LAMP1)	Negative	(Snijder et al., 2006; Ulasli et al., 2010)
Lipidated LC3-II/Intact Autophagy Pathway	Negative	(Snijder et al., 2006; Zhao et al., 2007)
Proximity/Continuity with ER	Positive	(Knoops et al., 2008; Snijder et al., 2006)
ER-associated degradation vesicle (nonlipidated LC3-I)	Positive	(Reggiori et al., 2010b)

Additionally, studies have shown that MHV infection led to an accumulation of both EDEM1 and OS-9 within the DMVs (Reggiori et al., 2010a). However, I was unable to determine any consistent change in OS-9 levels upon either transfection with SARS nsp3 or infection. I was also unable to reproduce the EDEM1 results at all using the same methodologies and reagents described in the aforementioned study. Another more recent study showed that neither truncated nsp3 nor nsp4 colocalized with EDEM1 (Hagemeijer et al., 2014). It may be that the early reports were incorrect or based on a cell type specific result. Based on these results, although the ERAD pathway may be involved in or important for coronavirus DMV and CM synthesis, I chose to continue along a different route of investigation.

A previous study in the Buchmeier lab attempted to determine potential host cell proteins interacting with some of the SARS-CoV nonstructural proteins during infection (Cornillez-Ty et al., 2009). Unpublished mass spectrometry data from this study yielded fatty acid synthase (FASN) as one among many potential interactors with SARS-CoV nsp3. Host cell FASN has been shown to be important for a number of positive sense single-stranded RNA viruses. FASN is 270 kDa dimeric enzyme responsible for catalyzing the formation of fatty acids from malonyl-coA and acetyl-coA precursors (Liu et al., 2010; Wakil, 1989). Mammalian FASN has seven functional domains: beta-ketoacyl synthase (KS), malonyl/acetyltransferase (MAT), dehydrogenase (DH), enoyl reductase (ER), beta-ketoacyl reductase (KR), acyl carrier protein (ACP), and thioesterase (TE) (Figure 1.5A) (Liu et al., 2010; Smith, 1994). These domains facilitate the condensation of acetyl- and malonyl-coA into palmitate (Figure 1.5B). Fatty acids

Figure 1.5. *FASN and inhibitors*. (A) Domain organization of dimeric mammalian FASN and (B) synthesis of palmitate from malonyl-coA and acetyl-coA. KS=beta ketoacyl synthase, MAT=malonyl/acetyltransferase, DH=dehydrogenase, ER=enoyl reducatse, KR=beta ketoacyle reductase, ACP=acyl carrier protein, TE=thioesterase. Initation begins with condensation of malonyl-coA and acetyl-coA via MAT. Subsequent addition of malonyl via KS, KR, ER, and DH elongates. TE domain terminates the chain, releasing palmitate from the FASN enzyme. (C) Chemical structures of cerulenin and C75 FASN inhibitors.

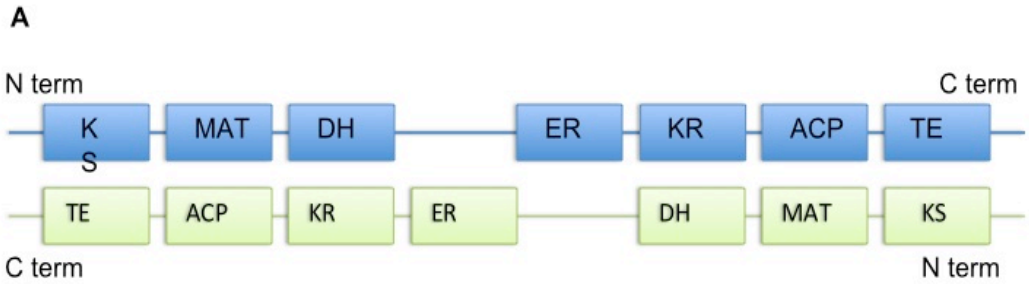
A
N term
C term
K
S
MAT
DH
ER
KR
ACP
TE
TE
ACP
KR
ER
DH
MAT
KS
C term
N term

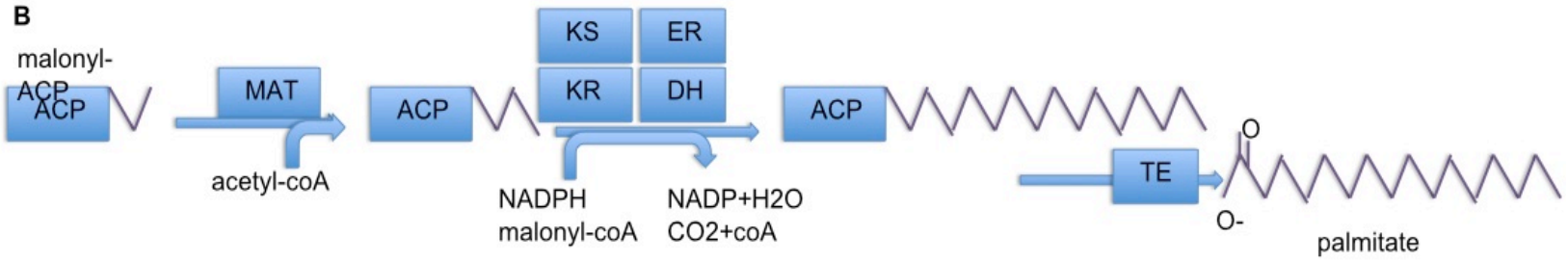
B
malonyl-
ACP
ACP
MAT
acetyl-coA
ACP
KS
ER
KR
DH
NADPH
malonyl-coA
NADP+H2O
CO2+coA
ACP
TE
O
O-
palmitate

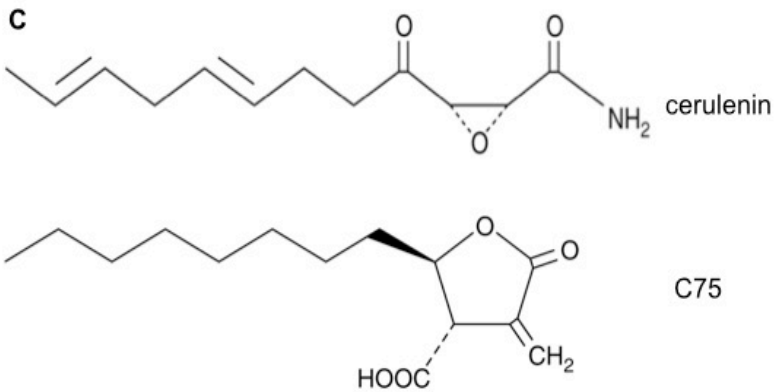
C
O
O
NH2
O
cerulenin
O
O
CH2
HOOC
C75

are the basic building components of cell membranes, serve important metabolic and messenger functions, and are found either free in the cell or as part of triacylglycerol (TAG), phospholipids, and cholesterol (Liu et al., 2010). FASN inhibition has been studied as a method of treatment for obesity and cancer and recently as a means of testing the effect of FASN on viral replication. Commonly used FASN inhibitors include cerulenin and C75, both of which inhibit FASN at the beta-ketoacyl synthase step of fatty acid synthesis (Figure 1.5C) (Kuhajda et al., 2000; Omura, 1976).

FASN was shown to be upregulated in coxsackievirus B3-infected cells and inhibition of FASN activity lowered viral infectivity (Rassmann et al., 2007; Wilsky et al., 2012). Hepatitis C virus (HCV) is probably the most well studied and understood virus that is intimately tied to host cell lipid metabolism. With respect to FASN, HCV infection upregulated FASN levels and/or FASN activity and both inhibition of FASN activity and knockdown of FASN levels via siRNA reduced viral replication (Huang et al., 2013; Nasheri et al., 2013; Yang et al., 2008). Additionally, both nonstructural protein 2 (NS2) and NS5b of HCV have been implicated in FASN interactions and HCV replication (Oem et al., 2008; Yang et al., 2008). West Nile Virus (WNV) infection did not cause a change in overall FASN levels, but WNV does requires the presence of FASN for successful synthesis of viral RNA (Martín-Acebes et al., 2011). Dengue virus NS3 recruits FASN to the sites of viral replication, and FASN activity is upregulated in dengue infected cells, despite no overall change in FASN levels (Heaton et al., 2010). It is important to distinguish between protein activity and protein upregulation, the latter of which can be measured by western blotting to determine protein level and quantitative PCR (qPCR) to determine upregulation of mRNA transcript levels. FASN activity can be

determined using a radioactive acetate incorporation assay (Pizer et al., 1998; Pizer et al., 1996). In dengue infected mosquito cells, the overall composition of the lipid environment was greatly changed compared to uninfected cells as determined by lipid mass spectrometry (Perera et al., 2012).

A quantitative proteomics study comparing SARS-CoV replicon cells to parental baby hamster kidney 21 (BHK-21) cells showed that a number of proteins involved in fatty acid maintenance were upregulated in the SARS-CoV replicon cells (Zhang et al., 2010). This study did not identify significant upregulation of FASN in the SARS-CoV replicon cells. Another study had similar findings in African green monkey Vero cells infected with infectious bronchitis virus (IBV), a coronavirus of poultry (Emmott et al., 2010). These changes in members involved in fatty acid biosynthesis and degradation are suggestive of the massive membrane remodeling occurring within infected cells and the possible importance of FASN for coronaviruses**.** Additionally, a study using tagged E-protein from SARS-CoV co-immunoprecipitated both SARS-CoV nsp3 and fatty acid synthase (Alvarez et al., 2010). Based on these studies, we examined the importance of FASN during coronavirus infection, as discussed in **Chapter 3**.

An understanding of the interplay between the viral proteins responsible for inducing membrane rearrangement and the host cell proteins involved in the membrane rearrangement process is necessary in order to begin describing the precise mechanism of action. In **Chapter 4,** the story thus far will be concluded and some potential future experiments that would be useful for leading the way towards a mechanism will be discussed.

CHAPTER 2

Severe Acute Respiratory Syndrome Coronavirus Nonstructural Proteins 3, 4, and 6 Induce Double-Membrane Vesicles

Abstract

Coronaviruses (CoV), like other positive-stranded RNA viruses, redirect and rearrange host cell membranes for use as part of the viral genome replication and transcription machinery. Specifically, coronaviruses induce the formation of double-membrane vesicles in infected cells. Although these double-membrane vesicles have been well characterized, the mechanism behind their formation remains unclear, including which viral proteins are responsible. This chapter describes the use of transfection of plasmid constructs encoding full-length versions of the three transmembrane-containing nonstructural proteins (nsps) of the severe acute respiratory syndrome (SARS) coronavirus to examine the ability of each to induce double-membrane vesicles in tissue culture. nsp3 has membrane disordering and proliferation ability, both in its full-length form and in a C-terminal-truncated form. nsp3 and nsp4 working together have the ability to pair membranes. nsp6 has membrane proliferation ability as well, inducing perinuclear vesicles localized around the microtubule organizing center. Together, nsp3, nsp4, and nsp6 have the ability to induce double-membrane vesicles that are similar to those observed in SARS coronavirus-infected cells. This activity appears to require the full-length form of nsp3 for action, as double-membrane vesicles were not seen in cells coexpressing the C-terminal truncation nsp3 with nsp4 and nsp6.

Importance

Although the majority of infections caused by coronaviruses in humans are relatively mild, the SARS outbreak of 2002 to 2003 and the emergence of the human coronavirus Middle Eastern respiratory syndrome (MERS-CoV) in 2012 highlight the ability of these viruses to cause severe morbidity and mortality. Insight into the molecular biology of how coronaviruses take over the host cell is critical for a full understanding of any known and possible future outbreaks caused by these viruses. Additionally, since membrane rearrangement is a tactic used by all known positive-sense single-stranded RNA viruses, this work adds to that body of knowledge and may prove beneficial in the development of future therapies not only for human coronavirus infections but for other pathogens as well.

Introduction

Severe acute respiratory syndrome, or SARS, emerged as a life- threatening disease of unknown origin in late 2002 in the Guangdong Province of southern China. The disease presented as an atypical pneumonia and rapidly spread throughout Asia and on to at least 29 countries worldwide, infecting over 8,000 individuals, with an approximately 10% mortality rate. Multiple laboratory groups ultimately identified the causative agent as a novel coronavirus: the SARS coronavirus (SARS-CoV) ((CDC), 2003; Drosten et al., 2003; Ksiazek et al., 2003; Pfefferle et al., 2011; Poutanen et al., 2003). Although there have not been any epidemic outbreaks of the SARS-CoV since the initial incident, the recent emergence of a related deadly human coronavirus, Middle

Eastern respiratory syndrome coronavirus (MERS-CoV), highlights the importance of continued research into this group of human pathogens (Chan et al., 2012; de Groot et al., 2013; Josset et al., 2013; Perlman and Zhao, 2013; van Boheemen et al., 2012; Zaki et al., 2012). Coronaviruses, members of the Nidovirales order, are enveloped, positive-sense, single-stranded RNA viruses (Hagemeijer et al., 2012; Sawicki et al., 2007; Ziebuhr, 2004). Their genome is the largest of all known RNA viruses, ranging from approximately 26 to 32 kb. The SARS coronavirus genome is 29.7kb in size, the first two-thirds of which encompasses the overlapping open reading frames 1a and 1b (ORF1a/b) (Pasternak et al., 2006; Snijder et al., 2003). ORF1a/b is translated into two large polyproteins (pp): pp1a and, via a frameshift event, pp1ab (Perlman and Netland, 2009; Sawicki et al., 2005; Ulferts et al., 2010). These polyproteins are co- and posttranslationally cleaved by viral proteases into the 16 nonstructural proteins (nsps) involved in viral genome replication and transcription (Harcourt et al., 2004; Prentice et al., 2004b).

Similar to other positive-sense, single-stranded RNA viruses, coronavirus genomic replication and transcription are moderated by a large RNA replication complex that is anchored in rearranged internal host membranes (den Boon and Ahlquist, 2010; den Boon et al., 2010; Miller and Krijnse-Locker, 2008; Netherton and Wileman, 2011; Salonen et al., 2005; Stertz et al., 2007; Suhy et al., 2000; van Hemert et al., 2008). These membranes act as a framework for viral genome replication by localizing and concentrating the necessary factors and possibly providing protection from host cell defenses. The hallmark membrane rearrangements observed upon coronavirus infection are double-membrane vesicles (DMVs), named for their distinctive double-lipid bilayer

as seen in electron micrographs. These DMVs are found in conjunction with reticular regions of a convoluted membrane (CM) between them, and contiguity with the endoplasmic reticulum (ER has been observed in electron microscopy (EM) despite a lack of canonical ER membrane markers (Gosert et al., 2002; Hagemeijer et al., 2011; Hagemeijer et al., 2010; Knoops et al., 2008; Snijder et al., 2006; Ulasli et al., 2010). Certain subsets of the coronavirus replication machinery have been shown to move in the cell in a manner that corresponds with microtubule-associated transport, but microtubule disruption does not have an effect on viral genome replication levels (Hagemeijer et al., 2010).

Although much has been done to study coronavirus-induced DMVs, it remains unclear which specific viral proteins are responsible for their induction and which host cellular membranes or processes are engaged (Knoops et al., 2010; Prentice et al., 2004a; Reggiori et al., 2011; Stertz et al., 2007; van den Worm et al., 2011). The nsps, also referred to as the replicase proteins, localize to the DMVs and CMs (Knoops et al., 2008). These vesicles, together with their localized proteins, are referred to as the "replication-transcription complex" (RTC). It has been seen for another group of the Nidovirales, the arteriviruses, that two nonstructural proteins alone were sufficient to induce double-membrane vesicles (Pedersen et al., 1999; Posthuma et al., 2008; Snijder et al., 2001). The two arterivirus nsps responsible for membrane rearrangement are related to SARS-CoV nsp3 and nsp4, which contain transmembrane domains. Additionally, SARS-CoV has a third integral membrane nonstructural protein, nsp6 (Baliji et al., 2009; Oostra et al., 2008). SARS-CoV nsp3 is a 215-kDa, transmembrane, glycosylated, multidomain protein that has been shown to interact with numerous other proteins involved in

replication and transcription and, as such, may serve as a scaffolding protein for these processes (Barretto et al., 2005; Imbert et al., 2008; Kanjanahaluethai et al., 2007; Neuman et al., 2008; von Brunn et al., 2007). nsp4 has been shown to cause aberrant DMV formation upon mutation, leading to a loss of nsp4 glycosylation (Beachboard et al., 2013; Clementz et al., 2008; Gadlage et al., 2010; Oostra et al., 2007; Sparks et al., 2007). nsp6 has been shown to activate autophagy, inducing vesicles containing Atg5 and LC3-II (Cottam et al., 2011). Expression of a construct encoding the last one-third of nsp3 with nsp4 suggested interaction of these two proteins via their ability to relocalize each other in immunofluorescence imaging (Hagemeijer et al., 2011). In these coexpressing cells, nsp6 was also relocalized (Hagemeijer et al., 2012). nsp6 has also been shown to interact with a truncated N-terminal region of nsp3 via yeast two-hybrid assays (Imbert et al., 2008). In this study, using both confocal and electron microscopy, I examined the ability of SARS-CoV nsp3, nsp4, and nsp6 to induce double-membrane vesicles via transfection.

Results

Expression of SARS-CoV nsp3, nsp4, and nsp6.

To determine if any of the three integral membrane nonstructural proteins of the SARS-CoV are capable of inducing double-membrane vesicles, I first validated the expression of our various nsp3, nsp4, and nsp6 constructs via Western blot analysis. Constructs were created (Fig. 2.1A) as described previously (Cornillez-Ty et al., 2009). Lysates from HEK293T cells transfected with our full-length nsp3 construct, termed nsp3 and featuring a C-terminal hemagglutinin (HA) tag followed by a tobacco etch virus

(TEV) cleavage site and a biotinylation signal, yield a pattern similar to that seen with SARS-CoV-infected cell lysates when probed using an anti-nsp3 antibody (Fig. 2.1B). A truncated form of nsp3 (N terminus through the group II-specific marker [GSM] domain), called nsp3N, was also detectable using an anti-nsp3 antibody (Fig. 2.1B). Our nsp3N-terminal construct, nsp3C-terminal construct (spanning the first transmembrane domain through the C terminus), nsp4 construct, and nsp6 construct, all featuring a C-terminal HA tag followed by a 3XFLAG tag, are detectable using an anti-FLAG antibody (Fig. 2.1C). I note here that the nsp3C-terminal construct that I used is distinct from that used by Hagemeijer et al. (Hagemeijer et al., 2010) mentioned in the introduction, which included the GSM domain. Immunofluorescence detection of all constructs was also performed (Fig. 2.2). Phenotypes observed in electron microscopy of transfected samples were categorized and can be found in Table 2.1. A comparison of our observed results versus expected results can be found in Table 2.2. An explanation of the quantitation methods used for both tables can be found in Materials and Methods.

Figure 2.1. *Expression of SARS-CoV nonstructural proteins.* (A) Schematic of nsp3, nsp3N, nsp3C, nsp4, and nsp6 constructs used. UB1, ubiquitin-like domain 1; AC, acidic region; ADRP, ADP-ribose-1''-phosphatase; SUD, SARS unique domain; UB2, ubiquitin-like domain2; $PLP2^{PRO}$, papain-like protease; NAB,nucleic acid binding domain; G2M, group II-specific marker; TM, transmembrane region; ZF, putative metal-binding region; Y, Y region; h, HA epitope tag; b, biotinylation signal sequence; f, FLAG epitope tag. (B) Left panel: detection of nsp3 in SARS-CoV-infected cell lysate and nsp3-transfected cell lysate via anti-nsp3. Right panel: detection of nsp3 and nsp3N in transfected cell lysates via anti-nsp3. (C) Detection of nsp4, nsp6, nsp3N, and nsp3C in transfected cell lysates via anti-FLAG.

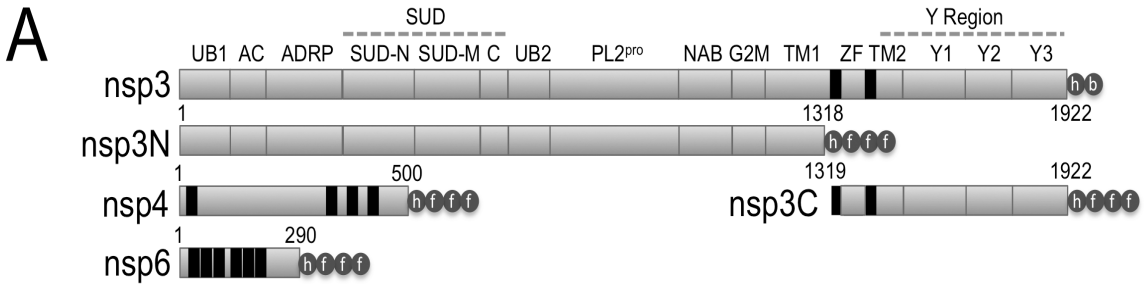
A
SUD
Y Region
UB1 AC ADRP SUD-N SUD-M C UB2 PL2pro NAB G2M TM1 ZF TM2 Y1 Y2 Y3
nsp3
1
1318
1922
nsp3N
1
500
nsp4
1
290
nsp6
1319
1922
nsp3C

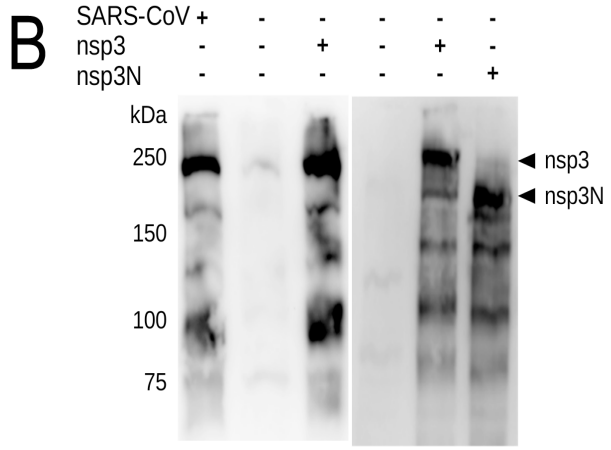
B
SARS-CoV + - - - - -
nsp3 - - + - + -
nsp3N - - - - - +
kDa
250
150
100
75
nsp3
nsp3N

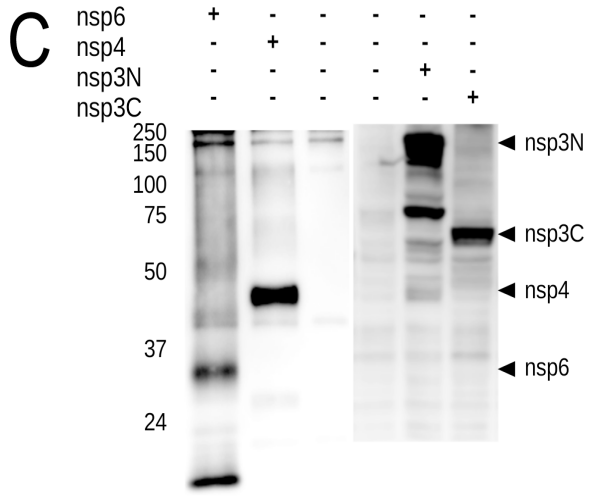
C
nsp6 + - - - - -
nsp4 - + - - - -
nsp3N - - - - + -
nsp3C - - - - - +
250
150
100
75
50
37
24
nsp3N
nsp3C
nsp4
nsp6

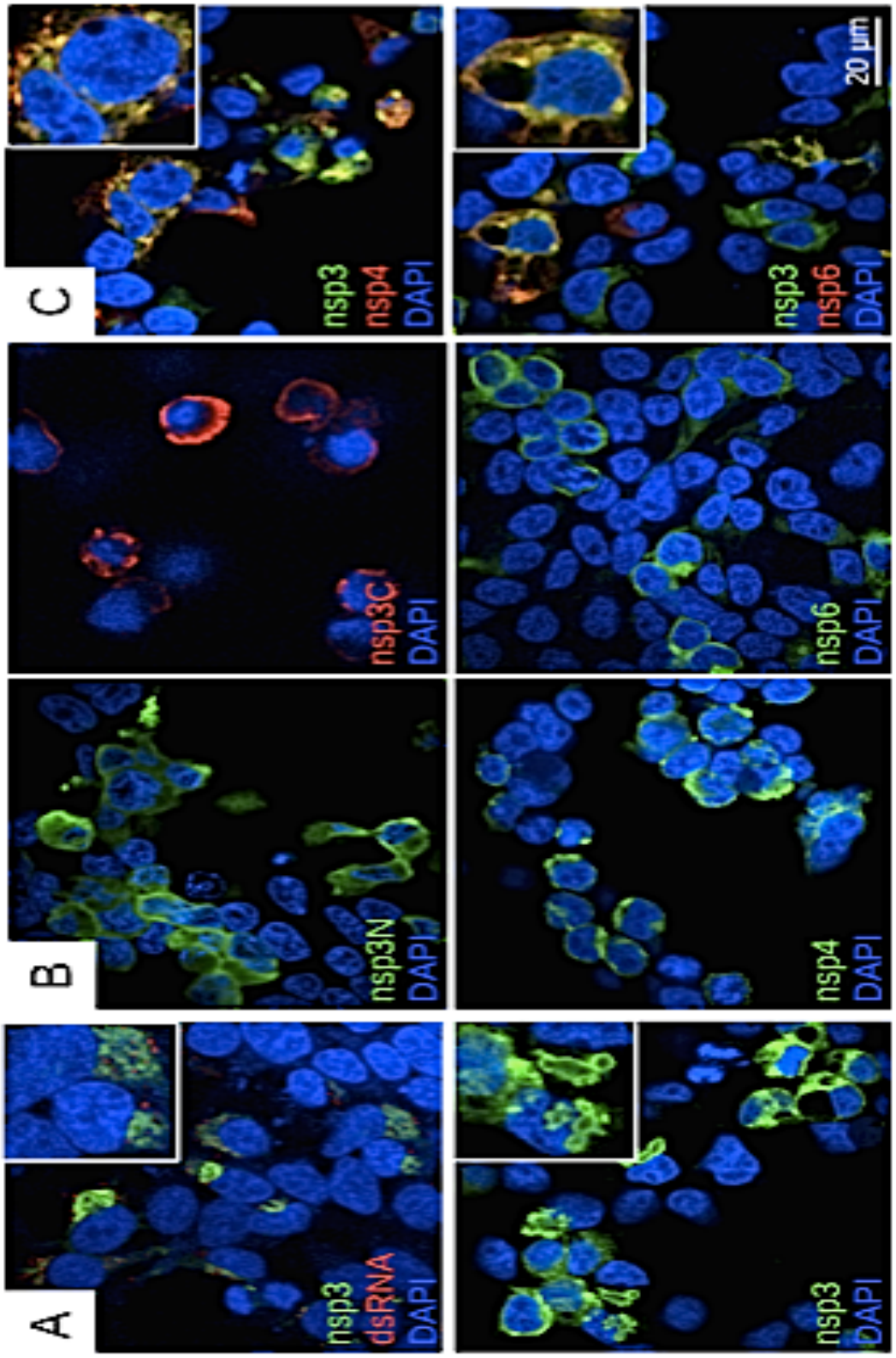
A
nsp3
dsRNA
DAPI
nsp3
DAPI
B
nsp3N
DAPI
nsp3C
DAPI
nsp4
DAPI
nsp6
DAPI
C
nsp3
nsp4
DAPI
nsp3
nsp6
DAPI
20 μm

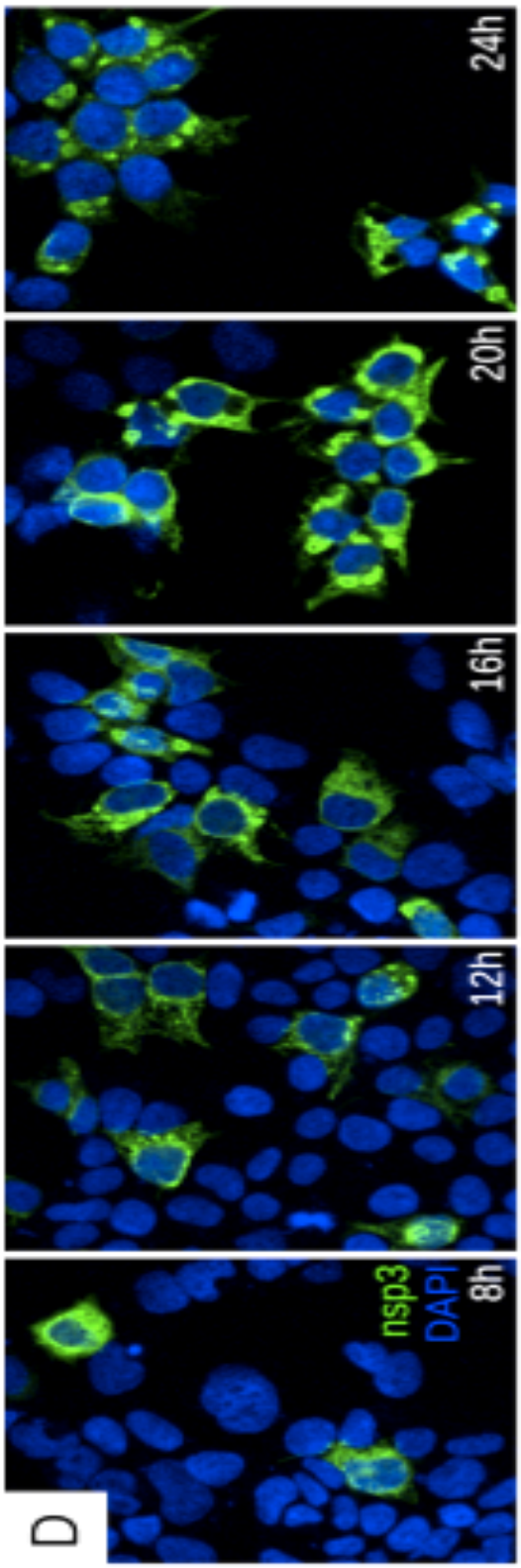
D
nsp3
DAPI
8h
12h
16h
20h
24h

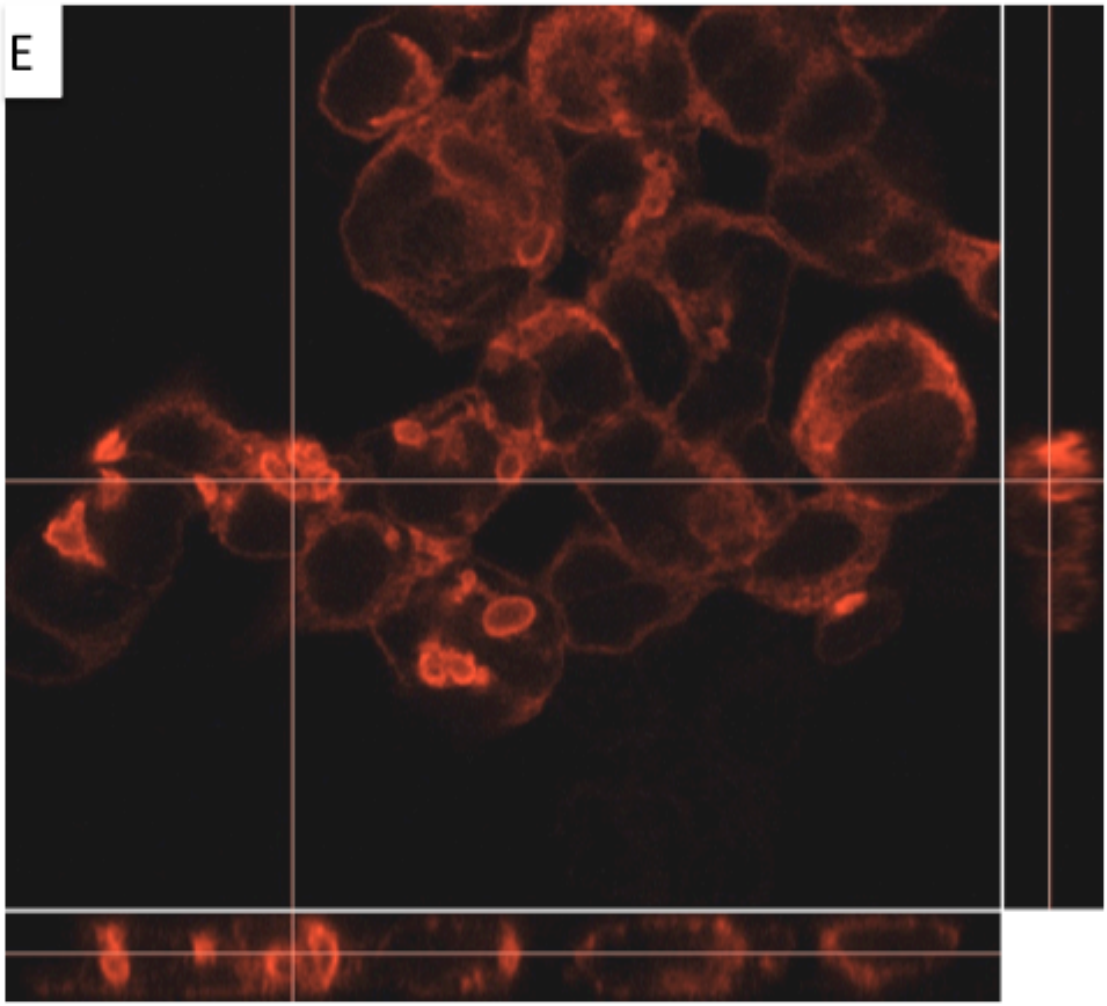

Figure 2.2. *Intracellular localization of accumulation of SARS-CoV nonstructural proteins.* (A) Upper panel: detection of nsp3 (green) and double-stranded RNA (dsRNA) (red) in SARS-CoV-infected HEK293T-ACE2 cells (MOI 0.1, fixed 24 h postinfection [hpi]). Lower panel: detection of nsp3 (green) in nsp3 transfected HEK293Tcells. (B) Detection of nsp3N (green), nsp3C (red), nsp4 (green), and nsp6 (green) in transfected HEK293T cells using anti-FLAG antibody. (C) Upper panel: detection of nsp3 (green) and nsp4 (red) in cotransfected HEK293T cells. Lower panel: detection of nsp3 (green) and nsp6 (red) in cotransfected HEK293T cells. (D) Time course experiment detecting nsp3 (green) in transfected cells (fixed at the indicated time points) over a 24-h period. (E) Close-up view of 3-dimensional Z-stack microscopy showing nsp3 (red) transfection-induced hollow accumulations, featuring side-slice view

Table 2.1. *Raw number of cells counted that contained a given phenotype compared to total number of cells counted.*

			Number (percent) of cell sections showing at least one instance of each phenotype							
Transfected	*Cell sections*	**Normal[a]**	**Disordered Membrane Body (DMB)**	**Multilamellar and Giant Vesiculation (MGV)**	**DMB with MGV**	**MTOC Vesicul-ation (MTOCV)**	**Maze-like Body (MLB)**	**DMB and MTOCV**	**MLB and MTOCV**	**Double-Membrane Vesicle Cluster**
None	*N=269*	269 (100%)	*no*[b]	*no*	*no*	*no*	*no*	*no*	*no*	*no*
nsp3	*N=170*	147 (86%)	7 (4%)	6 (4%)	4 (2%)	5 (3%)	*no*	1 (1%)	*no*	*no*
nsp3C	*N=217*	201 (93%)	4 (2%)	9 (4%)	*no*	3 (1%)	*no*	*no*	*no*	*no*
nsp3N	*N=102*	101 (99%)	*no*	*no*	*no*	1 (1%)	*no*	*no*	*no*	*no*
nsp4	*N=186*	186 (100%)	*no*	*no*	*no*	*no*	*no*	*no*	*no*	*no*
nsp6	*N=218*	181 (83%)	*no*	*no*	*no*	37 (17%)	*no*	*no*	*no*	*no*
nsp3+4	*N=424*	358 (84%)	13 (3%)	6 (1%)	1 (<1%)	1 (<1%)	45 (11%)	*no*	*no*	*no*
nsp3+6	*N=220*	171 (78%)	8 (4%)	*no*	*no*	36 (16%)	*no*	5 (2%)	*no*	*no*
nsp4+6	*N=359*	350 (97%)	*no*	*no*	*no*	9 (3%)	*no*	*no*	*no*	*no*
Nsp3+4+6	*N=613*	512 (84%)	4 (1%)	*no*	*no*	16 (3%)	61 (10%)	*no*	15 (2%)	5 (1%)
nsp3C+4+6	*N=220*	184 (84%)	4 (2%)	21 (10%)	*no*	9 (4%)	*no*	2 (1%)	*no*	*no*

[a]Encompassing the spectrum of phenotypes not listed elsewhere in this table

[b]Phenotype not observed in any of the cell sections examined

Table 2.2 *Observed frequency of nsp-related intracellular features compared to the expected frequency*

Transfected	*Phenotype Observed*[a]	**Expected Transfection Efficiency**[b]	**Approximate Diameter**	**Expected Frequency**[c]	**Observed Frequency**
nsp3	DMB/MGV	70%	4 µm	19%	11%
nsp3C	DMB/MGV	70%	4 µm	19%	6%
nsp6	MTOCV	70%	4 µm	19%	17%
nsp3+4	DMB/MGV	21%	4 µm	6%	5%
	MLB	49%	2 µm	7%	11%
nsp3+6	DMB/MGV	70%	4 µm	19%	4%
	MTOCV	70%	4 µm	19%	18%
nsp4+6	MTOCV	21%	4 µm	6%	3%
nsp3+4+6	DMB/MGV	21%	4 µm	6%	1%
	MTOCV	21%	4 µm	6%	5%
	MLB	15%	2 µm	2%	12%
	DMV Cluster	34%	0.5 µm	1%	1%
nsp3C+4+6	DMB/MGV	70%	4 µm	9%	13%
	MTOCV	54%	4 µm	7%	6%

[a] Combines both nsp3-induced membrane phenotypes under the heading DMB/MGV

[b] Assumes an independent 70% transfection efficiency for each plasmid, combining probabilities for plasmid combinations expected to result in the given phenotype; e.g., in nsp3+6 transfection, the nsp6 phenotype is expected in nsp6 single transfectants (21% of cells) plus nsp3+6 double-transfectants (49% of cells) because nsp3 and nsp6 phenotypes appear to be independent, whereas nsp4+6 transfection would only be expected to result in the nsp6 phenotype in nsp6 single transfectants (21% of cells) because nsp4 appeared to counteract the nsp6 phenotype

[c] Calculated as expected transfection efficiency × (average diameter of feature/15 µm average cell diameter)

Both full-length and truncated forms of nsp3 induce DMB and MGV.

Single transfection of both full-length nsp3 and nsp3C yielded similar phenotypes. Both appeared capable of causing the formation of large areas of disordered membrane (DMB) (Fig. 2.3A and C) as well as causing regions of proliferated membrane featuring multilamellar and giant vesiculation (MGV) (Fig. 2.3B and D). DMB differs from the classical SARS-induced convoluted membranes (CM) in that the DMB appears in larger masses without defined order or structure, often appearing as large tangled regions of membrane (Fig. 2.3A and C [insets]). nsp3- and nsp3C-induced DMB and MGV appeared similar, with the full-length nsp3 showing larger regions of hollow structures of nsp3 in immunofluorescence (Fig. 2.2A [lower panel, inset region] and 2.2E). These structures appear perinuclear, similar to nsp3 localization in SARS-CoV-infected cells (Fig. 2.2A) and do not colocalize with the ER markers calnexin and calregulin or with the actin marker phalloidin (Figure 2.3E-G). In a time course immunofluorescence experiment, the nsp3 hollow structures grew larger as time progressed, with the hollow centers being first visible at 12 h posttransfection (Fig. 2.2D). The nsp3N construct appeared to be dispersed throughout the cytoplasm in immunofluorescence (Fig. 2.2B) and showed no distinct phenotype in electron microscopy.

Figure 2.3. *Disordered membrane body (DMB) and multilamellar and giant vesiculation (MGV) in SARS-CoV nsp3- and nsp3C-transfected cells.* (A) DMB in nsp3-transfected cell. Zoomed region shows membrane detail. (B) MGV in nsp3-transfected cell. (C) DMB in nsp3C-transfected cell. Zoomed region shows membrane detail. (D) MGV in nsp3C-transfected cell. Nsp3- did not colocalize with the ER markers calnexin(E), calregulin(F), or the actin marker phalloidin(G). Scalebars = 50uM Green in (E) and (F)=nsp3, red=ER marker. Green in (G) = Phalloidin-FITC, red=nsp3

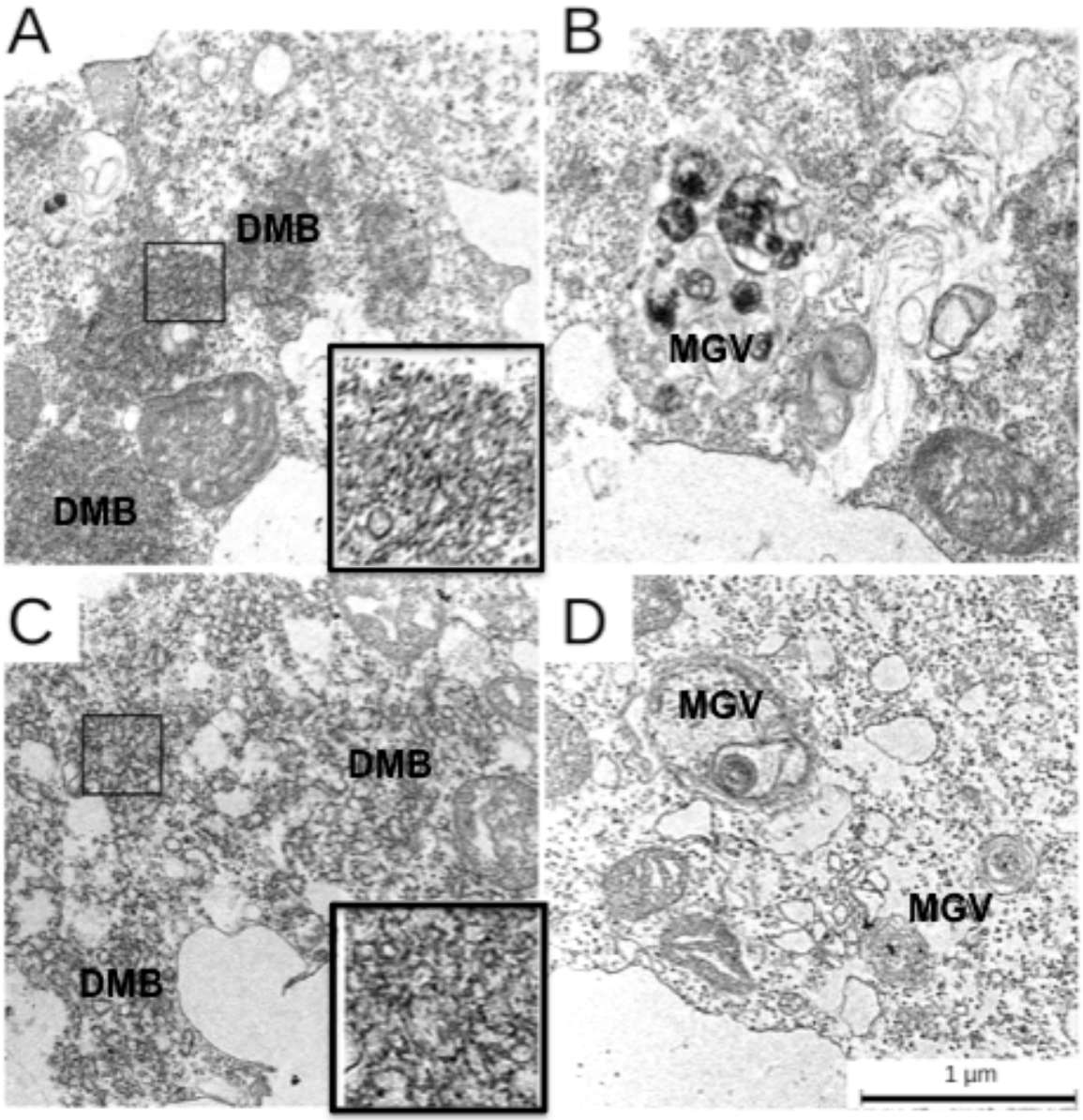
A
DMB
DMB
B
MGV
C
DMB
DMB
D
MGV
MGV
1 µm

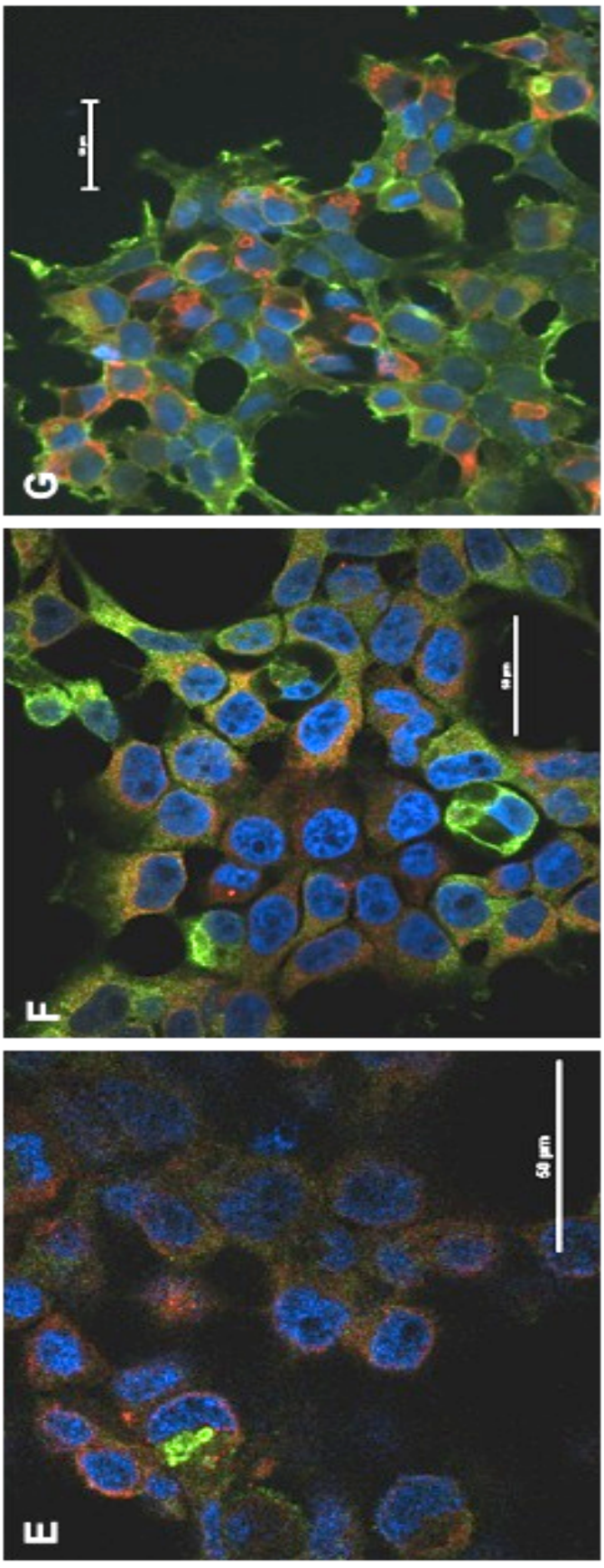
E
50 µm
F
G

Nsp4 with nsp3 produces MLBs featuring double-membrane walls.

Transfection of nsp4 alone induced a punctate pattern as observed via immunofluorescence microscopy, consistent with the localization of nsp4 to the ER (Fig.2.2B), as others have demonstrated (Hagemeijer et al., 2011; Oostra et al., 2007). In electron microscopy, cells transfected with nsp4 alone showed no distinct phenotype (Table 2.1). Cotransfection of nsp3 and nsp4 produced a pattern that was distinct from that seen for either nsp3 alone or nsp4 alone in immunofluorescence (Fig. 2.2C). In electron microscopy, it was observed that the membranes in this cotransfection form an extensive (typically ~2-um diameter) winding maze-like body (MLB), featuring paired membranes interspersed with double-membrane circular structures with an average diameter of ~80 nm (Fig. 2.4). The apposing walls of the MLB were typically separated from each other by approximately 20 nm. The MLB appear perinuclear, and interconnections with the ER were present (Fig. 2.4, black arrowheads).

Nsp6 induces single-membrane vesicles around microtubule organizing centers.

Transfection of nsp6, either alone or along with nsp3, yielded the presence of a large amount of smooth-walled single-membrane spherical vesicles approximately 280 +/- 60 nm in diameter (Fig. 2.5C). While this microtubule organizing center vesiculation (MTOCV) phenotype was not exclusive to nsp6 transfections, it was far more prevalent in nsp6-transfected cells (Table 2.1). This was consistent with what we observed in immunofluorescence with single nsp6 transfections, where the nsp6 signals clustered perinuclearly in one area of the cell and were frequently found clustered around gamma-tubulin centrosome staining (Figure 2.5E). Interestingly, when nsp6 was coexpressed

with nsp4, the MTOCV phenotype was lost (Fig. 2.5D) and regions surrounding the MTOC instead looked like the equivalent areas in untransfected or nsp4 singly transfected cells (Fig. 2.5A and B) (Table 2.1).

Nsp3, nsp4, and nsp6 together induce a pattern of double-membrane vesicles similar to that seen in SARS-CoV-infected cells.

A triple transfection of nsp3 and nsp4 and nsp6 yielded double membrane vesicles (Fig. 2.6 C to E) with connections to convoluted membranes of morphology similar to that of those induced in SARS coronavirus-infected cells (Fig. 2.6A and B). Whereas SARS-CoV-induced DMVs tend to remain approximately 210 +/- 30 nm in diameter, the DMVs induced by nsp3, nsp4, and nsp6 triple transfection exhibited a smaller average diameter of 120 +/- 40 nm. Both infection-induced and transfection-induced DMVs showed an approximate 20-nm separation between apposing membranes. As is the case for SARS-induced DMVs, the triple transfection induced interconnected DMVs that appeared perinuclear, showed contiguity with the ER, and exhibited dark membrane staining. In addition to the DMVs induced by the triple transfection, regions of MLB and MTOCV appearing in the same cell were found three times as frequently as DMVs were found. Interestingly, a triple transfection of nsp3C with nsp4 and nsp6 yielded regions of DMB, MGV, and MTOCV but never maze-like bodies, double-membrane vesicles, or any additional novel structures (Table 2.1)

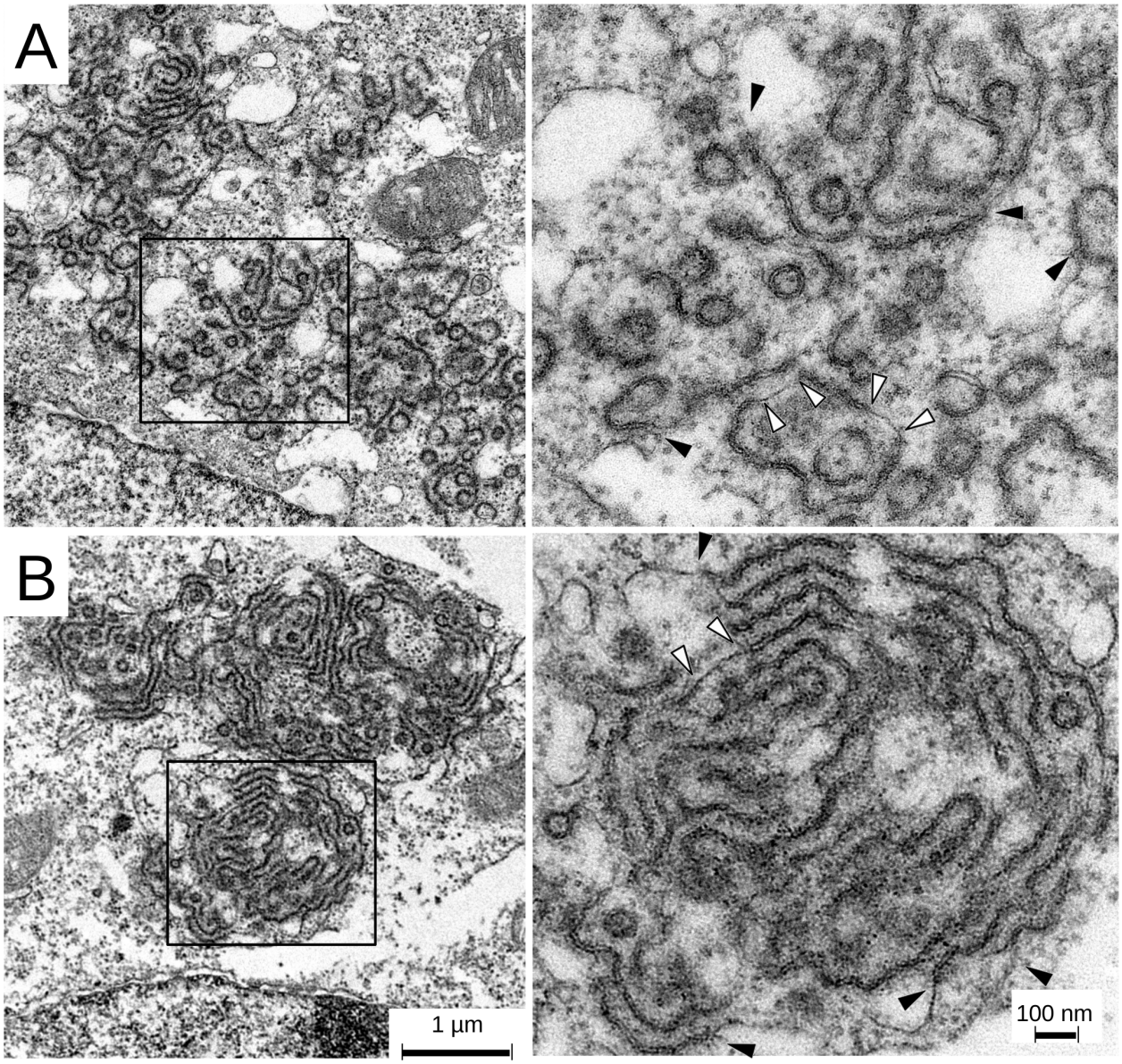

Figure 2.4. *Maze-like body (MLB) formation in SARS-CoV nsp3-nsp4-cotransfected cells.* (A and B) Perinuclear localization and double-wall highlights (zoomed region). Interconnections to the endoplasmic reticulum (black arrowheads) and smooth-sided single membranes interrupting maze-like bodies (white arrow-heads) are indicated

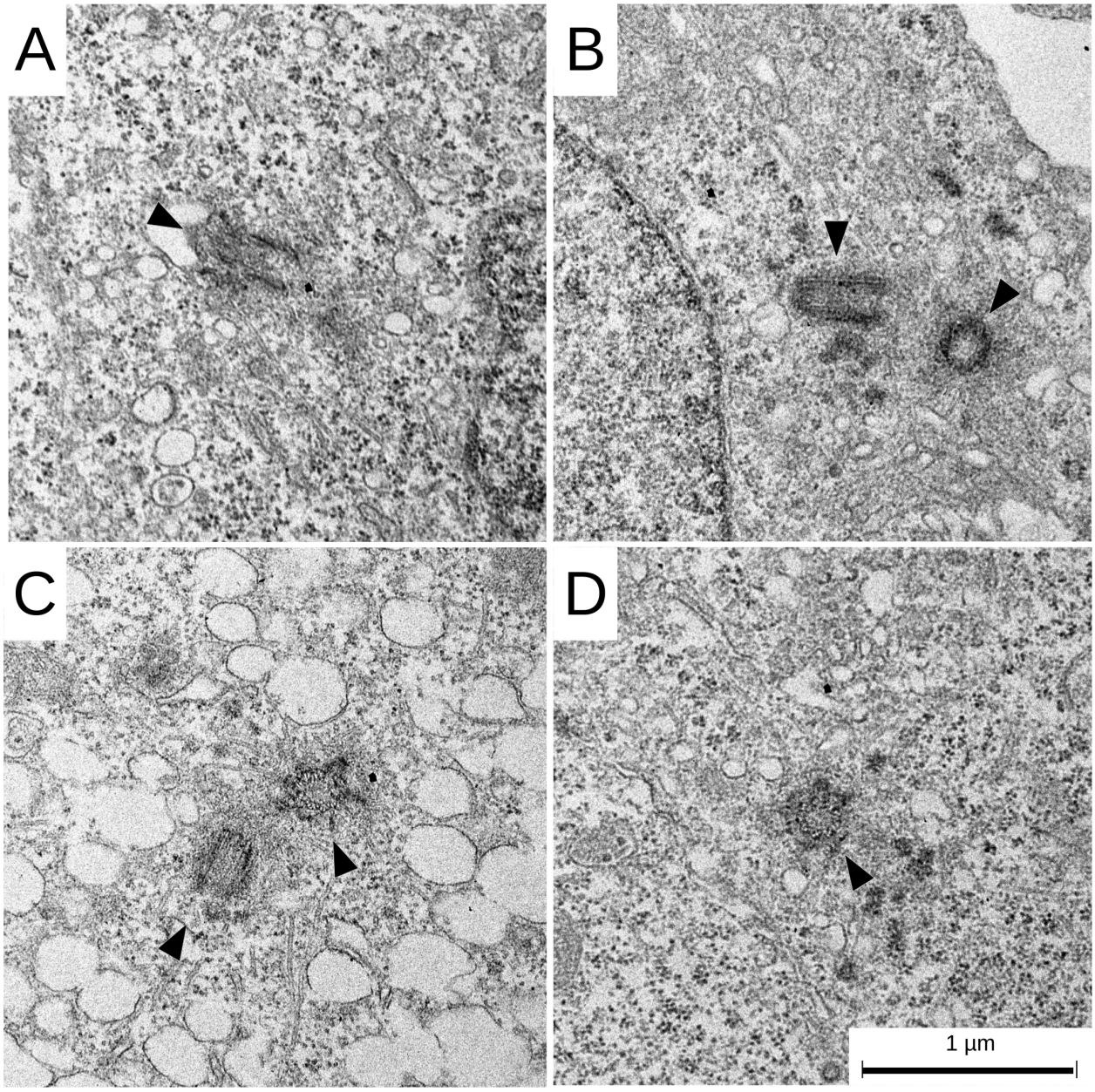
A
B
C
D
1 µm

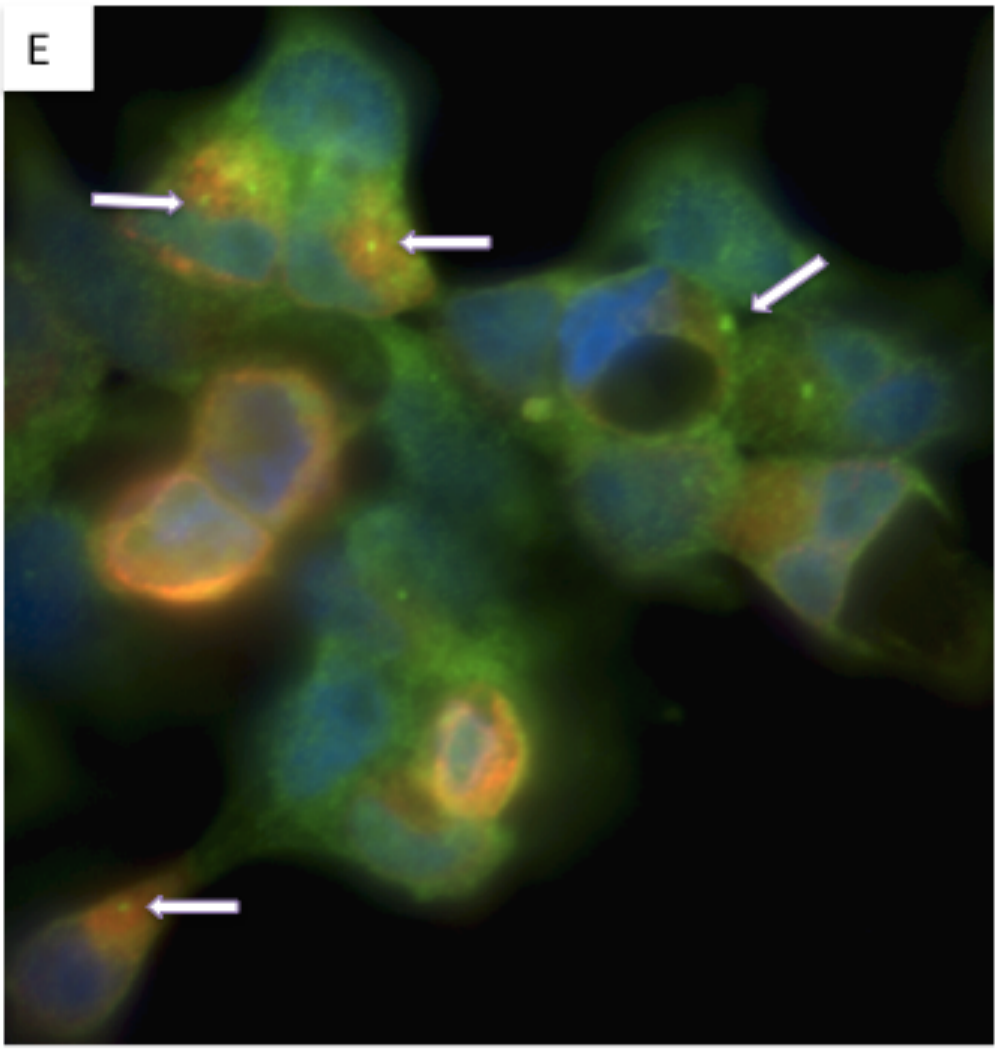

Figure 2.5. *Microtubule organizing center vesiculation (MTOCV) in SARS-CoV nsp6-transfected cells.* (A) Untransfected control. (B) SARS-CoV nsp4-transfected cell. (C) SARS-CoV nsp6-transfected cell featuring MTOCV. (D) SARS-CoV nsp4-nsp6-cotransfected cell. Centrioles (black arrowheads) are indicated. (E) Immunofluorescence of nsp6-transfected cells probed with anti-FLAG (red) and anti-gamma tubulin (green). Dark green puncta (white arrows) indicate centrosomes.

Discussion

Although it is understood that viral replicase interaction with host membranes is a requirement for successful coronavirus infection, it has not yet been determined which viral proteins are involved in double-membrane vesicle formation and the nature of the cellular organelles that are compromised. In this study, we used immunofluorescence and electron microscopy to examine the ability of the three membrane-spanning nonstructural proteins of the SARS-coronavirus to induce double membrane vesicles via transfection.

We found that exogenous nsp3 alone, both full length and the C-terminal transmembrane-containing region, was capable of inducing DMB as well as regions of MGV, suggesting a role for the C-terminus of nsp3 in membrane production or expansion of existing membranes. Transfected nsp3 did not colocalize with ER markers, suggesting that the membrane proliferation phenotype may be similar in its cellular membrane precursor to the infection-produced DMV precursor membranes, which also lack these canonical ER markers. In immunofluorescence time course experiments, nsp3 induced hollow accumulations that grew larger in size as time progressed posttransfection, eventually producing patterns much larger than the nsp3 signal observed in SARS-infected cells. These enlarged accumulations further support the idea of a role for nsp3 in membrane proliferation. It is interesting to note that the addition of either nsp4 or nsp6 with nsp3 reduces the appearance of the MGV phenotype but not the DMB phenotype, suggesting a regulatory role of these two nsps on nsp3's membrane proliferation ability.

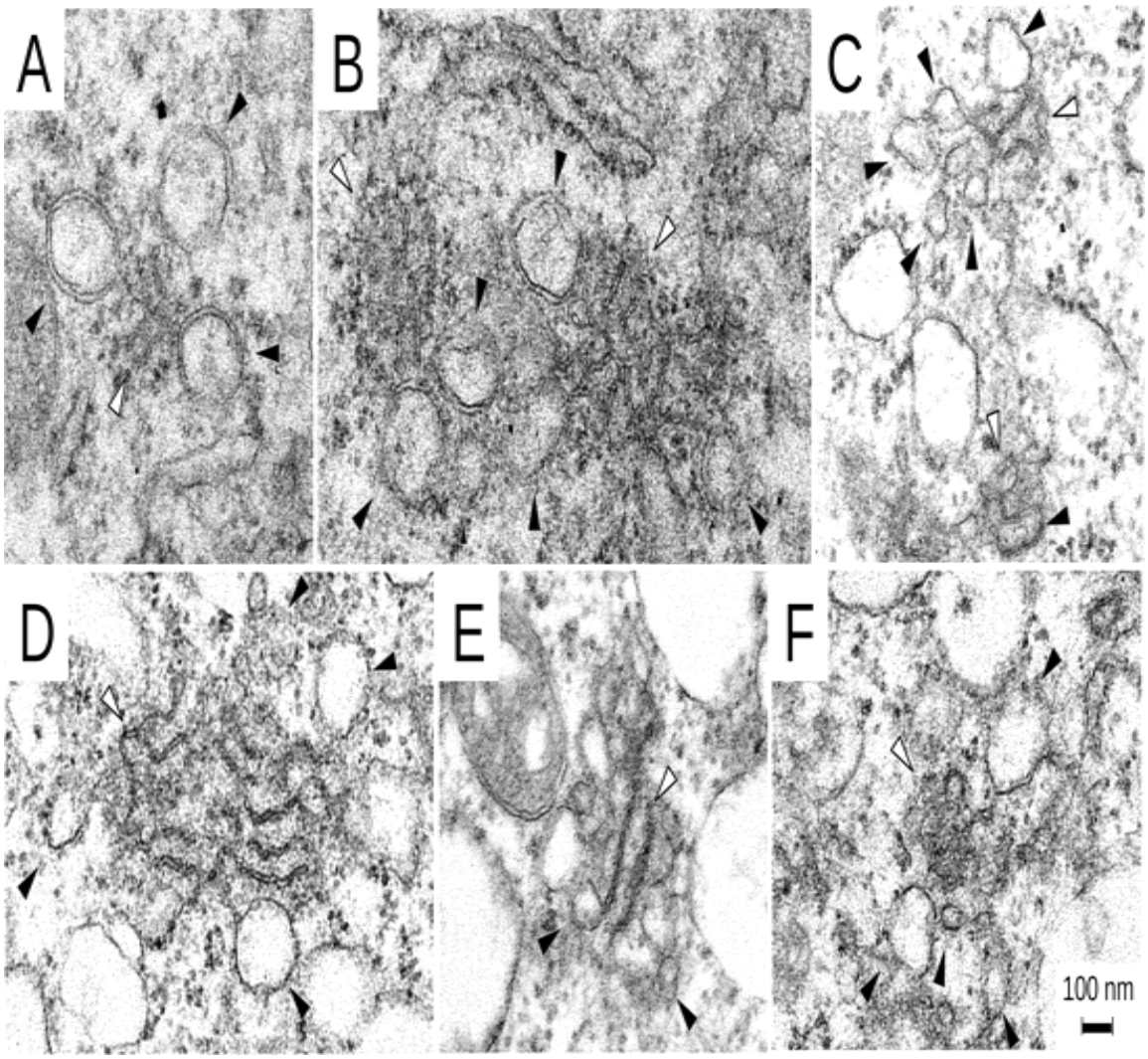
A
B
C
D
E
F
100 nm

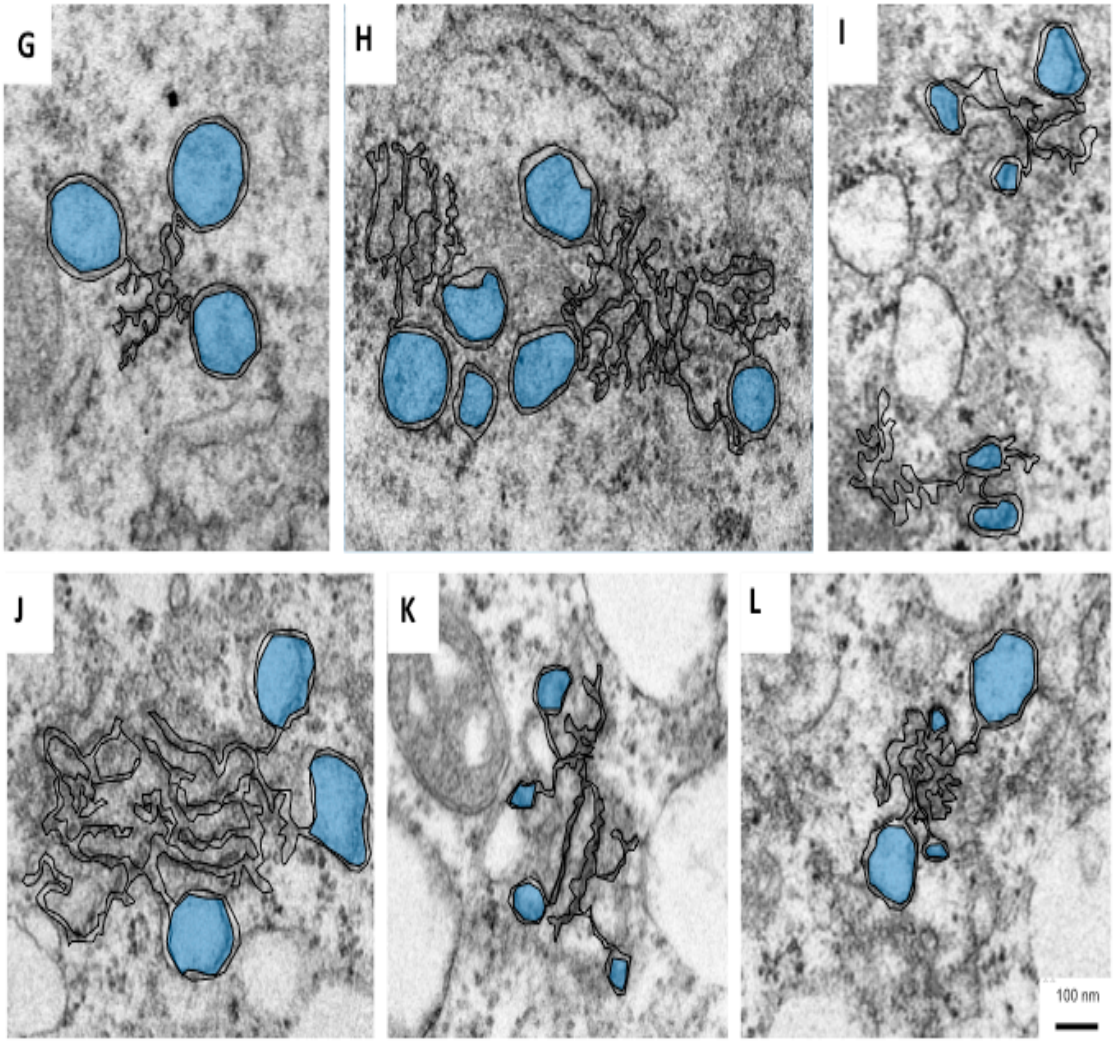

Figure 2.6. *SARS-CoV-induced DMVs versus triple-transfection SARS-CoV nsp3-nsp4-nsp6-induced DMVs.* (A and B) SARS-CoV-infected cells. MOI 1, fixed 7 h postinfection. (C to F) nsp3-nsp4-nsp6-transfected cells. Clusters consisting of convoluted membrane tubules (white arrowheads) ending in double- membrane vesicles (black arrowheads) are indicated. (G to L) Illustrative overlays showing the DMV and CM structures

Cotransfection of nsp3 with nsp4 showed a dramatic effect on membrane conformation, creating a perinuclear double-membrane walled maze-like body. The MLBs in our electron micrographs consist of roughly parallel rows spaced apart by approximately 80 nm and interspersed with double-membrane walled circular structures of about 80-nm diameter, suggesting that the rows and circles are longitudinal and cross sections of closely packed double-membrane walled tubules. Electron tomography studies would prove beneficial in this determination. The MLB produced by SARS nsp3 and nsp4 is distinct from what has been shown for arteriviruses, where the arterivirus homologues of coronavirus nsp3 and nsp4 are sufficient to induce complete DMVs that look like those of arterivirus-infected cells (Snijder et al., 2001). These results suggest that a biologically meaningful interaction occurs between nsp3 and nsp4, corroborating previously published data showing interactions between nsp3 and nsp4 via mammalian two-hybrid assays (Pan et al.) and Venus reporter fluorescence assays (Hagemeijer et al.) (Hagemeijer et al., 2011; Pan et al., 2008). There is immunofluorescence evidence that a truncated protein running from the GSM to nearly the C terminus of mouse hepatitis virus (MHV) nsp3 is able to change the localization of fluorescently tagged nsp4 to form perinuclear protein clusters (Hagemeijer et al., 2011), which were not investigated further but which may be similar to the nsp3-nsp4 maze-like bodies described here. If that is the case, then the determinants of nsp3-nsp4 interaction that lead to membrane pairing would be expected to lie in the relatively poorly conserved region between the start of the GSM domain and the amino-terminal transmembrane helix of nsp3. Further research is needed to investigate the determinants of nsp3-nsp4 interaction that results in membrane pairing.

Nsp6 alone induces small spherical vesicles featuring single membranes, which cluster around the microtubule organizing center. This MTOCV phenotype is mostly lost upon addition of nsp4. This apparent counteractive effect of nsp4 on the nsp6 MTOCV phenotype cannot simply be attributed to a reduced presence of nsp6 under double-transfection conditions because no reduction in MTOCV was observed in nsp3-nsp6 cotransfection. It would appear that nsp4 has a suppressive or negative effect on this phenotype or that nsp4 is relocalizing nsp6 to an area of the cell away from the MTOC. Previous studies of coronavirus RTCs have shown that certain members of the complex may traffic in the cell in a microtubule-dependent manner; however, microtubule integrity is not required for productive infection (Hagemeijer et al., 2010). Additionally, nsp6 expression may be disrupting Golgi vesicular transport mechanisms. Knockdown of RAB and ARF GTPases involved in Golgi trafficking has been shown to cause vesicle accumulation around centrioles in Drosophila (Giansanti et al., 2007; Schmidt et al., 2012). It has been shown that MHV replication is dependent on activation of ARF1, although it remains unclear whether this is related to the intracellular phenotype induced by nsp6 (Verheije et al., 2008).

Triple transfection of nsp3, nsp4, and nsp6 produced formations that looked very similar to the DMVs seen in coronavirus-infected cells, with double-membrane vesicles surrounding a central convoluted membrane structure (Knoops et al., 2008; Stertz et al., 2007; Ulasli et al., 2010). nsp6 appears to either break up or prevent the formation of the elongated stretches of double-membrane walls seen in the nsp3-nsp4 cotransfection mazes, leaving double-membrane vesicles and regions of convoluted membrane that are consistent with SARS-CoV-infected DMVs. Triply transfected cells containing both

MLB and MTOCV were about three times as frequent as cells containing DMVs (Table 2.1). Additionally, all cells from the triple transfection containing DMVs also contained evidence of MLBs and MTOCVs. This suggests that DMV formation from expressed nsp3, nsp4, and nsp6 is not particularly efficient. The presence of the MLBs and MTOCVs in DMV-containing cells further suggests that nsp3 and nsp4 interact more readily in this expression system than nsp4 and nsp6, which would result in loss of the MTOCV phenotype. Complementation studies using temperature-sensitive mutants of MHV have suggested that nsp4 through nsp10 may have functions in polyprotein forms prior to cleavage or that they are assembled into the RTC and then cleaved (Sawicki et al., 2005). The polyprotein may have a role in keeping nsp4 and nsp6 in close proximity, allowing more efficient DMV formation than in our expression system. Note that even though our nsp3C produced phenotypes very similar to those seen with the full-length nsp3 in single transfections, a triple transfection of nsp3C with nsp4 and nsp6 was unable to produce double-membrane vesicles. One explanation for the differences observed when using full-length nsp3 versus nsp3C is that the transmembrane domains, or domains C terminal to the transmembrane domains, may be responsible for membrane proliferation and convolution but some domain N terminal to the first transmembrane region of nsp3 is required for membrane pairing and regulation for the formation of DMVs. Since nsp6 was previously shown to interact with an N-terminal truncation of nsp3 via yeast two-hybrid screen, it is possible that this interaction is the critical missing link for DMV formation in the nsp3C-nsp4-nsp6 transfection (Imbert et al., 2008).

A possible explanation for DMV formation is that nsp3 is responsible for membrane proliferation that results in enough membrane to form the network of DMVs

that is required for RTC formation. The 20-nm distance typically found between the apposing membranes in SARS-CoV-induced DMVs and CMs was the same for nsp3-nsp4-nsp6 transfection-induced DMVs and CMs. This 20-nm distance was also found in nsp3-nsp4 MLBs, suggesting that nsp3 and nsp4 together are responsible for the DMV-like membrane pairing of the triple transfection. nsp3-nsp4 MLBs may represent a more organized version of SARS-CoV-induced convoluted membrane. The role of nsp6 may be to force the double-membrane structures mainly toward the formation of spherical vesicles as opposed to the MLBs seen in the absence of nsp6. These nsp6-induced structures appear to be consistent with what has been shown previously regarding the role of nsp6 in inducing autophagosomes (Cottam et al., 2011). Since cleavage of nsp3 and nsp4 occurs very rapidly upon polyprotein production and nsp6 cleavage may be comparatively delayed, one possibility for DMV formation could be that the MLBs and MTOCVs form in the cell somewhat independently and then rapidly meet to produce the DMVs (Harcourt et al., 2004; Kanjanahaluethai and Baker, 2000). However, the presence of all three at once may directly lead to production of DMVs without any of the intermediate structures. While the DMVs that are produced by nsp3- nsp4-nsp6 transfection are similar in structure and organization to authentic SARS-induced DMVs, they are smaller. This suggests a role for other proteins or the presence of viral RNA in determining DMV size.

The precise mechanism by which each of these nsps works to produce double-membrane vesicles is a topic for future study and is likely influenced by a variety of factors, including each nsp's production from the initial polyprotein precursor, how these

nsps recruit and exploit host cell proteins, and the interaction of each nsp with other viral proteins and host cell proteins.

Materials and Methods

Cells and virus. HEK293T human embryonic kidney epithelial cells (ATCC CRL-11268) were used for transfection experiments. HEK293T- ACE2 cells, which stably express the ACE2 receptor, were used for infection experiments. Cells were maintained in Dulbecco's modified Eagle's medium (HyClone) supplemented with 10% fetal bovine serum (FBS) and 1% penicillin-streptomycin. The Tor2 strain of SARS coronavirus was used for all infection experiments. Infections were performed at in- dicated multiplicities of infection (MOIs) for the indicated time lengths. All SARS-CoV work was performed under conditions of biosafety level 3 (BSL3) containment at the University of California, Irvine.

Antibodies. The primary antibodies used were anti-nsp3 (Rockland), anti-FLAG (Sigma), anti-calnexin (Santa Cruz), anti-calregulin (Santa Cruz), anti-gamma tubulin (Sigma). Alexafluor-488- and Alexafluor-594-conjugated secondary antibodies (Invitrogen) were used for immunofluorescence. Horseradish peroxidase (HRP)- conjugated secondary antibodies (Jackson Laboratories) were used for Western blotting.

Plasmids and transfection. All plasmids used were created as previously described using a Gateway expression system (Invitrogen) (Cornillez-Ty et al., 2009). Briefly, all constructs had a modified pCAGGs backbone containing a Woodchuck hepatitis virus posttranscriptional regulatory element (WPRE) and were C-terminally tagged with either

an HA tag sequence followed by a tobacco etch virus (TEV) cleavage site and a biotinylation signal sequence (HA-Bio) or an HA tag sequence followed by a 3*X*FLAG tag sequence (HA-3*X*FLAG). Transfections were conducted using Lipofectamine 2000 (Invitrogen) per the manufacturer's protocol.

Immunofluorescence assays. HEK293T cells were grown on poly-L- lysine-coated coverslips, transfected, and fixed 24h post-transfection using 3.7% paraformaldehyde, permeabilized with 0.1% Triton X-100, and mounted with DAPI (4',6-diamidino-2-phenylindole) Fluoromount D (Southern Biotech). Confocal microscopy was performed with a Nikon Eclipse Ti confocal microscope. Images were processed using NIS Elements software.

Western blotting assays. HEK293T cells were grown in 6-well plates and lysed 24 h posttransfection using either radioimmunoprecipitation assay (RIPA) or 1% NP-40 lysis buffer with 1*X* protease inhibitor cocktail (Research Products International Corp). Lysates were subjected to SDS-PAGE and transferred to a polyvinylidene difluoride (PVDF) membrane for immunoblotting.

Electron microscopy and phenotype quantification. Cells were grown in T-75 flasks, transfected, fixed 24 h posttransfection, and harvested with 2% EM-grade glutaraldehyde in 0.1 M sodium cacodylate buffer for at least 4h, postfixed in 1% osmium tetroxide–0.1M cacodylate buffer for 1 h, and stained in 2% uranyl acetate en bloc for 1 h. Samples were dehydrated in ethanol, embedded in epoxy resin, sectioned at intervals of 50 to 60 nm on a Leica UCT ultramicrotome, and picked up on Formvar and carbon-coated copper grids. Sections were stained with 2% uranyl acetate for 5 min and with Sato's lead stain for 1 min. Grids were viewed using either a Tecnai G2 Spirit BioTWIN transmission

electron microscope equipped with an Eagle 4k high-sensitivity (HS) digital camera (FEI, Hillsboro, OR) or a Phillips CM-20 camera equipped with a 2k charge-coupled device (CCD).

Percentages found in Table 2.1 are based on the raw number of cells counted that contained a given phenotype compared to total number of cells counted. Table 2.2 compares the observed frequency of nsp-related intracellular features to the expected frequency based on the size of the feature relative to the size of the cell and the number of plasmids required to produce the feature. The estimate assumes an independent 70% transfection rate for each plasmid and an average cell diameter of 15um. Expected frequencies were calculated as transfection efficiency times the ratio of feature size to cell size. Expected frequencies were summed for combinations that would produce the same feature.

CHAPTER 3

Fatty Acid Synthase is Important for Murine Hepatitis Virus Coronavirus Replication

Abstract

Coronaviruses, like most other positive sense single-stranded RNA (+RNA) viruses, induce rearrangements of host cell internal membranes to aid in viral replication. Host cellular fatty acid synthase (FASN), a multidomain enzyme responsible for fatty acid synthesis, has been shown to be important for the replication of a number of +RNA viruses. Here, we examine the importance of FASN to replication of the prototypical coronavirus, mouse hepatitis virus. Using both inhibition and knockdown of FASN we observed an overall decrease in viral titer, suggesting that FASN plays an important role in coronavirus replication. A time course addition of the FASN inhibitor, C75, showed that the loss of FASN activity had the greatest effect early during infection. Electron micrographs showed a massive decrease in the amount of double membrane vesicles and convoluted membranes, the membranous scaffold of the coronavirus replication-transcription complex, in infected cells treated with the inhibitor compared to vehicle. An increase of lipid droplets was also observed in infected cells treated with the inhibitor compared to vehicle. This work highlights the importance of FASN for coronavirus replication, while also hinting at the differences in mechanism by which these +RNA viruses may induce similar structures.

Introduction

Coronaviruses are positive sense single-stranded RNA viruses that can cause a range of moderate to severe disease in a variety of organisms, including infections of agriculturally important domestic livestock as well as human infection (Graham and Baric, 2010; Perlman and Netland, 2009; Sawicki et al., 2007; Weiss and Leibowitz, 2011). Until the 2003 emergence of the severe acute respiratory syndrome coronavirus (SARS-CoV), coronaviruses were not thought to cause widespread severe infection in humans (Drosten et al., 2003) (Goldsmith et al., 2004; Poutanen et al., 2003)). The recent appearance in 2012 of another severely pathogenic coronavirus, the middle eastern respiratory syndrome coronavirus (MERS-CoV), highlights the importance of studying this group of viruses (de Groot et al., 2013; Graham et al., 2013; Josset et al., 2013; Zaki et al., 2012).

Like all studied positive sense RNA viruses, coronaviruses induce membrane rearrangements in the infected host cell (Angelini et al., 2014; den Boon and Ahlquist, 2010; Hagemeijer et al., 2012; Netherton and Wileman, 2011; Paul and Bartenschlager, 2013). Coronaviruses specifically induce double-membrane vesicles (DMVs), so named for their distinctive double membraned walls, and convoluted membranes (CMs), at which viral genome replication and transcription occur (Hagemeijer et al., 2010; Knoops et al., 2008). Coronavirus DMVs and CMs are induced by three of the viral nonstructural proteins and feature continuity with the endoplasmic reticulum (ER) as imaged via electron microscopy, despite inconclusive staining for canonical ER markers (Angelini et al., 2013; Gosert et al., 2002; Hagemeijer et al., 2011; Snijder et al., 2006). Although

much work has been done to study these structures, the mechanism behind their formation remains elusive.

As might be expected for structures defined by their lipid membranes, members of the lipid biosynthesis pathway have come under scrutiny for their possible involvement in viral-induced membrane rearrangement. Specifically, fatty acid synthase (FASN) has been implicated as being important for replication of West Nile virus, dengue virus, hepatitis C virus, coxsackievirus, and rotavirus (Gaunt et al., 2013; Heaton et al., 2010; Martín-Acebes et al., 2011; Perera et al., 2012; Rassmann et al., 2007; Wilsky et al., 2012; Yang et al., 2008). FASN is a multi-domain enzyme responsible for palmitate synthesis from acetyl-coA and malonyl-coA precursors (Chirala and Wakil, 2004).

To determine is FASN is important for coronavirus replication, we performed a series of knockdown and inhibitor experiments. We used mouse hepatitis virus strain A59 (MHV-A59), the prototypic coronavirus, in combination with siRNAs directed against FASN or C75, a FASN inhibitor. We observed that either a reduction in the level of FASN or an inhibition of FASN both resulted in an overall reduced viral titers. Additionally, the effect appears to occur early in infection, during the timeframe that the viral replication-transcription complexes (RTCs) are forming.

Results

MHV infection does not change overall FASN levels

To determine if MHV infection had a change on global FASN protein levels, we infected DBT cells at an MOI of 1 for 8 hours and assayed FASN levels via western blot and immunofluorescence. We observed no discernable increase or decrease in protein expression level via western blotting and no overall change via immunofluorescence, indicating that the virus does not appear to affect overall FASN protein expression

Inhibition of FASN yields decreased viral titer with the most effect early in infection

To assess the importance of FASN on coronavirus infection, we performed inhibition studies using the FASN inhibitor C75. We first performed MTT cell viability assays and found the concentrations out to 50uM were not detrimental to DBT cell viability (Figure 3.2A). We then performed a dose-response curve using the inhibitor from 0-50uM and saw that viral titer decreased as levels of C75 increased. (Figure 3.2B) Results were similar when performed with cerulenin (Figure 3.3 A&B). However due to cerulenin's increased cellular toxicity as well as reagent availability, we chose to focus our further inhibitor studies on C75.

Using an antibody against double-stranded RNA (dsRNA), the viral replication intermediate, we sought to determine at what timepoint during the viral life cycle FASN inhibition had the greatest effect. To validate this technique, we first infected cells at MOI 1, 0.1, and 0.01. We fixed these cells and stained using the dsRNA antibody and quantified the ratio of cells presenting the dsRNA signal (shown in red) compared to total cell

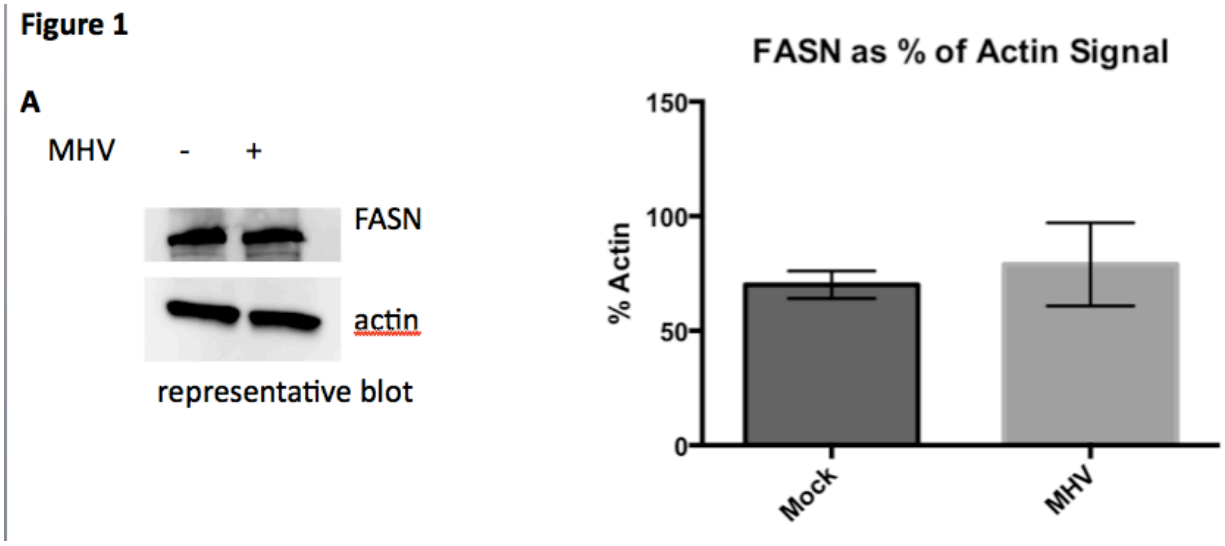

Figure 3.1. *Overall FASN levels remain unchanged upon MHV infection*. A) (left panel) Western blot of lysates prepared from mock or MHV-A59 infected DBT cells. MOI=1, harvest 8 hours post-infection. Blots were probed for FASN and actin. Bands were quantified using ImageJ. (Right panel) FASN signal expressed as percentage of actin signal. Data from 3 independent experiments, Error bars = SEM.

counts as determined by DAPI staining (shown in blue) (Figure 3.2 E). The results aligned with expected percentages for the varying MOIs (Figure 3.2F)

Following this validation, we moved on to examine the time course inhibition (Figure 3.2 C). We saw that the greatest reduction in viral titer took place when C75 was added at 0 and 2 hours post-infection. Importantly, pre-treatment with C75 did not have as great of an effect, indicating that it is likely a post-entry step that is being affected, possibly due to washout of C75. Studies remain unclear as to the reversibility of C75 binding. Since the dsRNA antibody recognizes a viral replication intermediate, the observation of decreased dsRNA signal with this time course addition of C75 suggests that C75 is affecting a step at or before viral genome replication. For further validation, viral supernatants were harvested and subjected to plaque assays to determine viral titer for the C75 time course addition. Again, C75 addition at 0 hr and 2 hr post-adsorption yielded the greatest decrease in viral titer, compared to vehicle treated cells (Figure 3.2D).

Figure 3.2. *Inhibition of FASN activity by C75 yields reduced viral titer and is most effective during early timepoints in infection*. A) MTT cell viability assay dose response curve of varying concentrations of C75 (0-50uM) or DMSO vehicle control of equal volume. B) Plaque assay results from supernatants of cells treated with either DMSO vehicle only or C75 concentrations from 0-50uM. Cells were adsorbed with MHV-A59, MOI=1, and either vehicle or C75 was added at media change. Data from 3 independent experiments, error bars =SEM. C) Quantification of % of cells showing dsRNA staining in C75 treated cells normalized to vehicle control. 1 hour adsorbtion with MHV-A59, MOI=1, and C75 added at timepoints 0, 2, 4, 6, and 8 hours post-infection. All cells fixed at 8 hours post-infection. "Pre-treat" condition cells were treated with 50uM C75 for 1 hour prior to MHV-A59 adsorbtion. Imaged at 20X magnification, 10 images counted per condition. D) Viral titers of C75 and vehicle treated cells. 1 hour adsorbtion with MHV-A59, MOI=1, C75 added at timepoints 0, 2, 4, 6, and 8 hours post-infection. Supernatants collected at 8 hours post-infection. "Pre-treat" condition cells were treated with 50uM of C75 for 1 hour prior to MHV-A59 adsorbtion. 3 independent experiments, error bars = SEM. (E) Representative images of the validation condition MOIs of 1, 0.1, 0.01, fixed 8 hours post-infection. Imaged 20X magnification, 10 images per condition. (F) Quantification of validation conditions. Data from 3 independent experiments, Error bars = SEM.

A

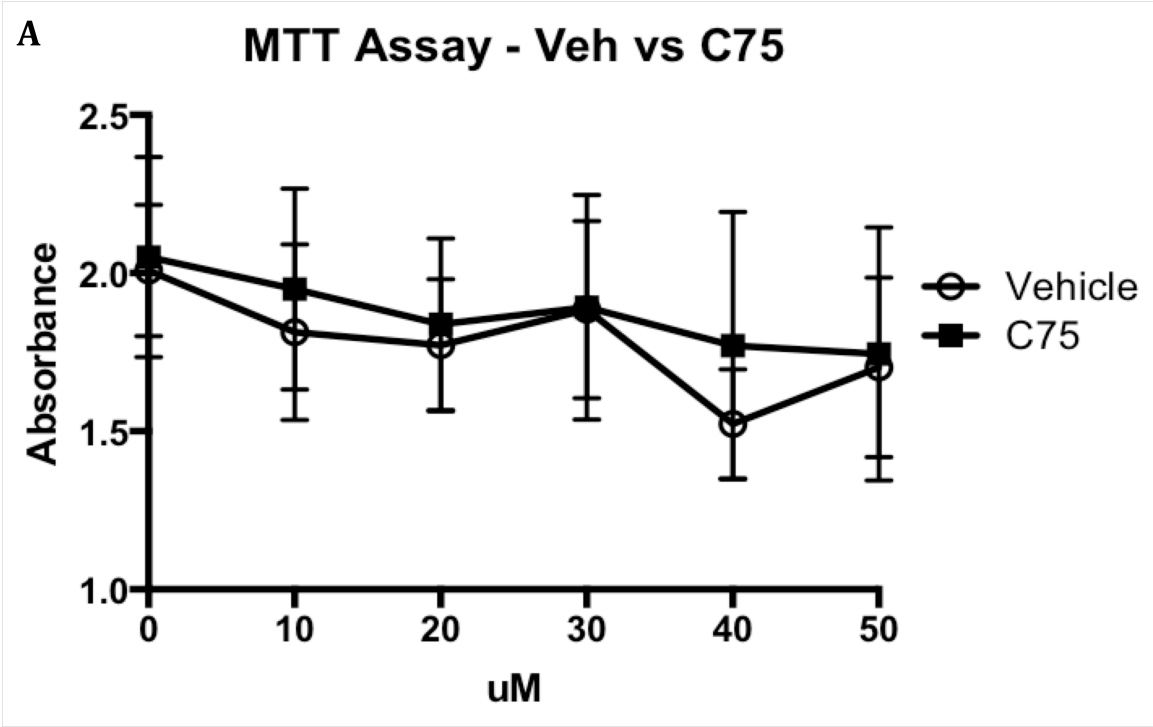
MTT Assay - Veh vs C75
Absorbance
2.5
2.0
1.5
1.0
0
10
20
30
40
50
uM
Vehicle
C75

B

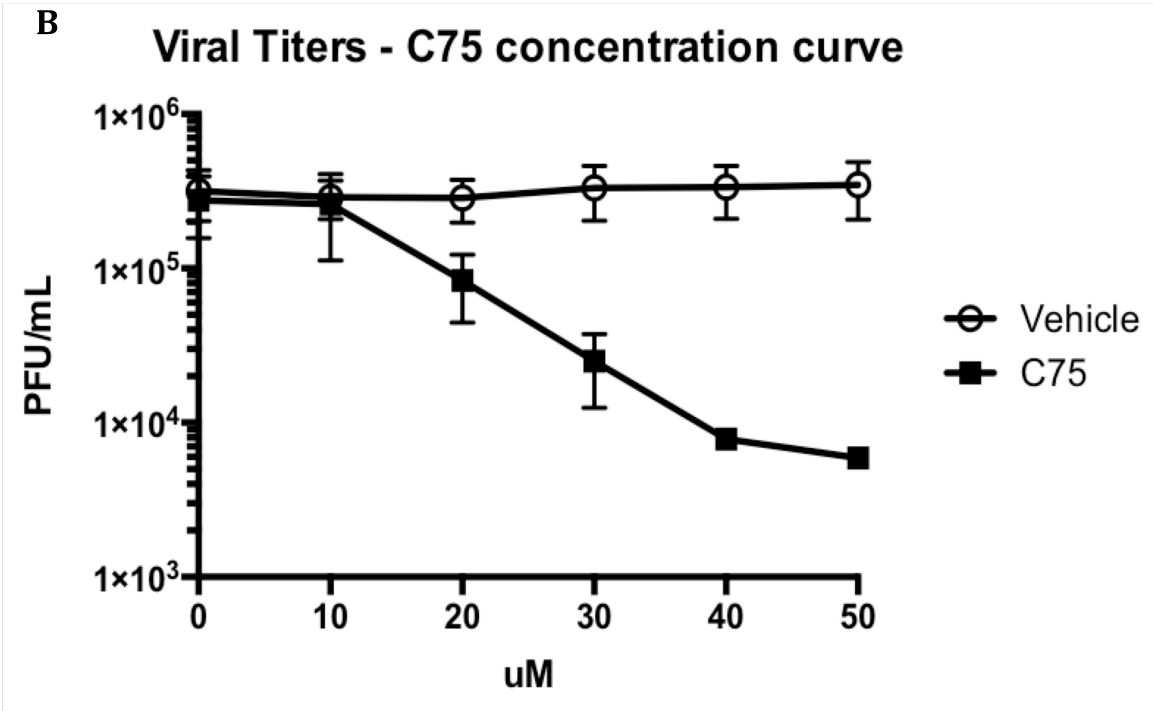
Viral Titers - C75 concentration curve
PFU/mL
1×10^6
1×10^5
1×10^4
1×10^3
0
10
20
30
40
50
uM
Vehicle
C75

C

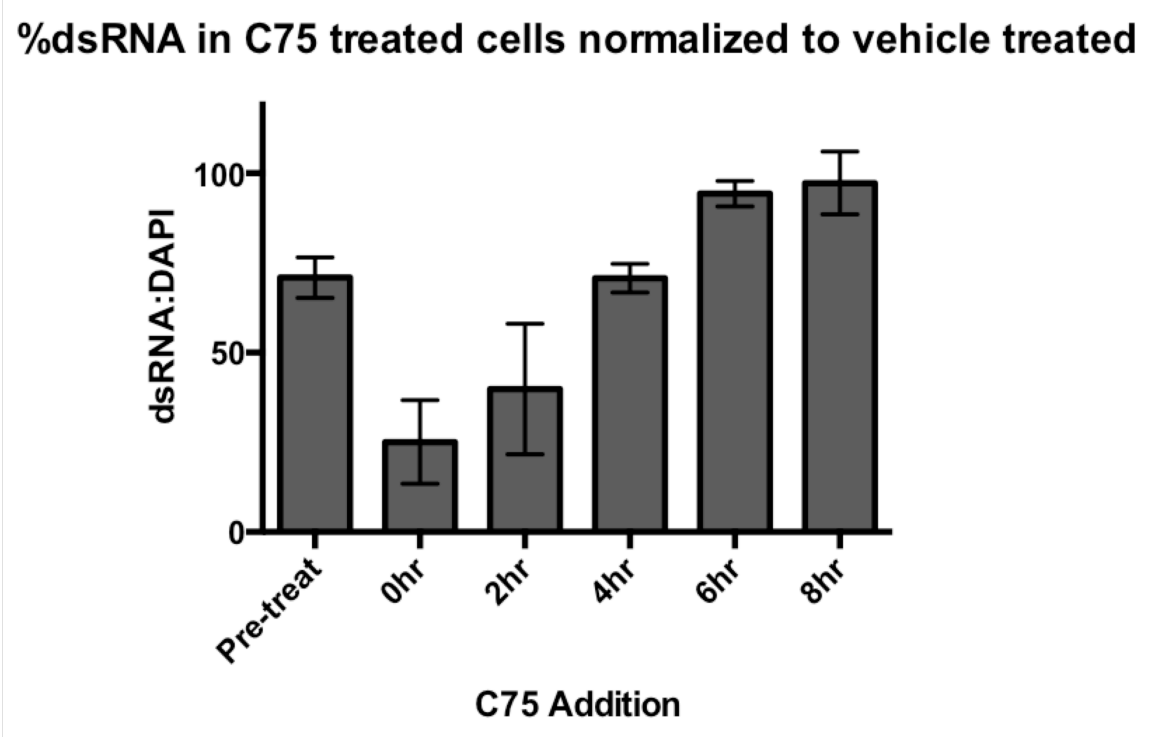
%dsRNA in C75 treated cells normalized to vehicle treated
dsRNA:DAPI
100
50
0
Pre-treat
0hr
2hr
4hr
6hr
8hr
C75 Addition

D

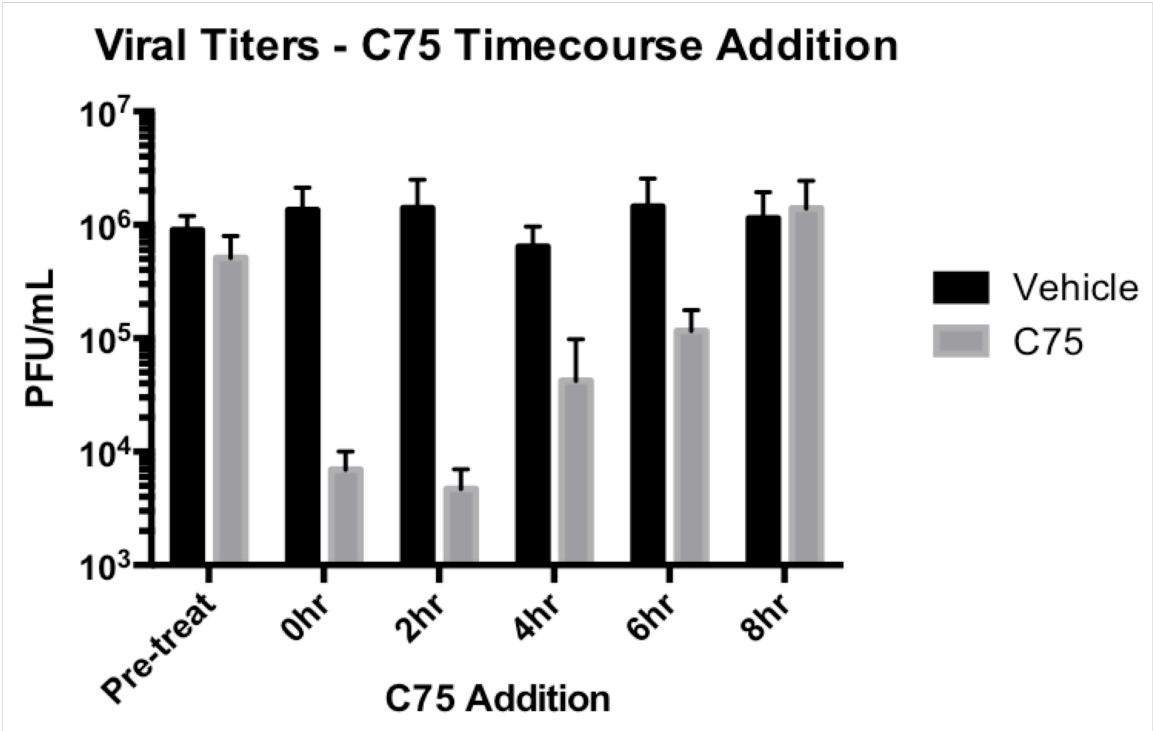
Viral Titers - C75 Timecourse Addition
PFU/mL
10^7
10^6
10^5
10^4
10^3
Vehicle
C75
Pre-treat
0hr
2hr
4hr
6hr
8hr
C75 Addition

E

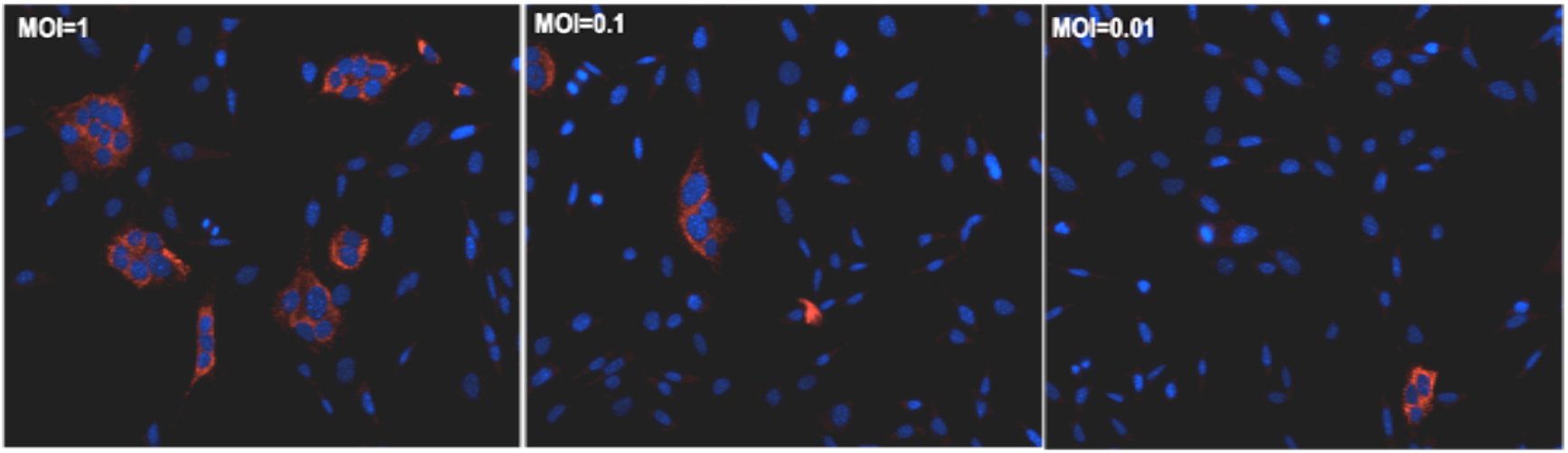
MOI=1
MOI=0.1
MOI=0.01

F

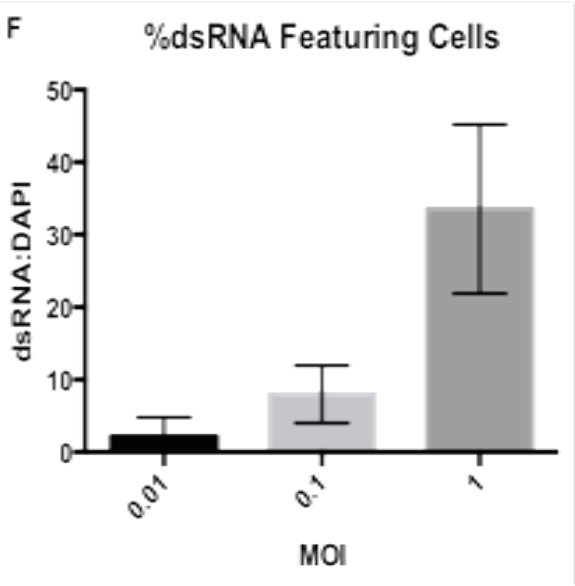
%dsRNA Featuring Cells
dsRNA:DAPI
50
40
30
20
10
0
0.01
0.1
1
MOI

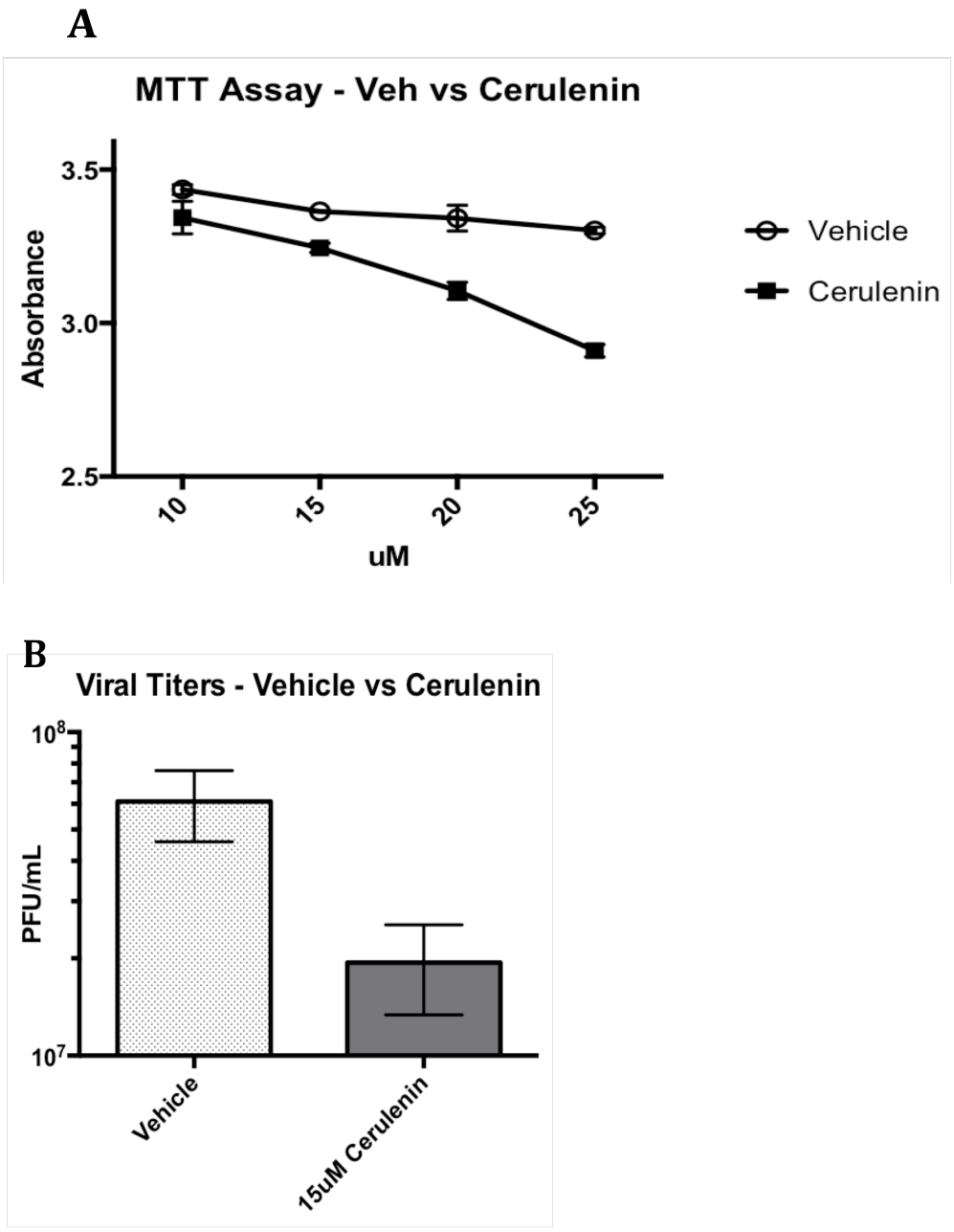

Figure 3.3. *FASN inhibition by cerulenin also decreases viral titer.* A) MTT cell viability assay dose response curve of varying concentrations of cerulenin (0-25uM) or DMSO vehicle control of equal volume. B) Plaque assay results from supernatants of cells treated with either DMSO vehicle only or 15uM cerulenin. Cells were adsorbed with MHV-A59, MOI=1, and either vehicle or cerulenin was added at media change. Virus was harvested 8 hours post-infection. Results of 2 independent experiments, error bars = SEM.

Knockdown of FASN yields a decreased viral titer

To complement the inhibitor study, we performed a knockdown study. We used a pool of four siRNAs targeting FASN. We first performed MTT assays to ensure that the FASN knockdown was not causing a reduction in cell viability (Figure 3.4A). There was no discernable difference in viability between cells treated with a scrambled pool of four nontargeting siRNAs and cells treated with siRNAs directed against FASN when used at a 25 nM concentration. We also performed western blots and determined that by using 25 nM concentration of siRNA against FASN, we could achieve and average ~70% knockdown of FASN (Figure 3.4A). Immunofluorescence showed that the FASN knockdown appeared to be affecting the cells at a reduced level uniformly within the monolayer, as opposed to complete knockdown in some cells and no knockdown in others, as would be evidenced by a lack of FASN signal in certain cells with full signal in others (Figure 3.4C). We then performed the FASN knockdowns and infected the cells 48 hours post-knockdown with MHV at an MOI of 1. Supernatants were harvested 8 hours post-infection and subjected to plaque assay analysis. We observed that, compared to the control siRNA, viral titers were ~1.5-2 log lower in the FASN knockdown cells (Figure 3.4D). Using the same dsRNA staining technique presented earlier in Figure 3.2 E & F, we saw that percent of cells featuring a dsRNA signal was ~80% lower in cells knocked down for FASN compared to the nontargeting control (Figure 3.4E).

Figure 3.4. *FASN knockdown causes decreased viral titer*. A) Western blot of lysates prepared from cells treated with nontargeting control knockdown (siNON) or FASN knockdown (siFASN). Blots were probed for FASN and actin. Bands were quantified using ImageJ. FASN signal expressed as percentage of actin signal. Data from 3 independent experiments, Error bars = SEM. B) Immunofluorescence microscopy of untreated, siNON, and siFASN treated cells. Cells infected with MHV, MOI=1, fixed 8hrs post-infection. Blue=DAPI, Green=FASN, Red=dsRNA. C) MTT cell viability assay 48 hours post-knockdown shows no significant difference between control nontargeting knockdown (siNON) and FASN knockdown (siFASN). Scalebars = 10uM D) Plaque assay results from supernatants of cells knocked down using either control nontargeting siRNA (siNON) or siRNAs against FASN (siFASN), 48 hours post knockdown infected with MHV-A59, MOI=1, supernatant harvested 8 hours post-infection. Data from 3 independent experiments, Error bars = SEM. (E) dsRNA quantification of siFASN vs. siNON. All cells fixed 8 hours post-infection. Imaged 20X magnification, 10 images per condition. (F) Quantification of validation conditions. Data from 3 independent experiments, Error bars = SEM.

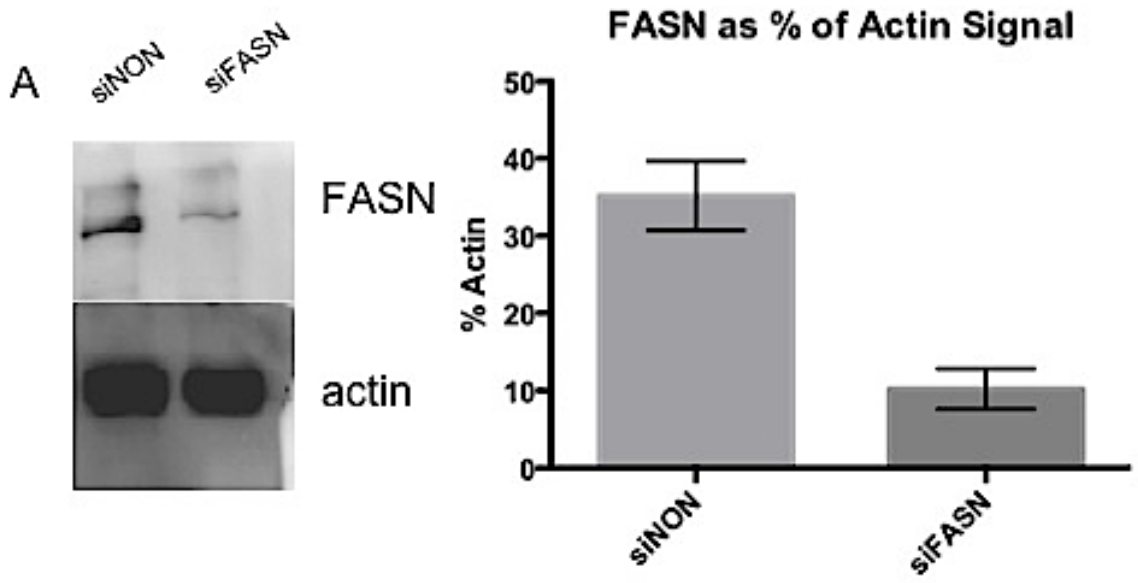
A
siNON
siFASN
FASN
actin
FASN as % of Actin Signal
% Actin
50
40
30
20
10
0
siNON
siFASN

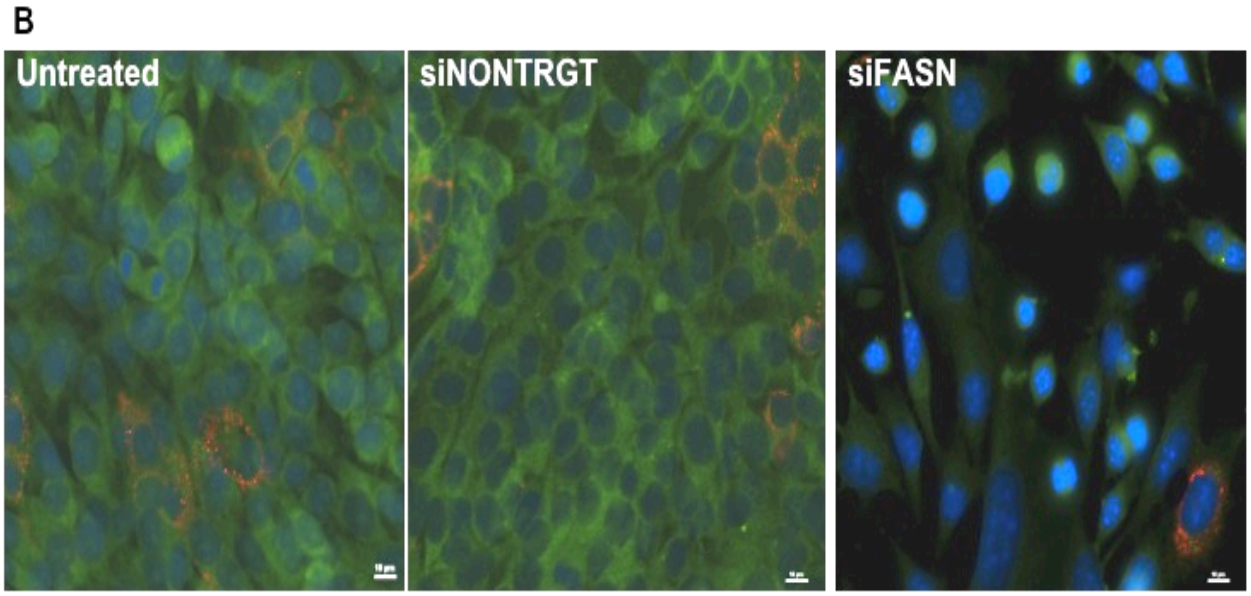
B
Untreated
siNONTRGT
siFASN

C

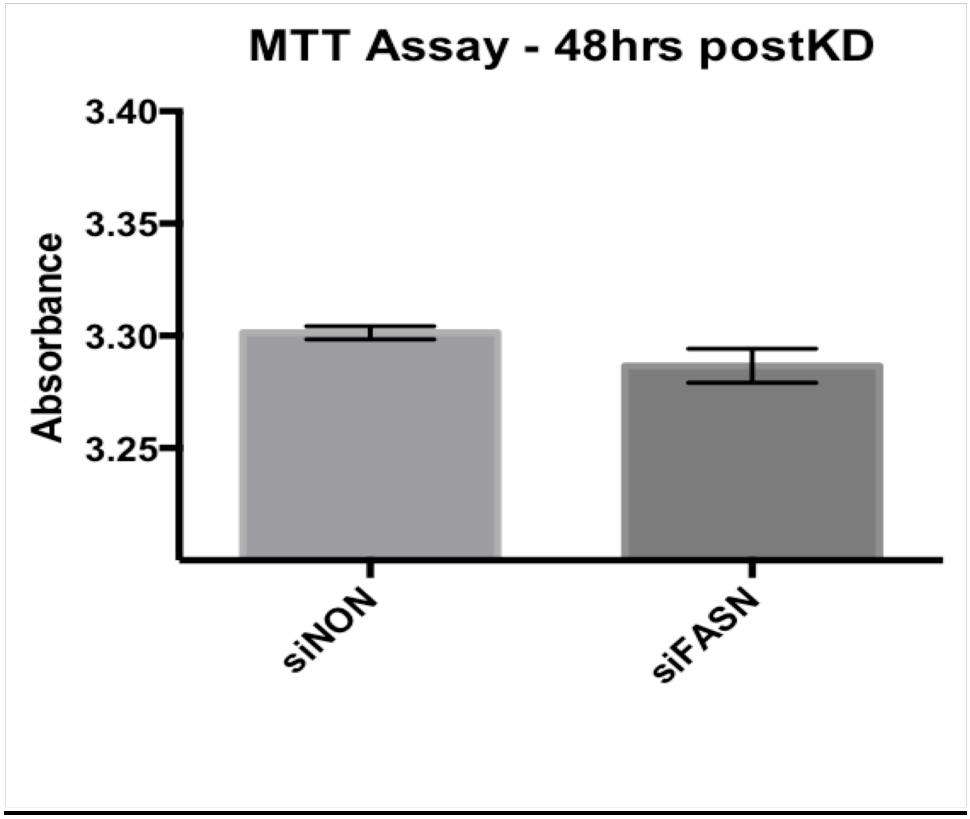
MTT Assay - 48hrs postKD
Absorbance
3.40
3.35
3.30
3.25
siNON
siFASN

D

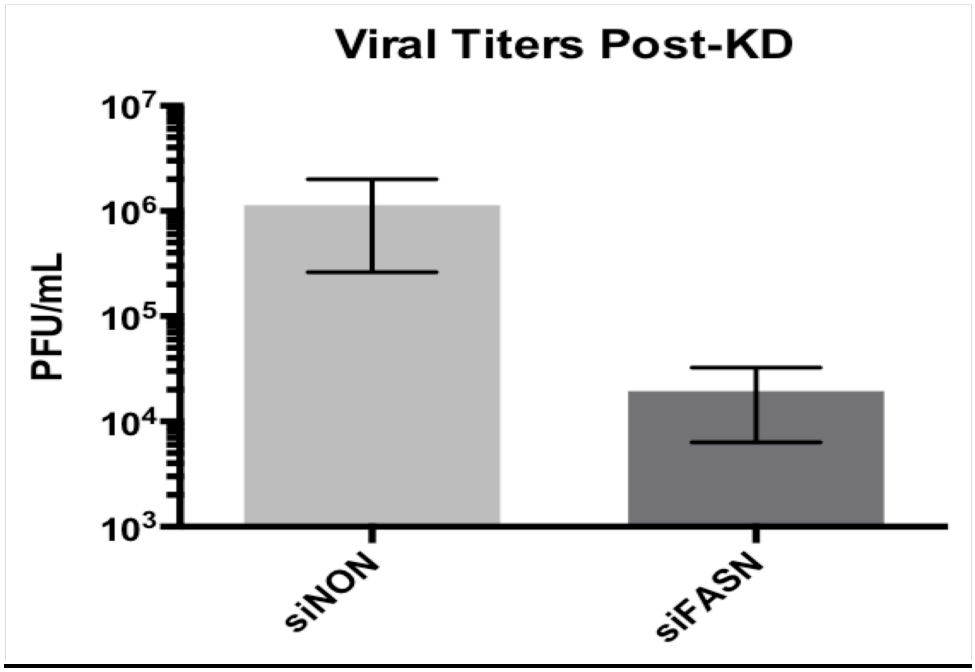
Viral Titers Post-KD
PFU/mL
10^7
10^6
10^5
10^4
10^3
siNON
siFASN

E

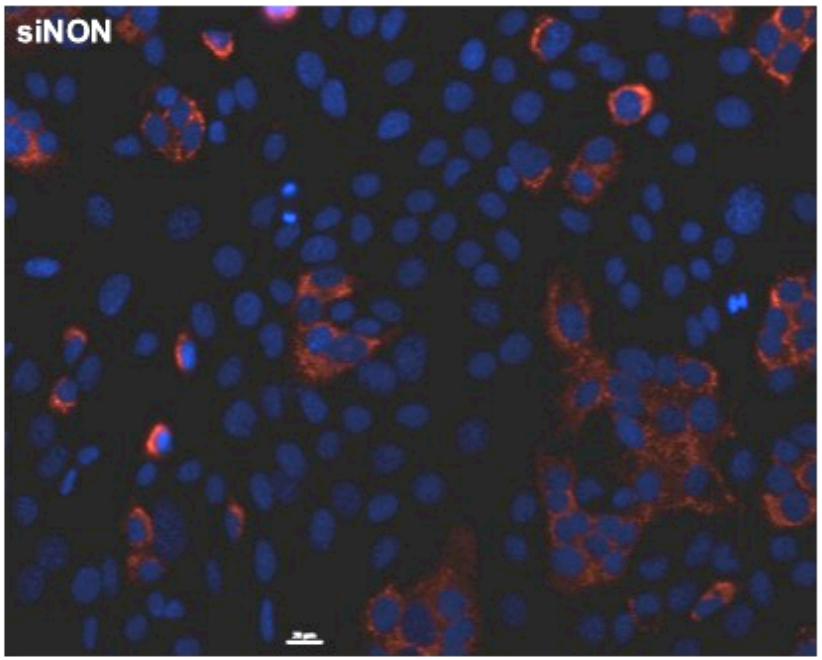
siNON

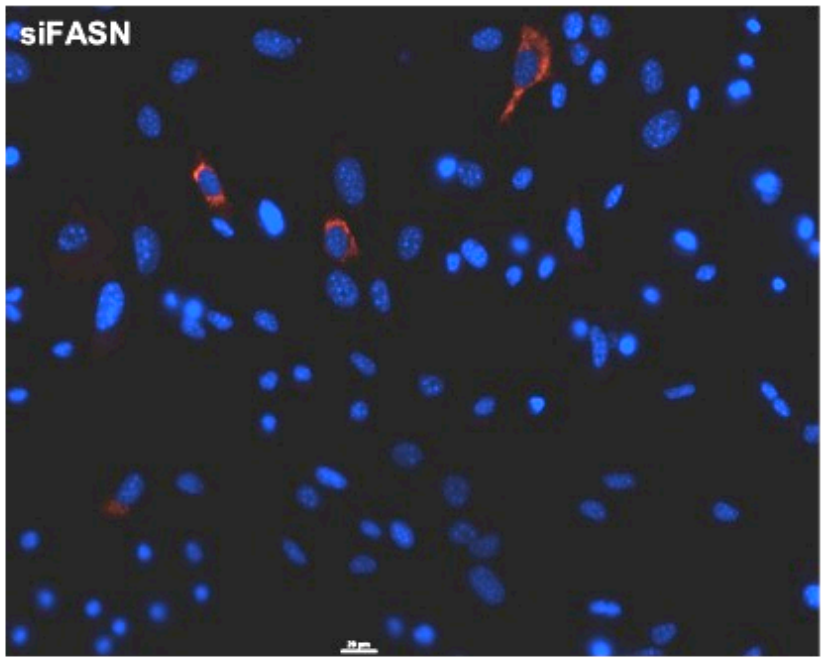
siFASN

F

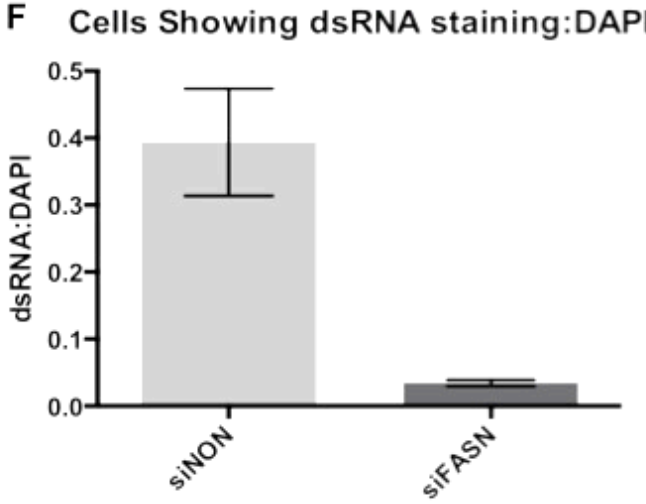
Cells Showing dsRNA staining:DAPI
dsRNA:DAPI
0.5
0.4
0.3
0.2
0.1
0.0
siNON
siFASN

C75 treatment results in loss of DMVs and CMs

We performed electron microscopy (EM) on vehicle and C75 treated cells, both uninfected and infected with MHV at an MOI of 3 for 5.5 hours to determine if the replication-transcription complex membranes were being disrupted when FASN activity was inhibited. As Table 3.1 shows, double membrane vesicles and convoluted membranes were completely absent in MHV infected cells treated with 50uM of C75 (Table 3.1-shaded region).

Interestingly, lipid droplets were present in much higher quantities in MHV infected cells treated with 50 uM of C75 compared with either MHV infected cells treated with vehicle or mock infected cells treated with 50 uM C75 (Table 3.1-shaded region). Lipid droplet amount jumped from 0.5% in mock infected/untreated cells to 8.1% in mock infected/C75 treated cells. MHV infected cells with no C75 showed lipid droplets in 3% of cells, jumping to 30% of cells in MHV infected/C75 treated cells. Representative EM images are shown in Figure 3.5. Treatment of DBT cells with 50uM of C75 increases the number and size of lipid droplets, observed both in EM (Figure 3.5 and Table 3.1-shaded region) and immunofluorescence (Figure 3.7A-D). C75 treatment in the presence of MHV infection further increases the number of lipid droplets observed.

Table 3.1. Ultrastructural study of C75 vs. vehicle treated cells in the absence or presence of MHV infection.

	MHV+C75	MHV	C75	Uninfected
Normal	7%	37.4%	20.7%	94.8%
Golgi present	0%	24.2%	0.0%	34.6%
Compacted Golgi	32%	7.1%	23.4%	0.5%
Mitochondrial Dysfunction	76%	2.0%	63.1%	0.2%
DMV	0%	34.3%	0.0%	0.0%
Nuclear degradation	3%	5.1%	8.1%	0.9%
Condensed cytosol	13%	0.0%	13.5%	0.0%
Lipid droplet	30%	3.0%	8.1%	0.5%
Cytoskeleton prominent	7%	11.1%	12.6%	1.2%
LVCV	0%	12.1%	0.0%	0.0%
Single Membrane Degradation Vesicles	24%	27.3%	20.7%	12.6%
Total Cells Imaged	147	99	111	422

MHV=mouse hepatitis virus, DMV = double membrane vesicle, LVCV = large virion containing vacuoles, MTOC = microtubule organizing center

A
Mock/Vehicle
Mock/C75
MHV/Vehicle
MHV/C75
M
N
500 nm

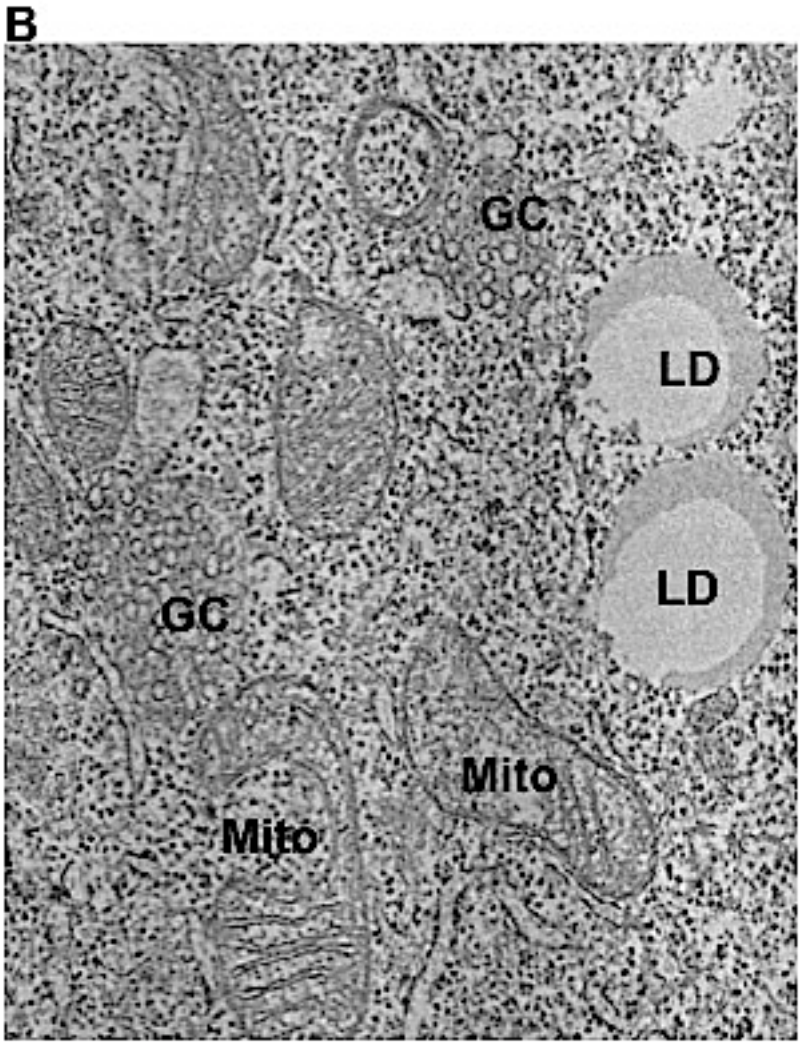

Figure 3.5. *Electron microscopy of mock vs MHV infected, vehicle vs C75 treated.* A) Representative images of conditions used for quantification in Table 1. Cells were either mock of MHV infected MOI = 3 for 1hr, media changed included either DMSO of 50uM C75. B) Image of an MHV infection/C75 treated cell illustrating some of the phenotypes from Table 3.1. CG= compacted golgi, LD= lipid droplet, Mito=mitochondria with some dysfunction apparent

The EM studies also showed a significant change in the morphology of the Golgi, with the traditional Golgi pattern being replaced with the condensed Golgi phenotype of small, single-membrane rounded vesicles clustered in areas typically expected for the Golgi. Upon C75 treatment, either in the absence or presence of MHV infection, detection of standard morphology Golgi in EM dropped to 0%, while the compacted vesicular phenotype was present (Table 3.1). To follow-up on this change, we performed immunofluorescence microscopy staining for both the Golgi using the cis-Golgi marker GRASP65. The staining showed that the Golgi signal was contracted in the overall sample in the C75 treated cells (Figure 3.6B) compared with the vehicle treated cells (Figure 3.6A). We compared the length to width (L:W) ratio of the Golgi signals in both samples and found that there was a statistically significant difference in the L:W ratios. The C75 treated cells had a ratio closer to 1 whereas the vehicle ratio was much higher, indicating that the Golgi compaction we observed in microscopy was a measurable difference (Figure 3.6C).

A
Vehicle
B
50uM C75
C
Vehicle
D
+C75

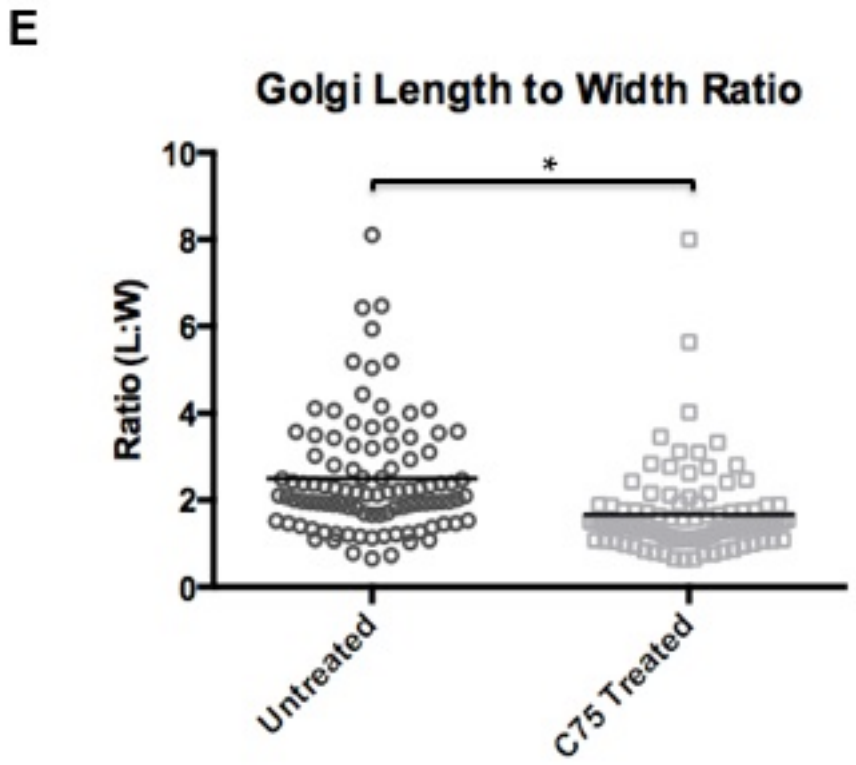

Figure 3.6. *C75 treatment leads to Golgi compaction and increased lipid droplets*. Immunofluorescence micrscopy of DBT cells treated with DMSO vehicle (A) or 50uM C75 (B). Blue=DAPI, Red=GRASP65 Golgi. Scalebars = 20uM C) and D) Higher magnification images illustrating the Golgi morphology changes seen in A and B. Scalebar = 20uM E) ImageJ quantification of the L:W ratios of vehicle vs. C75 treated cells. 100 cells measured per condition. *= $p<0.01$

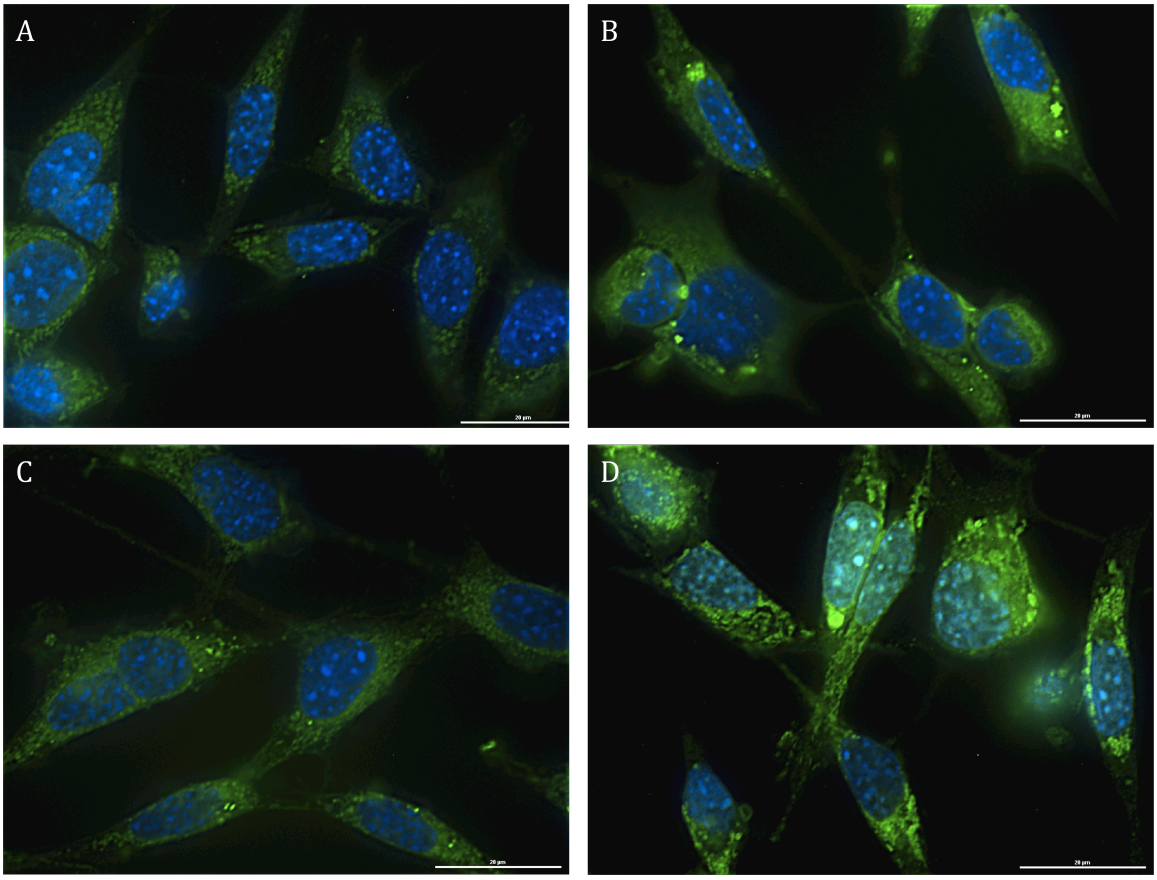

Figure 3.7. *C75 treatment leads to increased lipid droplets*. Cells were treated with either DMSO vehicle or 50uM of C75, then were either mock infected of infected with MHV MOI=1 for 6 hours. A) Mock infected/vehicle treated B) Mock infected/50uM C75 treated C) MHV infected/vehicle treated D) MHV infected/50uM C75 treated. Green=Bodipy493/503 lipid droplet marker. Scalebars = 20uM.

Discussion

Although it was recently shown which viral proteins appear to be sufficient to induce coronavirus DMVs and CMs, which host cell proteins are important for RTC formation remains unclear. In this study, we sought to determine the importance of FASN on coronavirus replication. Overall, MHV infection did not appear to have any significant effect on total FASN levels in the cell. This differs from coxsackievirus and HCV, where infection increases the total FASN present (Nasheri et al., 2013; Rassmann et al., 2007). However, since we did not assay for FASN activity, it is possible that although total FASN levels remain constant during MHV infection FASN activity may be changed. Similarly, we did not observe any significant change in FASN localization within the cell in the presence of MHV. This is comparable to what has been observed for HCV (Nasheri et al., 2013).

We observed that both reduction of the level of FASN present, as well as inhibition of FASN activity via C75 treatment led to an overall reduction in viral titer. Inhibiting FASN early in infection (0-2 hrs) had a greater impact on viral titer than either pre-treatment or later timepoint addition. Finally, we saw that inhibition of FASN led to decreased levels of DMVs and CMs formed in infected cells. The fact that FASN is important for coronavirus replication mimics what has been shown for a number of other positive sense single-stranded RNA viruses. However, the results seen in both electron microscopy and immunofluorescence microscopy show that FASN inhibited cells exhibit higher numbers of lipid droplets than non-inhibited cells and that FASN inhibited cells in the presence of MHV infection had the highest amount of lipid droplets. This suggests that the mechanism of action by which FASN inhibition or depletion affects coronavirus

replication may differ from what has been seen for dengue infected cells, where an increase in lipid droplets is beneficial for dengue virus replication. It is possible that to gain enough membrane in order to form membranous structures during infection, coronaviruses must induce cellular lipid catabolism, or lipophagy, in addition to the production of new fatty acids. In the absence of FASN activity, MHV causes the cell to go into lipophagy overdrive as a means of compensation and partial storage of the newly freed fatty acids occuring in lipid droplets. It is useful to consider what Gruber, et al. have seen for C75 and cerulenin treatment in CHO-K1 cells under starvation conditions (Gubern et al., 2009). That study showed that, in the absence of serum, C75 and cerulenin treated cells showed an increase in lipid droplet numbers. The author posed that the reason for this was that in the absence of serum and active FASN, the cell needs to degrade existing phospholipids to sustain itself and some of the newly freed fatty acids get incorporated as triacylglycerol and are stored in the lipid droplets. If the virus imposes a similar "starvation" stress situation on the cell, it is reasonable that in the absence of FASN activity, a similar condition could occur as described by Gruber, et al.

Although we observed no overall change in the total amount of FASN present in either uninfected or MHV infected cells, it would be useful to determine whether the activity of FASN changes in response to infection, as has been seen for HCV and dengue virus (Nasheri et al., 2013). It is possible that the virus needs increased activity to sustain itself. This would explain the lowered titers when the enzyme activity is inhibited or the enzyme is not present. A study using SARS-CoV featuring a tagged E-protein co-immunoprecipitated both nsp3 as well as FASN with the E-protein, suggesting a possible interaction between nsp3 and FASN (Alvarez et al., 2010). This might account for the

membrane proliferation activity seen in our previous study when expressing nsp3 alone in cells.

The Golgi compaction seen in both EM and IF has not been observed before, to the best of our knowledge. It is unclear if this is novel to DBT cells, similar to the lipid droplet formation, or if it is common to all C75 treated cells but has never been studied. If novel to DBT cells, it could again indicate why DBT cells are susceptible to MHV infection and to the mechanism of infection. Although the virus assembles and buds at the ER-Golgi intermediate compartment (ERGIC) it does not appear that this is the step at which viral production is being initially halted. If this were the case, we would have expected to see RTCs still formed in EM and a stable amount or even an increase and buildup of dsRNA as seen in IF. It is possible that the disruption of the Golgi contributed to the inability of the virus to produced DMVs and CMs, thus preventing replication. A recent study showed that, in addition to inhibiting FASN, C75 also has an inhibitory effect on human mitochondrial B-ketoacyl synthase carrier protein, a member of the mitochondrial fatty acid synthesis pathway (Chen et al., 2014). However, this study demonstrated that FASN knockdown did not affect the mitochondrial fatty acid synthesis pathway. Since our C75 inhibitor studies mimic the results of our FASN knockdown studies, I conclude that the result seen in our C75 inhibitor study is not due to the inhibition of the mitochondrial fatty acid synthesis pathway.

It will be interesting to determine if FASN interacts with a viral protein, particularly the nonstructural proteins. NS5B from hepatitis C virus interacts with FASN in pull down studies and dengue virus NS3 relocalizes FASN to the sites of viral replication (Heaton et al., 2010). I have previously shown that the SARS-CoV nsp3 has

membrane proliferation activity, suggesting a possible interaction with FASN (Angelini et al., 2013)

Whether directly or indirectly, the inhibition of fatty acid synthase has important detrimental effects on MHV infection and could be exploited when studying future avenues for coronavirus treatments. Indeed, a FASN inhibitor drug has shown promise in animal models as an anti-HCV drug (Baugh et al., 2013; Evanchik et al., 2012). If the same applies for FASN importance in coronavirus infection, this could be a viable route for therapeutic development.

Materials and Methods

Cells and virus. DBT (mouse delayed brain tumor) cells were used for all experiments. Cells were maintained in Dulbecco's modified Eagle's medium (HyClone) supplemented with 10% fetal bovine serum (FBS) and 1% penicillin-streptomycin. The A59 strain of murine hepatitis virus (MHV) was used for all experiments. Infections were performed at indicated multiplicities of infection (MOIs) for the indicated time lengths.

Antibodies. The primary antibodies used were K1 mouse monoclonal antibody against dsRNA (English and Scientific Consulting), rabbit anti-fatty acid synthase (Osman et al.), rabbit anti-GRASP65 cis Golgi (obtained from Suetterlin lab, UCI). Alexafluor-488- and Alexafluor-594-conjugated secondary antibodies (Invitrogen) were used for immunofluorescence. Horseradish peroxidase (HRP)- conjugated secondary antibodies (Jackson Laboratories) were used for Western blotting.

Immunofluorescence assays. Cells were grown on coverslips and fixed designated number of hours using 3.7% paraformaldehyde, permeabilized with 0.1% Triton X-100,

and mounted with DAPI (4',6-diamidino-2-phenylindole) Fluoromount D (Southern Biotech). Microscopy was performed with a Nikon Eclipse Ti microscope. Images were processed using NIS Elements software.

Western blotting assays. Cells were grown in 6-well plates and lysed using 1% NP-40 lysis buffer with 1*X* protease inhibitor cocktail (Research Products International Corp). Lysates were subjected to SDS-PAGE and transferred to a polyvinylidene difluoride (PVDF) membrane for immunoblotting.

Electron microscopy. Cells were grown in T-75 flasks, transfected, fixed and harvested with 2% EM-grade glutaraldehyde in 0.1 M sodium cacodylate buffer for at least 4h, postfixed in 1% osmium tetroxide–0.1M cacodylate buffer for 1 h, and stained in 2% uranyl acetate en bloc for 1 h. Samples were dehydrated in ethanol, embedded in epoxy resin, sectioned at intervals of 50 to 60 nm on a Leica UCT ultramicrotome, and picked up on Formvar and carbon-coated copper grids. Sections were stained with 2% uranyl acetate for 5 min and with Sato's lead stain for 1 min. Grids were viewed using either a Tecnai G2 Spirit BioTWIN transmission electron microscope equipped with an Eagle 4k high-sensitivity (HS) digital camera (FEI, Hillsboro, OR) or a Phillips CM-20 camera equipped with a 2k charge-coupled device (CCD).

Lipid staining. Cells were infected and treated as described. BODIPY 493/503 (Life Technologies) was diluted in DMSO and used at a final concentration of 1ug/uL in PBS. Cells were incubated for 15-30 min at 37 degrees and fixed and imaged as described above.

CHAPTER 4

Conclusions, current model for coronavirus DMV formation, and future directions

This thesis has described the work undertaken to decipher the mechanisms behind host cell internal membrane rearrangement caused by coronaviruses. Specifically, the studies herein have elucidated which viral proteins are sufficient for producing membranes rearranged into DMVs and CMs, as well as pinpointed a particular host cell protein of importance for coronavirus replication, although the precise mechanism driving these changes remains unclear. These findings give important insight into the molecular biology of coronavirus infections that can also be applied to examine how coronaviruses fit in with other positive sense single-stranded RNA viruses, highlighting similarities and differences. This work also has possible practical applications in identifying druggable targets for inhibiting coronavirus replication and thereby infection and disease.

Our initial work focused on identifying the viral factors responsible for inducing host cell membrane rearrangement associating with viral genome transcription and replication. In **Chapter 2**, we demonstrated that transfection with three of the SARS-coronavirus nonstructural proteins was sufficient to induce double membrane vesicles and convoluted membranes similar to those observed in SARS-infected cells. Individually, these three nsps: nsp3, nsp4, and nsp6 had effects on the cells. Specifically, nsp3 alone induced an intriguing membrane proliferation phenotype wherein regions of extended membrane whirled and gathered in an unstructured manner. This phenotype

was also observable upon transfection of a truncated form of nsp3 containing the C-terminal transmembrane domains, thus pinpointing this region of the protein as having membrane proliferative properties. Nsp4 alone in the cell had no distinguishable effect and appeared to reside within the ER. Nsp6 alone caused a gathering of single membraned vesicles around the microtubule organizing center (MTOC) which could point to some importance for the MTOC in membrane rearrangement. The microtubules have been shown to be involved with coronavirus nonstructural proteins, with nsp2 having been shown to traffic in a microtubule-dependant manner in one live imaging study (Hagemeijer et al., 2010). Further study into the role that microtubules may play in coronavirus infection and nonstructural protein interaction could prove fruitful. Specifically, our results suggest that nsp6, in addition to nsp2, should be looked into.

As the identity of the viral proteins important for membrane rearrangement has become clear and the cellular membranes and pathways involved begin to be distinguished, the mechanism of membrane deformation can be deciphered. DMVs and CMs are comprised of highly curved membranes. Presumably this curvature is induced via the transmembrane domains located in coronavirus nsp3, nsp4, and nsp6 (nsp2, nsp3, and nsp5 for arteriviruses) as well as protein–protein interactions of these nsps with each other, with other viral proteins, and with host cellular proteins. Transmembrane domains that feature conical shapes will induce membrane curvature as a product of their shape by forcing the membrane to accommodate and deform around the conical region in a wedge-like manner (McMahon and Gallop, 2005; Shibata et al., 2009). Additionally, suites of proteins may form together like a scaffold that has the ability to deform lipid bilayers and steric effects of these membrane-interacting proteins may also aid in deformation (Schley

et al., 2013). Since nsp3, nsp4, and nsp6 (and their *Nidovirales* homologs) contain transmembrane domains and work together in a scaffold-like fashion, it is possible that both of these approaches work together to induce DMVs and CMs. As I propose in Figure 4.1, following initial genome polyprotein translation and proteolytic processing, nsp3 (dark blue), nsp4 (teal), and nsp6 (green) remain inserted in the lipid bilayer (Figure 4.1- upper left inset).

The intracellular phenotypes of cells expressing both nsp3 and nsp6 suggest that these proteins may promote membrane curvature, inducing proliferated membranes and vesiculation respectively on their own. Nsp4 alone appears incapable of inducing membrane curvature but, in conjunction with nsp3, is able to produce paired membranes, suggesting that some combination of homotypic and/or heterotypic interactions is driving this pairing (Figure 4.1- lower right inset). Nsp3–nsp3, nsp4–nsp4, and nsp3–nsp4 interactions have all been previously identified by mass spectrometry-based approaches, yeast two-hybrid assays, and co-immunoprecipition studies (Hagemeijer et al., 2011; Imbert et al., 2008; Neuman et al., 2008; von Brunn et al., 2007). Since this membrane pairing was not observed when using a C-terminal region of nsp3, it is likely that the scaffolding function relies on interaction of nsp4 with some region of nsp3 that is N-terminal to its transmembrane domain. The addition of nsp6 changes the organization of paired membranes from remarkably consistent maze-like swirls to a mixture of heterogeneous DMVs and CMs that resemble the viral replicative organelles found in infected cells. This suggests that nsp6 modifies the long-range organization of paired membranes without disrupting membrane pairing, possibly by inducing deep curvature into the nsp3+nsp4 scaffold. Nsp4–nsp6 heterotypic interaction has been previously

shown via co-immunoprecipitation and Venus reporter protein complementation assay (Hagemeijer et al., 2011). Due to the high homology of these three transmembrane regions across the *Nidovirales*, this proposed mechanism may apply generally (Fig. 1.2). It is important to note though that despite this high homology, a recent study showed that transfection of nsp3 and nsp4 from different coronavirus species did not appear to localize in the same patterns seen when using nsp3 and nsp4 from the same species (Hagemeijer et al., 2014). This study also suggests that the luminal loops of nsp3 and nsp4 could play a crucial role in protein-protein interaction that could serve to "zipper" membranes together to form double membrane structures. This agrees with our results showing that nsp3 and nsp4 together are sufficient to form double walled mazes. Additionally, although nsp3, nsp4, and nsp6 appear to have a major role in membrane rearrangement, they also likely play a secondary role in recruiting and anchoring other viral proteins and host cell proteins to the replication complex sites and no mechanism of replication complex formation would be complete without an understanding of these interactions. Indeed, it has been shown that the cytosolic nsp2 can be recruited to replication sites by nsp3 and nsp4 alone (Hagemeijer et al., 2014).

Another factor to consider in determining a final mechanism is the kinetics of the nonstructural protein cleavage. Although nsp3, nsp4, and nsp6 are all produced from a single polyproteins and therefore should be found in 1:1:1 ratios within the infected cell, the proteolytic cleavage timing could affect the availability of these nsps. Nsp3 and the N-terminal region of nsp4 are cleaved from the polyprotein by the one or two papain-like proteases encoded within nsp3, whereas the C-terminus of nsp4 and nsp6 are cleaved by the main protease encoded within nsp5. The timing of polyprotein cleavage has been

studied somewhat and it is known that certain intermediates are present for extended periods of time during infection, such as an uncleaved nsp2-3 intermediate which can be found from 30-60 minutes post-infection and is found simultaneously alongside mature nsp2 and nsp3 (Graham and Denison, 2006). The function of such uncleaved intermediates remains undetermined but could play an important regulatory role. Our studies were unable to address this topic due to our plasmid constructs encoding only a single nsp per plasmid.

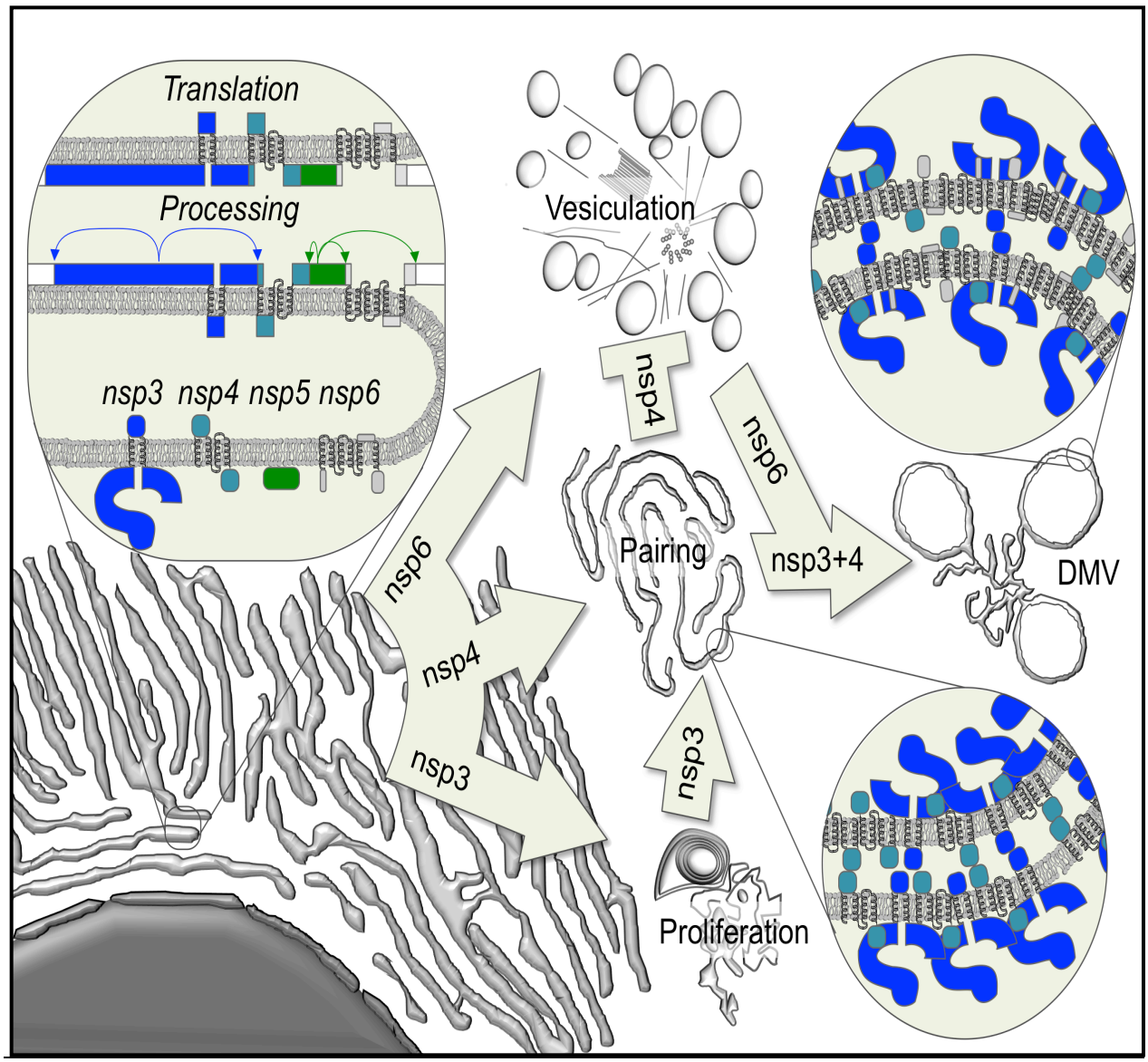

Figure 4.1 *Theoretical mechanism for DMV and CM formation using CoV nsps as examples*. Polyprotein translation occurs from genome, featuring co- and post-translational cleavage of nsps, including nsp3 (dark blue), nsp4 (teal), nsp5 (green), and nsp6 (light grey). Nsp3 alone produces proliferated membrane, nsp4 alone has no membrane phenotype, nsp6 alone produces vesiculation. Nsp4 has a negative effect on nsp6's vesiculation. Nsp3 and nsp4 together induce paired membranes. Nsp3, nsp4, and nsp6 together induce DMVs

The lipid environment may also be affected in nidovirus-infected cells for the purposes of membrane rearrangement. The virus may induce changes in the lipid composition of the progenitor membranes to better facilitate DMV and CM formation as increased amounts of certain species of lipids may aid in certain types of membrane deformation (Bacia et al., 2005; Baumgart et al., 2003; McMahon and Gallop, 2005). In **Chapter 3**, I present the work begun to identify important host cell factors that might be involved in membrane rearrangement. We chose to investigate the role that fatty acid synthase (FASN) might play in coronavirus infection and membrane rearrangement based on studies performed using other positive sense single-stranded RNA viruses. We found that loss of FASN or inhibition of FASN activity has an overall detrimental effect on viral replication as measured by viral titer and dsRNA staining, with a loss of DMVs and CMs observed in EM imaging.

FASN may be play a role in inducing or enhancing the membrane proliferation phenotype observed upon expression of nsp3 (Figure 4.1). Although there is no change in FASN protein levels in coronavirus infected cells, performing FASN enzyme activity assays would determine if the virus changes the rate of FASN during infection. Similarly, performing such assays in the presence of the individual nsps, with particular interest on nsp3 due to its membrane proliferation phenotype, could yield useful information as to whether these viral proteins have a direct effect and to determine whether FASN is interacting with any of the viral nsps, particularly with nsp3, nsp4, or nsp6. There is some evidence from previously performed mass spectrometry data that SARS-CoV nsp3 may interact with FASN. It has also been shown that the SARS

envelope (E) protein interacts with both nsp3 and FASN in tandem affinity purification pull-down experiments (Alvarez et al., 2010). This information, in conjunction with the observation that nsp3 appears to be capable of inducing a membrane proliferation phenotype, strongly points towards the idea that nsp3 may be interacting with or stimulating FASN in some manner. If so, FASN could begin to become incorporated into our model of membrane rearrangement. Our attempts to co-immunoprecipitate nsp3 with host cell proteins have proven unsuccessful, partly due to the harsh conditions required for removing nsp3 from the host cell membranes.

A mass spectrometric study of the profile of the cellular lipid environment in the absence and presence of coronavirus infection would also be informative. For flaviviruses, it has been shown that a distinct change in the composition of the host cell lipids occurs during infection. A similar study for coronaviruses would help profile further insight into the coronavirus mechanism as well as providing a comparison for the existing flavivirus studies. Whether or not the control of the overall lipid environment varies between positive sense single-stranded RNA viruses could suggest similarities between mechanisms across viruses.

A method of experimentation that would be intriguing would be the creation of a FASN inhibition-resistant virus. Attempts in our hands to create such a virus by serially passaging the virus in cells with C75 present in the media have not produced a resistance mutant. It may well be that FASN inhibition by C75 is a cellular condition so disastrous for the virus that it cannot overcome the obstacle. If such a resistant virus were to be produced, however, sequencing the virus could yield novel insight into regions of importance within the viral proteins for interacting or affecting FASN. This is similar to

what has been shown using K22, a viral membrane rearrangement replication inhibitor molecule, where virus resistance under pressure was obtained (Lundin et al., 2014). This K22-resistant virus featured mutations within the nsp6-coding region. The K22 inhibitor is thought to be broadly effective against multiple coronaviruses and is being investigated as a possible therapeutic. Although C75 itself is likely not a viable drug for humans, targeting FASN with other FASN inhibitors may prove useful as a therapeutic option. Our studies using MHV as the viral model could be extended into working in MHV infected mice. Indeed, C75 is already regularly administered to mice in studies of the role of FASN in cancer and obesity (Kuhajda et al., 2005).

Overall, while the results presented in this thesis represent a significant advance towards our understanding of the mechanism by which coronaviruses induce membrane rearrangement in host cells for means of viral genome replication and transcription, there are still many unanswered questions. A more precise understanding of the mechanisms behind this process is still needed to aid in future research and potential therapies for these viruses and possibly for other positive sense RNA viruses as well.

References

(CDC), C.f.D.C.a.P. 2003. Update: Outbreak of severe acute respiratory syndrome--worldwide, 2003. *MMWR Morb Mortal Wkly Rep*. 52:241-246, 248.

Ahlquist, P. 2006. Parallels among positive-strand RNA viruses, reverse-transcribing viruses and double-stranded RNA viruses. *Nat Rev Microbiol*. 4:371-382.

Alexopoulou, L., A.C. Holt, R. Medzhitov, and R.A. Flavell. 2001. Recognition of double-stranded RNA and activation of NF-kappaB by Toll-like receptor 3. *Nature*. 413:732-738.

Alvarez, E., M.L. DeDiego, J.L. Nieto-Torres, J.M. Jiménez-Guardeño, L. Marcos-Villar, and L. Enjuanes. 2010. The envelope protein of severe acute respiratory syndrome coronavirus interacts with the non-structural protein 3 and is ubiquitinated. *Virology*. 402:281-291.

Angelini, M.M., M. Akhlaghpour, B.W. Neuman, and M.J. Buchmeier. 2013. Severe acute respiratory syndrome coronavirus nonstructural proteins 3, 4, and 6 induce double-membrane vesicles. *MBio*. 4.

Angelini, M.M., B.W. Neuman, and M.J. Buchmeier. 2014. Untangling Membrane Rearrangement in the Nidovirales. *DNA Cell Biol*.

Bacia, K., P. Schwille, and T. Kurzchalia. 2005. Sterol structure determines the separation of phases and the curvature of the liquid-ordered phase in model membranes. *Proc Natl Acad Sci U S A*. 102:3272-3277.

Bailey, D., W.J. Kaiser, M. Hollinshead, K. Moffat, Y. Chaudhry, T. Wileman, S.V. Sosnovtsev, and I.G. Goodfellow. 2010. Feline calicivirus p32, p39 and p30 proteins localize to the endoplasmic reticulum to initiate replication complex formation. *J Gen Virol*. 91:739-749.

Baliji, S., S.A. Cammer, B. Sobral, and S.C. Baker. 2009. Detection of nonstructural protein 6 in murine coronavirus-infected cells and analysis of the transmembrane topology by using bioinformatics and molecular approaches. *J Virol*. 83:6957-6962.

Barajas, D., Y. Jiang, and P.D. Nagy. 2009. A unique role for the host ESCRT proteins in replication of Tomato bushy stunt virus. *PLoS Pathog*. 5:e1000705.

Barretto, N., D. Jukneliene, K. Ratia, Z. Chen, A.D. Mesecar, and S.C. Baker. 2005. The papain-like protease of severe acute respiratory syndrome coronavirus has deubiquitinating activity. *J Virol*. 79:15189-15198.

Baugh, J.M., J.A. Garcia-Rivera, and P.A. Gallay. 2013. Host-targeting agents in the treatment of hepatitis C: a beginning and an end? *Antiviral Res*. 100:555-561.

Baumgart, T., S.T. Hess, and W.W. Webb. 2003. Imaging coexisting fluid domains in biomembrane models coupling curvature and line tension. *Nature*. 425:821-824.

Beachboard, D.C., X. Lu, S.C. Baker, and M.R. Denison. 2013. Murine hepatitis virus nsp4 N258T mutants are not temperature-sensitive. *Virology*. 435:210-213.

Belov, G.A., V. Nair, B.T. Hansen, F.H. Hoyt, E.R. Fischer, and E. Ehrenfeld. 2012. Complex dynamic development of poliovirus membranous replication complexes. *J Virol*. 86:302-312.

Bernasconi, R., and M. Molinari. 2011. ERAD and ERAD tuning: disposal of cargo and of ERAD regulators from the mammalian ER. *Curr Opin Cell Biol*. 23:176-183.

Bernasconi, R., T. Pertel, J. Luban, and M. Molinari. 2008. A dual task for the Xbp1-responsive OS-9 variants in the mammalian endoplasmic reticulum: inhibiting secretion of misfolded protein conformers and enhancing their disposal. *J Biol Chem*. 283:16446-16454.

Boine, B., R.L. Kingston, and M.N. Pearson. 2012. Recombinant expression of the coat protein of Botrytis virus X and development of an immunofluorescence detection method to study its intracellular distribution in Botrytis cinerea. *J Gen Virol*. 93:2502-2511.

Braden, C.R., S.F. Dowell, D.B. Jernigan, and J.M. Hughes. 2013. Progress in global surveillance and response capacity 10 years after severe acute respiratory syndrome. *Emerg Infect Dis*. 19:864-869.

Brian, D.A., and R.S. Baric. 2005. Coronavirus genome structure and replication. *Curr Top Microbiol Immunol*. 287:1-30.

Britton, P., and D. Cavanagh. 2008. Nidovirus Genome Organization and Expression Mechanisms. *In* Nidoviruses. S. Perlman, T. Gallagher, and E.J. Snijder, editors. ASM Press, Washington, DC. 29-46.

Calì, T., C. Galli, S. Olivari, and M. Molinari. 2008. Segregation and rapid turnover of EDEM1 by an autophagy-like mechanism modulates standard ERAD and folding activities. *Biochem Biophys Res Commun*. 371:405-410.

Chan, J.F., K.S. Li, K.K. To, V.C. Cheng, H. Chen, and K.Y. Yuen. 2012. Is the discovery of the novel human betacoronavirus 2c EMC/2012 (HCoV-EMC) the beginning of another SARS-like pandemic? *J Infect*. 65:477-489.

Chen, C., X. Han, X. Zou, Y. Li, L. Yang, K. Cao, J. Xu, J. Long, J. Liu, and Z. Feng. 2014. 4-Methylene-2-octyl-5-oxotetrahydrofuran-3-carboxylic Acid (C75), an Inhibitor of Fatty-acid Synthase, Suppresses the Mitochondrial Fatty Acid Synthesis Pathway and Impairs Mitochondrial Function. *J Biol Chem*. 289:17184-17194.

Chirala, S.S., and S.J. Wakil. 2004. Structure and function of animal fatty acid synthase. *Lipids*. 39:1045-1053.

Clementz, M.A., A. Kanjanahaluethai, T.E. O'Brien, and S.C. Baker. 2008. Mutation in murine coronavirus replication protein nsp4 alters assembly of double membrane vesicles. *Virology*. 375:118-129.

Cong, Y., and X. Ren. 2014. Coronavirus entry and release in polarized epithelial cells: a review. *Rev Med Virol*.

Cornillez-Ty, C.T., L. Liao, J.R. Yates, P. Kuhn, and M.J. Buchmeier. 2009. Severe acute respiratory syndrome coronavirus nonstructural protein 2 interacts with a host protein complex involved in mitochondrial biogenesis and intracellular signaling. *J Virol*. 83:10314-10318.

Cottam, E.M., H.J. Maier, M. Manifava, L.C. Vaux, P. Chandra-Schoenfelder, W. Gerner, P. Britton, N.T. Ktistakis, and T. Wileman. 2011. Coronavirus nsp6 proteins generate autophagosomes from the endoplasmic reticulum via an omegasome intermediate. *Autophagy*. 7:1335-1347.

Cotten, M., S.J. Watson, A.I. Zumla, H.Q. Makhdoom, A.L. Palser, S.H. Ong, A.A. Al Rabeeah, R.F. Alhakeem, A. Assiri, J.A. Al-Tawfiq, A. Albarrak, M. Barry, A. Shibl, F.A. Alrabiah, S. Hajjar, H.H. Balkhy, H. Flemban, A. Rambaut, P. Kellam,

and Z.A. Memish. 2014. Spread, circulation, and evolution of the Middle East respiratory syndrome coronavirus. *MBio*. 5.
Cowley, J.A., C.M. Dimmock, K.M. Spann, and P.J. Walker. 2000. Gill-associated virus of Penaeus monodon prawns: an invertebrate virus with ORF1a and ORF1b genes related to arteri- and coronaviruses. *J Gen Virol*. 81:1473-1484.
de Groot, R.J., S.C. Baker, R.S. Baric, C.S. Brown, C. Drosten, L. Enjuanes, R.A. Fouchier, M. Galiano, A.E. Gorbalenya, Z. Memish, S. Perlman, L.L. Poon, E.J. Snijder, G.M. Stephens, P.C. Woo, A.M. Zaki, M. Zambon, and J. Ziebuhr. 2013. Middle East Respiratory Syndrome Coronavirus (MERS-CoV); Announcement of the Coronavirus Study Group. *J Virol*.
de Haan, C.A., and F. Reggiori. 2008. Are nidoviruses hijacking the autophagy machinery? *Autophagy*. 4:276-279.
de Wilde, A.H., V.S. Raj, D. Oudshoorn, T.M. Bestebroer, S. van Nieuwkoop, R.W. Limpens, C.C. Posthuma, Y. van der Meer, M. Bárcena, B.L. Haagmans, E.J. Snijder, and B.G. van den Hoogen. 2013. MERS-coronavirus replication induces severe in vitro cytopathology and is strongly inhibited by cyclosporin A or interferon-α treatment. *J Gen Virol*. 94:1749-1760.
den Boon, J.A., and P. Ahlquist. 2010. Organelle-like membrane compartmentalization of positive-strand RNA virus replication factories. *Annu Rev Microbiol*. 64:241-256.
den Boon, J.A., A. Diaz, and P. Ahlquist. 2010. Cytoplasmic viral replication complexes. *Cell Host Microbe*. 8:77-85.
Denison, M.R. 2008. Seeking membranes: positive-strand RNA virus replication complexes. *PLoS Biol*. 6:e270.
Drosten, C., S. Günther, W. Preiser, S. van der Werf, H.R. Brodt, S. Becker, H. Rabenau, M. Panning, L. Kolesnikova, R.A. Fouchier, A. Berger, A.M. Burguière, J. Cinatl, M. Eickmann, N. Escriou, K. Grywna, S. Kramme, J.C. Manuguerra, S. Müller, V. Rickerts, M. Stürmer, S. Vieth, H.D. Klenk, A.D. Osterhaus, H. Schmitz, and H.W. Doerr. 2003. Identification of a novel coronavirus in patients with severe acute respiratory syndrome. *N Engl J Med*. 348:1967-1976.
Dveksler, G.S., M.N. Pensiero, C.B. Cardellichio, R.K. Williams, G.S. Jiang, K.V. Holmes, and C.W. Dieffenbach. 1991. Cloning of the mouse hepatitis virus (MHV) receptor: expression in human and hamster cell lines confers susceptibility to MHV. *J Virol*. 65:6881-6891.
Edwardson, J.R., and R.G. Christie. 1978. Use of virus-induced inclusions in classification and diagnosis. *Annual Reviews Phytopathology*. 16:24.
Egloff, M.P., H. Malet, A. Putics, M. Heinonen, H. Dutartre, A. Frangeul, A. Gruez, V. Campanacci, C. Cambillau, J. Ziebuhr, T. Ahola, and B. Canard. 2006. Structural and functional basis for ADP-ribose and poly(ADP-ribose) binding by viral macro domains. *J Virol*. 80:8493-8502.
Emmott, E., M.A. Rodgers, A. Macdonald, S. McCrory, P. Ajuh, and J.A. Hiscox. 2010. Quantitative proteomics using stable isotope labeling with amino acids in cell culture reveals changes in the cytoplasmic, nuclear, and nucleolar proteomes in Vero cells infected with the coronavirus infectious bronchitis virus. *Mol Cell Proteomics*. 9:1920-1936.

Evanchik, M., H.Y. Cai, Q.S. Feng, L. Hu, R. Johnson, G. Kemble, Y. Kosaka, J. Lai, J.D. Oslob, M. Sivaraja, S. Tep, H.B. Yan, C.A. Zaharia, and R. McDowell. 2012. TVB-2640, a novel anti-HCV agent, safely causes sustained host-target inhibition in vivo. *Hepatology*. 56:1.

Faaberg, K.S. 2008. Arterivirus Structural Proteins and Assembly. *In* Nidoviruses. S. Perlman, T. Gallagher, and E.J. Snijder, editors. ASM Press, Washington DC. 211-234.

Fontana, J., C. López-Iglesias, W.P. Tzeng, T.K. Frey, J.J. Fernández, and C. Risco. 2010. Three-dimensional structure of Rubella virus factories. *Virology*. 405:579-591.

Fowler, R.A., S.E. Lapinsky, D. Hallett, A.S. Detsky, W.J. Sibbald, A.S. Slutsky, T.E. Stewart, and T.S.C.C. Group. 2003. Critically ill patients with severe acute respiratory syndrome. *JAMA*. 290:367-373.

Froshauer, S., J. Kartenbeck, and A. Helenius. 1988. Alphavirus RNA replicase is located on the cytoplasmic surface of endosomes and lysosomes. *J Cell Biol*. 107:2075-2086.

Gadlage, M.J., J.S. Sparks, D.C. Beachboard, R.G. Cox, J.D. Doyle, C.C. Stobart, and M.R. Denison. 2010. Murine hepatitis virus nonstructural protein 4 regulates virus-induced membrane modifications and replication complex function. *J Virol*. 84:280-290.

Gantier, M.P. 2014. Processing of double-stranded RNA in Mammalian cells: a direct antiviral role? *J Interferon Cytokine Res*. 34:469-477.

Gaunt, E.R., W. Cheung, J.E. Richards, A. Lever, and U. Desselberger. 2013. Inhibition of rotavirus replication by downregulation of fatty acid synthesis. *J Gen Virol*. 94:1310-1317.

Gauthier, L., M. Ravallec, M. Tournaire, F. Cousserans, M. Bergoin, B. Dainat, and J.R. de Miranda. 2011. Viruses associated with ovarian degeneration in Apis mellifera L. queens. *PLoS One*. 6:e16217.

Giansanti, M.G., G. Belloni, and M. Gatti. 2007. Rab11 is required for membrane trafficking and actomyosin ring constriction in meiotic cytokinesis of Drosophila males. *Mol Biol Cell*. 18:5034-5047.

Gillespie, L.K., A. Hoenen, G. Morgan, and J.M. Mackenzie. 2010. The endoplasmic reticulum provides the membrane platform for biogenesis of the flavivirus replication complex. *J Virol*. 84:10438-10447.

Goldsmith, C.S., K.M. Tatti, T.G. Ksiazek, P.E. Rollin, J.A. Comer, W.W. Lee, P.A. Rota, B. Bankamp, W.J. Bellini, and S.R. Zaki. 2004. Ultrastructural characterization of SARS coronavirus. *Emerg Infect Dis*. 10:320-326.

González, J.M., P. Gomez-Puertas, D. Cavanagh, A.E. Gorbalenya, and L. Enjuanes. 2003. A comparative sequence analysis to revise the current taxonomy of the family Coronaviridae. *Arch Virol*. 148:2207-2235.

Gorbalenya, A.E., L. Enjuanes, J. Ziebuhr, and E.J. Snijder. 2006. Nidovirales: evolving the largest RNA virus genome. *Virus Res*. 117:17-37.

Gosert, R., A. Kanjanahaluethai, D. Egger, K. Bienz, and S.C. Baker. 2002. RNA replication of mouse hepatitis virus takes place at double-membrane vesicles. *J Virol*. 76:3697-3708.

Graham, R., and M. Denison. 2006. Replication of murine hepatitis virus is regulated by papain-like proteinase 1 processing of nonstructural proteins 1, 2, and 3. *J Virol*. 80:11610-11620.

Graham, R.L., and R.S. Baric. 2010. Recombination, reservoirs, and the modular spike: mechanisms of coronavirus cross-species transmission. *J Virol*. 84:3134-3146.

Graham, R.L., E.F. Donaldson, and R.S. Baric. 2013. A decade after SARS: strategies for controlling emerging coronaviruses. *Nat Rev Microbiol*. 11:836-848.

Grangeon, R., M. Agbeci, J. Chen, G. Grondin, H. Zheng, and J.F. Laliberté. 2012. Impact on the endoplasmic reticulum and Golgi apparatus of turnip mosaic virus infection. *J Virol*. 86:9255-9265.

Gubern, A., M. Barceló-Torns, J. Casas, D. Barneda, R. Masgrau, F. Picatoste, J. Balsinde, M.A. Balboa, and E. Claro. 2009. Lipid droplet biogenesis induced by stress involves triacylglycerol synthesis that depends on group VIA phospholipase A2. *J Biol Chem*. 284:5697-5708.

Guix, S., S. Caballero, A. Bosch, and R.M. Pintó. 2004. C-terminal nsP1a protein of human astrovirus colocalizes with the endoplasmic reticulum and viral RNA. *J Virol*. 78:13627-13636.

Hagemeijer, M.C., I. Monastyrska, J. Griffith, P. van der Sluijs, J. Voortman, P.M. van Bergen En Henegouwen, A.M. Vonk, P.J. Rottier, F. Reggiori, and C.A. de Haan. 2014. Membrane rearrangements mediated by coronavirus nonstructural proteins 3 and 4. *Virology*. 458-459C:125-135.

Hagemeijer, M.C., P.J. Rottier, and C.A. de Haan. 2012. Biogenesis and dynamics of the coronavirus replicative structures. *Viruses*. 4:3245-3269.

Hagemeijer, M.C., M. Ulasli, A.M. Vonk, F. Reggiori, P.J. Rottier, and C.A. de Haan. 2011. Mobility and interactions of coronavirus nonstructural protein 4. *J Virol*. 85:4572-4577.

Hagemeijer, M.C., M.H. Verheije, M. Ulasli, I.A. Shaltiël, L.A. de Vries, F. Reggiori, P.J. Rottier, and C.A. de Haan. 2010. Dynamics of coronavirus replication-transcription complexes. *J Virol*. 84:2134-2149.

Harcourt, B.H., D. Jukneliene, A. Kanjanahaluethai, J. Bechill, K.M. Severson, C.M. Smith, P.A. Rota, and S.C. Baker. 2004. Identification of severe acute respiratory syndrome coronavirus replicase products and characterization of papain-like protease activity. *J Virol*. 78:13600-13612.

Heaton, N.S., R. Perera, K.L. Berger, S. Khadka, D.J. Lacount, R.J. Kuhn, and G. Randall. 2010. Dengue virus nonstructural protein 3 redistributes fatty acid synthase to sites of viral replication and increases cellular fatty acid synthesis. *Proc Natl Acad Sci U S A*. 107:17345-17350.

Hogue, B.G., and C.E. Machamer. 2008. Coronavirus Structural Proteins and Virus Assembly. *In* Nidoviruses. S. Perlman, T. Gallagher, and E.J. Snijder, editors. ASM Press, Washington DC.

Hsu, N.Y., O. Ilnytska, G. Belov, M. Santiana, Y.H. Chen, P.M. Takvorian, C. Pau, H. van der Schaar, N. Kaushik-Basu, T. Balla, C.E. Cameron, E. Ehrenfeld, F.J. van Kuppeveld, and N. Altan-Bonnet. 2010. Viral reorganization of the secretory pathway generates distinct organelles for RNA replication. *Cell*. 141:799-811.

Huang, J.T., C.P. Tseng, M.H. Liao, S.C. Lu, W.Z. Yeh, N. Sakamoto, C.M. Chen, and J.C. Cheng. 2013. Hepatitis C virus replication is modulated by the interaction of nonstructural protein NS5B and fatty acid synthase. *J Virol*. 87:4994-5004.

Imbert, I., E.J. Snijder, M. Dimitrova, J.C. Guillemot, P. Lécine, and B. Canard. 2008. The SARS-Coronavirus PLnc domain of nsp3 as a replication/transcription scaffolding protein. *Virus Res*. 133:136-148.

Johnson, M.A., A. Chatterjee, B.W. Neuman, and K. Wüthrich. 2010. SARS coronavirus unique domain: three-domain molecular architecture in solution and RNA binding. *J Mol Biol*. 400:724-742.

Josset, L., V.D. Menachery, L.E. Gralinski, S. Agnihothram, P. Sova, V.S. Carter, B.L. Yount, R.L. Graham, R.S. Baric, and M.G. Katze. 2013. Cell Host Response to Infection with Novel Human Coronavirus EMC Predicts Potential Antivirals and Important Differences with SARS Coronavirus. *MBio*. 4.

Kanjanahaluethai, A., and S.C. Baker. 2000. Identification of mouse hepatitis virus papain-like proteinase 2 activity. *J Virol*. 74:7911-7921.

Kanjanahaluethai, A., Z. Chen, D. Jukneliene, and S.C. Baker. 2007. Membrane topology of murine coronavirus replicase nonstructural protein 3. *Virology*. 361:391-401.

Kawakami, S., Y. Watanabe, and R.N. Beachy. 2004. Tobacco mosaic virus infection spreads cell to cell as intact replication complexes. *Proc Natl Acad Sci U S A*. 101:6291-6296.

Kirkegaard, K., and W.T. Jackson. 2005. Topology of double-membraned vesicles and the opportunity for non-lytic release of cytoplasm. *Autophagy*. 1:182-184.

Knobler, R.L., M. Rodriguez, P.W. Lampert, and M.B. Oldstone. 1983. Virologic models of chronic relapsing demyelinating disease. *Acta Neuropathol Suppl*. 9:31-37.

Knoops, K., M. Kikkert, S.H. Worm, J.C. Zevenhoven-Dobbe, Y. van der Meer, A.J. Koster, A.M. Mommaas, and E.J. Snijder. 2008. SARS-coronavirus replication is supported by a reticulovesicular network of modified endoplasmic reticulum. *PLoS Biol*. 6:e226.

Knoops, K., C. Swett-Tapia, S.H. van den Worm, A.J. Te Velthuis, A.J. Koster, A.M. Mommaas, E.J. Snijder, and M. Kikkert. 2010. Integrity of the early secretory pathway promotes, but is not required for, severe acute respiratory syndrome coronavirus RNA synthesis and virus-induced remodeling of endoplasmic reticulum membranes. *J Virol*. 84:833-846.

Kopek, B.G., G. Perkins, D.J. Miller, M.H. Ellisman, and P. Ahlquist. 2007. Three-dimensional analysis of a viral RNA replication complex reveals a virus-induced mini-organelle. *PLoS Biol*. 5:e220.

Kopek, B.G., E.W. Settles, P.D. Friesen, and P. Ahlquist. 2010. Nodavirus-induced membrane rearrangement in replication complex assembly requires replicase protein a, RNA templates, and polymerase activity. *J Virol*. 84:12492-12503.

Ksiazek, T.G., D. Erdman, C.S. Goldsmith, S.R. Zaki, T. Peret, S. Emery, S. Tong, C. Urbani, J.A. Comer, W. Lim, P.E. Rollin, S.F. Dowell, A.E. Ling, C.D. Humphrey, W.J. Shieh, J. Guarner, C.D. Paddock, P. Rota, B. Fields, J. DeRisi, J.Y. Yang, N. Cox, J.M. Hughes, J.W. LeDuc, W.J. Bellini, L.J. Anderson, and S.W. Group. 2003.

A novel coronavirus associated with severe acute respiratory syndrome. *N Engl J Med*. 348:1953-1966.
Kuhajda, F.P., L.E. Landree, and G.V. Ronnett. 2005. The connections between C75 and obesity drug-target pathways. *Trends Pharmacol Sci*. 26:541-544.
Kuhajda, F.P., E.S. Pizer, J.N. Li, N.S. Mani, G.L. Frehywot, and C.A. Townsend. 2000. Synthesis and antitumor activity of an inhibitor of fatty acid synthase. *Proc Natl Acad Sci U S A*. 97:3450-3454.
Kupfer, B., A. Simon, C.M. Jonassen, S. Viazov, V. Ditt, R.L. Tillmann, A. Müller, B. Matz, and O. Schildgen. 2007. Two cases of severe obstructive pneumonia associated with an HKU1-like coronavirus. *Eur J Med Res*. 12:134-138.
Lau, E.H., C.A. Hsiung, B.J. Cowling, C.H. Chen, L.M. Ho, T. Tsang, C.W. Chang, C.A. Donnelly, and G.M. Leung. 2010. A comparative epidemiologic analysis of SARS in Hong Kong, Beijing and Taiwan. *BMC Infect Dis*. 10:50.
Lauber, C., J.J. Goeman, M.e.C. Parquet, P. Thi Nga, E.J. Snijder, K. Morita, and A.E. Gorbalenya. 2013. The footprint of genome architecture in the largest genome expansion in RNA viruses. *PLoS Pathog*. 9:e1003500.
Leong, H.N., A. Earnest, H.H. Lim, C.F. Chin, C. Tan, M.E. Puhaindran, A. Tan, M.I. Chen, and Y.S. Leo. 2006. SARS in Singapore--predictors of disease severity. *Ann Acad Med Singapore*. 35:326-331.
Lesemann, D.E. 1977. Virus Group-specific and Virus-specific Cytological Alterations induced by Members of the Tymovirus Group. *Journal of phytopathology*. 90:21.
Leung, G.M., A.J. Hedley, L.M. Ho, P. Chau, I.O. Wong, T.Q. Thach, A.C. Ghani, C.A. Donnelly, C. Fraser, S. Riley, N.M. Ferguson, R.M. Anderson, T. Tsang, P.Y. Leung, V. Wong, J.C. Chan, E. Tsui, S.V. Lo, and T.H. Lam. 2004. The epidemiology of severe acute respiratory syndrome in the 2003 Hong Kong epidemic: an analysis of all 1755 patients. *Ann Intern Med*. 141:662-673.
Li, W., M.J. Moore, N. Vasilieva, J. Sui, S.K. Wong, M.A. Berne, M. Somasundaran, J.L. Sullivan, K. Luzuriaga, T.C. Greenough, H. Choe, and M. Farzan. 2003. Angiotensin-converting enzyme 2 is a functional receptor for the SARS coronavirus. *Nature*. 426:450-454.
Limpens, R.W., H.M. van der Schaar, D. Kumar, A.J. Koster, E.J. Snijder, F.J. van Kuppeveld, and M. Bárcena. 2011. The transformation of enterovirus replication structures: a three-dimensional study of single- and double-membrane compartments. *MBio*. 2.
Linnik, O., J. Liesche, J. Tilsner, and K.J. Oparka. 2013. Unraveling the structure of viral replication complexes at super-resolution. *Front Plant Sci*. 4:6.
Liu, H., J.Y. Liu, X. Wu, and J.T. Zhang. 2010. Biochemistry, molecular biology, and pharmacology of fatty acid synthase, an emerging therapeutic target and diagnosis/prognosis marker. *Int J Biochem Mol Biol*. 1:69-89.
Lundin, A., R. Dijkman, T. Bergström, N. Kann, B. Adamiak, C. Hannoun, E. Kindler, H.R. Jónsdóttir, D. Muth, J. Kint, M. Forlenza, M.A. Müller, C. Drosten, V. Thiel, and E. Trybala. 2014. Targeting membrane-bound viral RNA synthesis reveals potent inhibition of diverse coronaviruses including the middle East respiratory syndrome virus. *PLoS Pathog*. 10:e1004166.

Mackenzie, J. 2005. Wrapping things up about virus RNA replication. *Traffic*. 6:967-977.
Magliano, D., J.A. Marshall, D.S. Bowden, N. Vardaxis, J. Meanger, and J.Y. Lee. 1998. Rubella virus replication complexes are virus-modified lysosomes. *Virology*. 240:57-63.
Maier, H.J., and P. Britton. 2012. Involvement of autophagy in coronavirus replication. *Viruses*. 4:3440-3451.
Maier, H.J., P.C. Hawes, E.M. Cottam, J. Mantell, P. Verkade, P. Monaghan, T. Wileman, and P. Britton. 2013. Infectious bronchitis virus generates spherules from zippered endoplasmic reticulum membranes. *MBio*. 4:e00801-00813.
Martín-Acebes, M.A., A.B. Blázquez, N. Jiménez de Oya, E. Escribano-Romero, and J.C. Saiz. 2011. West Nile virus replication requires fatty acid synthesis but is independent on phosphatidylinositol-4-phosphate lipids. *PLoS One*. 6:e24970.
McBride, R., and B.C. Fielding. 2012. The role of severe acute respiratory syndrome (SARS)-coronavirus accessory proteins in virus pathogenesis. *Viruses*. 4:2902-2923.
McMahon, H.T., and J.L. Gallop. 2005. Membrane curvature and mechanisms of dynamic cell membrane remodelling. *Nature*. 438:590-596.
Medina, V., T. Tian, J. Wierzchos, and B.W. Falk. 1998. Specific inclusion bodies are associated with replication of lettuce infectious yellows virus RNAs in Nicotiana benthamiana protoplasts. *J Gen Virol*. 79 (Pt 10):2325-2329.
Miller, D.J., M.D. Schwartz, and P. Ahlquist. 2001. Flock house virus RNA replicates on outer mitochondrial membranes in Drosophila cells. *J Virol*. 75:11664-11676.
Miller, S., S. Kastner, J. Krijnse-Locker, S. Bühler, and R. Bartenschlager. 2007. The non-structural protein 4A of dengue virus is an integral membrane protein inducing membrane alterations in a 2K-regulated manner. *J Biol Chem*. 282:8873-8882.
Miller, S., and J. Krijnse-Locker. 2008. Modification of intracellular membrane structures for virus replication. *Nat Rev Microbiol*. 6:363-374.
Miorin, L., I. Romero-Brey, P. Maiuri, S. Hoppe, J. Krijnse-Locker, R. Bartenschlager, and A. Marcello. 2013. Three-dimensional architecture of tick-borne encephalitis virus replication sites and trafficking of the replicated RNA. *J Virol*. 87:6469-6481.
Monastyrska, I., M. Ulasli, P.J. Rottier, J.L. Guan, F. Reggiori, and C.A. de Haan. 2012. An autophagy-independent role for LC3 in equine arteritis virus replication. *Autophagy*. 9.
Moreira, A.G., E.W. Kitajima, and J.A.M. Rezende. 2010. Identification and partial characterization of a Carica papaya-infecting isolate of Alfalfa mosaic virus in Brazil. *Journal of General Plant Pathology*. 76:3.
Méndez, E., G. Aguirre-Crespo, G. Zavala, and C.F. Arias. 2007. Association of the astrovirus structural protein VP90 with membranes plays a role in virus morphogenesis. *J Virol*. 81:10649-10658.
Nagy, P.D., and J. Pogany. 2012. The dependence of viral RNA replication on co-opted host factors. *Nat Rev Microbiol*. 10:137-149.

Nasheri, N., M. Joyce, Y. Rouleau, P. Yang, S. Yao, D.L. Tyrrell, and J.P. Pezacki. 2013. Modulation of fatty acid synthase enzyme activity and expression during hepatitis C virus replication. *Chem Biol*. 20:570-582.

Netherton, C.L., and T. Wileman. 2011. Virus factories, double membrane vesicles and viroplasm generated in animal cells. *Curr Opin Virol*. 1:381-387.

Neuman, B.W., J.S. Joseph, K.S. Saikatendu, P. Serrano, A. Chatterjee, M.A. Johnson, L. Liao, J.P. Klaus, J.R. Yates, K. Wüthrich, R.C. Stevens, M.J. Buchmeier, and P. Kuhn. 2008. Proteomics analysis unravels the functional repertoire of coronavirus nonstructural protein 3. *J Virol*. 82:5279-5294.

Nishihara, T. 2003. Various morphological aspects of Escherichia coli lysis by RNA bacteriophage MS2 observed by transmission and scanning electron microscopes. *New Microbiol*. 26:163-168.

Novoa, R.R., G. Calderita, R. Arranz, J. Fontana, H. Granzow, and C. Risco. 2005. Virus factories: associations of cell organelles for viral replication and morphogenesis. *Biol Cell*. 97:147-172.

Oem, J.K., C. Jackel-Cram, Y.P. Li, Y. Zhou, J. Zhong, H. Shimano, L.A. Babiuk, and Q. Liu. 2008. Activation of sterol regulatory element-binding protein 1c and fatty acid synthase transcription by hepatitis C virus non-structural protein 2. *J Gen Virol*. 89:1225-1230.

Omura, S. 1976. The antibiotic cerulenin, a novel tool for biochemistry as an inhibitor of fatty acid synthesis. *Bacteriol Rev*. 40:681-697.

Oostra, M., M.C. Hagemeijer, M. van Gent, C.P. Bekker, E.G. te Lintelo, P.J. Rottier, and C.A. de Haan. 2008. Topology and membrane anchoring of the coronavirus replication complex: not all hydrophobic domains of nsp3 and nsp6 are membrane spanning. *J Virol*. 82:12392-12405.

Oostra, M., E.G. te Lintelo, M. Deijs, M.H. Verheije, P.J. Rottier, and C.A. de Haan. 2007. Localization and membrane topology of coronavirus nonstructural protein 4: involvement of the early secretory pathway in replication. *J Virol*. 81:12323-12336.

Osman, C., C. Merkwirth, and T. Langer. 2009. Prohibitins and the functional compartmentalization of mitochondrial membranes. *J Cell Sci*. 122:3823-3830.

Pan, J., X. Peng, Y. Gao, Z. Li, X. Lu, Y. Chen, M. Ishaq, D. Liu, M.L. Dediego, L. Enjuanes, and D. Guo. 2008. Genome-wide analysis of protein-protein interactions and involvement of viral proteins in SARS-CoV replication. *PLoS One*. 3:e3299.

Pasternak, A.O., W.J. Spaan, and E.J. Snijder. 2006. Nidovirus transcription: how to make sense...? *J Gen Virol*. 87:1403-1421.

Paul, D., and R. Bartenschlager. 2013. Architecture and biogenesis of plus-strand RNA virus replication factories. *World J Virol*. 2:32-48.

Pedersen, K.W., Y. van der Meer, N. Roos, and E.J. Snijder. 1999. Open reading frame 1a-encoded subunits of the arterivirus replicase induce endoplasmic reticulum-derived double-membrane vesicles which carry the viral replication complex. *J Virol*. 73:2016-2026.

Perales-Linares, R., and S. Navas-Martin. 2013. Toll-like receptor 3 in viral pathogenesis: friend or foe? *Immunology*. 140:153-167.

Perera, R., C. Riley, G. Isaac, A.S. Hopf-Jannasch, R.J. Moore, K.W. Weitz, L. Pasa-Tolic, T.O. Metz, J. Adamec, and R.J. Kuhn. 2012. Dengue virus infection perturbs lipid homeostasis in infected mosquito cells. *PLoS Pathog*. 8:e1002584.

Perlman, S., and J. Netland. 2009. Coronaviruses post-SARS: update on replication and pathogenesis. *Nat Rev Microbiol*. 7:439-450.

Perlman, S., and J. Zhao. 2013. Human Coronavirus EMC Is Not the Same as Severe Acute Respiratory Syndrome Coronavirus. *MBio*. 4.

Pfefferle, S., J. Schöpf, M. Kögl, C.C. Friedel, M.A. Müller, J. Carbajo-Lozoya, T. Stellberger, E. von Dall'Armi, P. Herzog, S. Kallies, D. Niemeyer, V. Ditt, T. Kuri, R. Züst, K. Pumpor, R. Hilgenfeld, F. Schwarz, R. Zimmer, I. Steffen, F. Weber, V. Thiel, G. Herrler, H.J. Thiel, C. Schwegmann-Wessels, S. Pöhlmann, J. Haas, C. Drosten, and A. von Brunn. 2011. The SARS-coronavirus-host interactome: identification of cyclophilins as target for pan-coronavirus inhibitors. *PLoS Pathog*. 7:e1002331.

Pizer, E.S., F.J. Chrest, J.A. DiGiuseppe, and W.F. Han. 1998. Pharmacological inhibitors of mammalian fatty acid synthase suppress DNA replication and induce apoptosis in tumor cell lines. *Cancer Res*. 58:4611-4615.

Pizer, E.S., F.D. Wood, G.R. Pasternack, and F.P. Kuhajda. 1996. Fatty acid synthase (FAS): a target for cytotoxic antimetabolites in HL60 promyelocytic leukemia cells. *Cancer Res*. 56:745-751.

Plant, E.P., and J.D. Dinman. 2008. The role of programmed-1 ribosomal frameshifting in coronavirus propagation. *Front Biosci*. 13:4873-4881.

Posthuma, C.C., K.W. Pedersen, Z. Lu, R.G. Joosten, N. Roos, J.C. Zevenhoven-Dobbe, and E.J. Snijder. 2008. Formation of the arterivirus replication/transcription complex: a key role for nonstructural protein 3 in the remodeling of intracellular membranes. *J Virol*. 82:4480-4491.

Poutanen, S.M., D.E. Low, B. Henry, S. Finkelstein, D. Rose, K. Green, R. Tellier, R. Draker, D. Adachi, M. Ayers, A.K. Chan, D.M. Skowronski, I. Salit, A.E. Simor, A.S. Slutsky, P.W. Doyle, M. Krajden, M. Petric, R.C. Brunham, A.J. McGeer, C.n. National Microbiology Laboratory, and C.S.A.R.S.S. Team. 2003. Identification of severe acute respiratory syndrome in Canada. *N Engl J Med*. 348:1995-2005.

Prentice, E., W.G. Jerome, T. Yoshimori, N. Mizushima, and M.R. Denison. 2004a. Coronavirus replication complex formation utilizes components of cellular autophagy. *J Biol Chem*. 279:10136-10141.

Prentice, E., J. McAuliffe, X. Lu, K. Subbarao, and M.R. Denison. 2004b. Identification and characterization of severe acute respiratory syndrome coronavirus replicase proteins. *J Virol*. 78:9977-9986.

Pringle, F.M., K.N. Johnson, C.L. Goodman, A.H. McIntosh, and L.A. Ball. 2003. Providence virus: a new member of the Tetraviridae that infects cultured insect cells. *Virology*. 306:359-370.

Pyrc, K., B. Berkhout, and L. van der Hoek. 2007. Identification of new human coronaviruses. *Expert Rev Anti Infect Ther*. 5:245-253.

Quinkert, D., R. Bartenschlager, and V. Lohmann. 2005. Quantitative analysis of the hepatitis C virus replication complex. *J Virol*. 79:13594-13605.

Rassmann, A., A. Henke, N. Jarasch, F. Lottspeich, H.P. Saluz, and T. Munder. 2007. The human fatty acid synthase: a new therapeutic target for coxsackievirus B3-induced diseases? *Antiviral Res*. 76:150-158.

Reed, S.E. 1984. The behaviour of recent isolates of human respiratory coronavirus in vitro and in volunteers: evidence of heterogeneity among 229E-related strains. *J Med Virol*. 13:179-192.

Reggiori, F., C.A. de Haan, and M. Molinari. 2011. Unconventional use of LC3 by coronaviruses through the alleged subversion of the ERAD tuning pathway. *Viruses*. 3:1610-1623.

Reggiori, F., I. Monastyrska, M. Verheije, T. Calì, M. Ulasli, S. Bianchi, R. Bernasconi, C. de Haan, and M. Molinari. 2010a. Coronaviruses Hijack the LC3-I-positive EDEMosomes, ER-derived vesicles exporting short-lived ERAD regulators, for replication. *Cell Host Microbe*. 7:500-508.

Reggiori, F., I. Monastyrska, M.H. Verheije, T. Calì, M. Ulasli, S. Bianchi, R. Bernasconi, C.A. de Haan, and M. Molinari. 2010b. Coronaviruses Hijack the LC3-I-positive EDEMosomes, ER-derived vesicles exporting short-lived ERAD regulators, for replication. *Cell Host Microbe*. 7:500-508.

Rehman, S., N. Kapur, H. Durgapal, and S.K. Panda. 2008. Subcellular localization of hepatitis E virus (HEV) replicase. *Virology*. 370:77-92.

Reichel, C., P. Más, and R.N. Beachy. 1999. The role of the ER and cytoskeleton in plant viral trafficking. *Trends Plant Sci*. 4:458-462.

Richards, A.L., J.A. Soares-Martins, G.T. Riddell, and W.T. Jackson. 2014. Generation of unique poliovirus RNA replication organelles. *MBio*. 5:e00833-00813.

Roberts, I.M., and B.D. Harrison. 1970. Inclusion bodies and tubular structures in Chenopodium amaranticolor plants infected with strawberry latent ringspot virus. *J Gen Virol*. 7:47-54.

Romero-Brey, I., A. Merz, A. Chiramel, J.Y. Lee, P. Chlanda, U. Haselman, R. Santarella-Mellwig, A. Habermann, S. Hoppe, S. Kallis, P. Walther, C. Antony, J. Krijnse-Locker, and R. Bartenschlager. 2012. Three-dimensional architecture and biogenesis of membrane structures associated with hepatitis C virus replication. *PLoS Pathog*. 8:e1003056.

Roosendaal, J., E.G. Westaway, A. Khromykh, and J.M. Mackenzie. 2006. Regulated cleavages at the West Nile virus NS4A-2K-NS4B junctions play a major role in rearranging cytoplasmic membranes and Golgi trafficking of the NS4A protein. *J Virol*. 80:4623-4632.

Ruch, T.R., and C.E. Machamer. 2012. The coronavirus E protein: assembly and beyond. *Viruses*. 4:363-382.

Rudzinska-Langwald, A. 1990. Cytological changes in phloem parenchyma cells of Solanum rostratum (Dunal.) related to the replication of potato virus M (PVM). *Acta societatis botanicorum poloniae*. 59:9.

Saikatendu, K.S., J.S. Joseph, V. Subramanian, T. Clayton, M. Griffith, K. Moy, J. Velasquez, B.W. Neuman, M.J. Buchmeier, R.C. Stevens, and P. Kuhn. 2005. Structural basis of severe acute respiratory syndrome coronavirus ADP-ribose-1''-phosphate dephosphorylation by a conserved domain of nsP3. *Structure*. 13:1665-1675.

Salonen, A., T. Ahola, and L. Kääriäinen. 2005. Viral RNA replication in association with cellular membranes. *Curr Top Microbiol Immunol*. 285:139-173.
Salonen, A., L. Vasiljeva, A. Merits, J. Magden, E. Jokitalo, and L. Kääriäinen. 2003. Properly folded nonstructural polyprotein directs the semliki forest virus replication complex to the endosomal compartment. *J Virol*. 77:1691-1702.
Satija, N., and S.K. Lal. 2007. The molecular biology of SARS coronavirus. *Ann N Y Acad Sci*. 1102:26-38.
Sawicki, S.G., D.L. Sawicki, and S.G. Siddell. 2007. A contemporary view of coronavirus transcription. *J Virol*. 81:20-29.
Sawicki, S.G., D.L. Sawicki, D. Younker, Y. Meyer, V. Thiel, H. Stokes, and S.G. Siddell. 2005. Functional and genetic analysis of coronavirus replicase-transcriptase proteins. *PLoS Pathog*. 1:e39.
Schaad, M.C., P.E. Jensen, and J.C. Carrington. 1997. Formation of plant RNA virus replication complexes on membranes: role of an endoplasmic reticulum-targeted viral protein. *EMBO J*. 16:4049-4059.
Schley, D., R.J. Whittaker, and B.W. Neuman. 2013. Arenavirus budding resulting from viral-protein-associated cell membrane curvature. *J R Soc Interface*. 10:20130403.
Schmidt, K.N., S. Kuhns, A. Neuner, B. Hub, H. Zentgraf, and G. Pereira. 2012. Cep164 mediates vesicular docking to the mother centriole during early steps of ciliogenesis. *J Cell Biol*. 199:1083-1101.
Schwartz, M., J. Chen, M. Janda, M. Sullivan, J. den Boon, and P. Ahlquist. 2002. A positive-strand RNA virus replication complex parallels form and function of retrovirus capsids. *Mol Cell*. 9:505-514.
Serrano, P., M.A. Johnson, A. Chatterjee, B.W. Neuman, J.S. Joseph, M.J. Buchmeier, P. Kuhn, and K. Wüthrich. 2009. Nuclear magnetic resonance structure of the nucleic acid-binding domain of severe acute respiratory syndrome coronavirus nonstructural protein 3. *J Virol*. 83:12998-13008.
Sharma, M., Z. Sasvari, and P.D. Nagy. 2011. Inhibition of phospholipid biosynthesis decreases the activity of the tombusvirus replicase and alters the subcellular localization of replication proteins. *Virology*. 415:141-152.
Shibata, Y., J. Hu, M.M. Kozlov, and T.A. Rapoport. 2009. Mechanisms shaping the membranes of cellular organelles. *Annu Rev Cell Dev Biol*. 25:329-354.
Short, J.R., and R.A. Dorrington. 2012. Membrane targeting of an alpha-like tetravirus replicase is directed by a region within the RNA-dependent RNA polymerase domain. *J Gen Virol*. 93:1706-1716.
Simon, A., S. Völz, K. Höfling, A. Kehl, R. Tillman, A. Müller, B. Kupfer, A.M. Eis-Hübinger, M.J. Lentze, U. Bode, and O. Schildgen. 2007. Acute life threatening event (ALTE) in an infant with human coronavirus HCoV-229E infection. *Pediatr Pulmonol*. 42:393-396.
Smith, S. 1994. The animal fatty acid synthase: one gene, one polypeptide, seven enzymes. *FASEB J*. 8:1248-1259.
Snijder, E.J., P.J. Bredenbeek, J.C. Dobbe, V. Thiel, J. Ziebuhr, L.L. Poon, Y. Guan, M. Rozanov, W.J. Spaan, and A.E. Gorbalenya. 2003. Unique and conserved features of genome and proteome of SARS-coronavirus, an early split-off from the coronavirus group 2 lineage. *J Mol Biol*. 331:991-1004.

Snijder, E.J., M. Kikkert, and Y. Fang. 2013. Arterivirus molecular biology and pathogenesis. *J Gen Virol*.
Snijder, E.J., Y. van der Meer, J. Zevenhoven-Dobbe, J.J. Onderwater, J. van der Meulen, H.K. Koerten, and A.M. Mommaas. 2006. Ultrastructure and origin of membrane vesicles associated with the severe acute respiratory syndrome coronavirus replication complex. *J Virol*. 80:5927-5940.
Snijder, E.J., H. van Tol, N. Roos, and K.W. Pedersen. 2001. Non-structural proteins 2 and 3 interact to modify host cell membranes during the formation of the arterivirus replication complex. *J Gen Virol*. 82:985-994.
Spann, K.M., J.E. Vickers, and R.J.G. Lester. 1995. Lymphoid organ virus of Penaeus monodon from Australia. *Diseases of aquatic organisms*. 23:8.
Sparks, J.S., X. Lu, and M.R. Denison. 2007. Genetic analysis of Murine hepatitis virus nsp4 in virus replication. *J Virol*. 81:12554-12563.
Spuul, P., G. Balistreri, L. Kääriäinen, and T. Ahola. 2010. Phosphatidylinositol 3-kinase-, actin-, and microtubule-dependent transport of Semliki Forest Virus replication complexes from the plasma membrane to modified lysosomes. *J Virol*. 84:7543-7557.
Stern, D.F., and S.I. Kennedy. 1980. Coronavirus multiplication strategy. I. Identification and characterization of virus-specified RNA. *J Virol*. 34:665-674.
Stertz, S., M. Reichelt, M. Spiegel, T. Kuri, L. Martínez-Sobrido, A. García-Sastre, F. Weber, and G. Kochs. 2007. The intracellular sites of early replication and budding of SARS-coronavirus. *Virology*. 361:304-315.
Subramaniam, S. 2005. Bridging the imaging gap: visualizing subcellular architecture with electron tomography. *Curr Opin Microbiol*. 8:316-322.
Subramaniam, S., A. Bartesaghi, J. Liu, A.E. Bennett, and R. Sougrat. 2007. Electron tomography of viruses. *Curr Opin Struct Biol*. 17:596-602.
Suhy, D.A., T.H. Giddings, and K. Kirkegaard. 2000. Remodeling the endoplasmic reticulum by poliovirus infection and by individual viral proteins: an autophagy-like origin for virus-induced vesicles. *J Virol*. 74:8953-8965.
Takao, Y., K. Nagasaki, K. Mise, T. Okuno, and D. Honda. 2005. Isolation and characterization of a novel single-stranded RNA Virus infectious to a marine fungoid protist, Schizochytrium sp. (Thraustochytriaceae, Labyrinthulea). *Appl Environ Microbiol*. 71:4516-4522.
Tan, K., B.D. Zelus, R. Meijers, J.H. Liu, J.M. Bergelson, N. Duke, R. Zhang, A. Joachimiak, K.V. Holmes, and J.H. Wang. 2002. Crystal structure of murine sCEACAM1a[1,4]: a coronavirus receptor in the CEA family. *EMBO J*. 21:2076-2086.
Teterina, N.L., K. Bienz, D. Egger, A.E. Gorbalenya, and E. Ehrenfeld. 1997. Induction of intracellular membrane rearrangements by HAV proteins 2C and 2BC. *Virology*. 237:66-77.
Tilsner, J., O. Linnik, K.M. Wright, K. Bell, A.G. Roberts, C. Lacomme, S. Santa Cruz, and K.J. Oparka. 2012. The TGB1 movement protein of Potato virus X reorganizes actin and endomembranes into the X-body, a viral replication factory. *Plant Physiol*. 158:1359-1370.

Tirotta, E., K.S. Carbajal, C.S. Schaumburg, L. Whitman, and T.E. Lane. 2010. Cell replacement therapies to promote remyelination in a viral model of demyelination. *J Neuroimmunol*. 224:101-107.

Tomaru, Y., N. Katanozaka, K. Nishida, Y. Shirai, K. Taruntani, M. Yamaguchi, and K. Nagasaki. 2004. Isolation and characterization of two distinct types of HcRNAV, a single-stranded RNA virus infecting the bivalve-killing microalga Heterocapsa circularisquama. *Aquatic microbial ecology*. 34:12.

Ulasli, M., M.H. Verheije, C.A. de Haan, and F. Reggiori. 2010. Qualitative and quantitative ultrastructural analysis of the membrane rearrangements induced by coronavirus. *Cell Microbiol*. 12:844-861.

Ulferts, R., I. Imbert, B. Canard, and J. Ziebuhr. 2010. Expression and Functions of SARS Coronavirus Replicative Proteins. *In* Molecular Biology of the SARS-Coronavirus. S.K. Lal, editor. Springer, Berlin Heidelberg. 75-98.

van Boheemen, S., M. de Graaf, C. Lauber, T.M. Bestebroer, V.S. Raj, A.M. Zaki, A.D. Osterhaus, B.L. Haagmans, A.E. Gorbalenya, E.J. Snijder, and R.A. Fouchier. 2012. Genomic characterization of a newly discovered coronavirus associated with acute respiratory distress syndrome in humans. *MBio*. 3.

van den Worm, S.H., K. Knoops, J.C. Zevenhoven-Dobbe, C. Beugeling, Y. van der Meer, A.M. Mommaas, and E.J. Snijder. 2011. Development and RNA-synthesizing activity of coronavirus replication structures in the absence of protein synthesis. *J Virol*. 85:5669-5673.

van Hemert, M.J., S.H. van den Worm, K. Knoops, A.M. Mommaas, A.E. Gorbalenya, and E.J. Snijder. 2008. SARS-coronavirus replication/transcription complexes are membrane-protected and need a host factor for activity in vitro. *PLoS Pathog*. 4:e1000054.

Verheije, M.H., M. Raaben, M. Mari, E.G. Te Lintelo, F. Reggiori, F.J. van Kuppeveld, P.J. Rottier, and C.A. de Haan. 2008. Mouse hepatitis coronavirus RNA replication depends on GBF1-mediated ARF1 activation. *PLoS Pathog*. 4:e1000088.

von Brunn, A., C. Teepe, J.C. Simpson, R. Pepperkok, C.C. Friedel, R. Zimmer, R. Roberts, R. Baric, and J. Haas. 2007. Analysis of intraviral protein-protein interactions of the SARS coronavirus ORFeome. *PLoS One*. 2:e459.

Wakil, S.J. 1989. Fatty acid synthase, a proficient multifunctional enzyme. *Biochemistry*. 28:4523-4530.

Wei, T., and A. Wang. 2008. Biogenesis of cytoplasmic membranous vesicles for plant potyvirus replication occurs at endoplasmic reticulum exit sites in a COPI- and COPII-dependent manner. *J Virol*. 82:12252-12264.

Weiss, S.R., S.A. Hughes, P.J. Bonilla, J.D. Turner, J.L. Leibowitz, and M.R. Denison. 1994. Coronavirus polyprotein processing. *Arch Virol Suppl*. 9:349-358.

Weiss, S.R., and J.L. Leibowitz. 2011. Coronavirus pathogenesis. *Adv Virus Res*. 81:85-164.

Welsch, S., S. Miller, I. Romero-Brey, A. Merz, C.K. Bleck, P. Walther, S.D. Fuller, C. Antony, J. Krijnse-Locker, and R. Bartenschlager. 2009. Composition and three-dimensional architecture of the dengue virus replication and assembly sites. *Cell Host Microbe*. 5:365-375.

Wilsky, S., K. Sobotta, N. Wiesener, J. Pilas, N. Althof, T. Munder, P. Wutzler, and A. Henke. 2012. Inhibition of fatty acid synthase by amentoflavone reduces coxsackievirus B3 replication. *Arch Virol*. 157:259-269.

Wood, O., N. Tauraso, and H. Liebhaber. 1970. Electron microscopic study of tissue cultures infected with simian haemorrhagic fever virus. *J Gen Virol*. 7:129-136.

Yang, W., B.L. Hood, S.L. Chadwick, S. Liu, S.C. Watkins, G. Luo, T.P. Conrads, and T. Wang. 2008. Fatty acid synthase is up-regulated during hepatitis C virus infection and regulates hepatitis C virus entry and production. *Hepatology*. 48:1396-1403.

Zaki, A.M., S. van Boheemen, T.M. Bestebroer, A.D. Osterhaus, and R.A. Fouchier. 2012. Isolation of a novel coronavirus from a man with pneumonia in Saudi Arabia. *N Engl J Med*. 367:1814-1820.

Zhang, L., Z.P. Zhang, X.E. Zhang, F.S. Lin, and F. Ge. 2010. Quantitative proteomics analysis reveals BAG3 as a potential target to suppress severe acute respiratory syndrome coronavirus replication. *J Virol*. 84:6050-6059.

Zhao, Z., L.B. Thackray, B.C. Miller, T.M. Lynn, M.M. Becker, E. Ward, N.N. Mizushima, M.R. Denison, and H.W. Virgin. 2007. Coronavirus replication does not require the autophagy gene ATG5. *Autophagy*. 3:581-585.

Ziebuhr, J. 2004. Molecular biology of severe acute respiratory syndrome coronavirus. *Curr Opin Microbiol*. 7:412-419.

Ziebuhr, J. 2006. The coronavirus replicase: insights into a sophisticated enzyme machinery. *Adv Exp Med Biol*. 581:3-11.

Zirkel, F., A. Kurth, P.L. Quan, T. Briese, H. Ellerbrok, G. Pauli, F.H. Leendertz, W.I. Lipkin, J. Ziebuhr, C. Drosten, and S. Junglen. 2011. An insect nidovirus emerging from a primary tropical rainforest. *MBio*. 2:e00077-00011.